CHAPTER 2

Pharmacophore-based Virtual Screening-guided Design, Synthesis and Biological Evaluation of Thioacetamide-tethered 1,3,4-Thiadiazole-1,2,4-Triazole Hybrids

2. Thioacetamide-tethered 1,3,4-thiadiazole-1,2,4-triazole hybrids (STT Series)

2.1. Design rationale and plan of work

2.1.1. Design rationale

With an objective to identify a novel SHP2 inhibitory scaffold, we performed pharmacophore-based virtual screening of Enamine^{TM} Advanced Collection of 551,907 molecules against an anti-SHP2 pharmacophore model (i.e. a 'PCP Query') built by creating hypothetical space regions on **SHP099** by Molecular Operating Environment (MOE) software to identify a sizable number of potential hit molecules which were subsequently filtered with the aid of flexible molecular docking against the tunnel allosteric site of SHP2 with **SHP099** as the co-crystallized ligand (PDB ID: 5EHR) and specialized techniques like PreADMET, PAINS-Remover to arrive upon a refined list of virtual hits. Based upon the binding affinity of the molecules towards SHP2, a couple of virtual leads were selected having the best binding affinity and structure-guided molecular dynamics simulation studies were done on them to understand their plausible binding mode and interaction pattern with SHP2.

Upon successful virtual screening and *in silico* studies of the virtual hit(s), the topmost molecule was synthesized, characterized and evaluated for SHP2 inhibition to obtain its IC_{50}. Interestingly, all the features (or sites) of the thus identified lead SHP2 inhibitor, **111675** (IC_{50} = 0.878 ± 0.008 μM) corresponded well with **SHP099** within the binding

site of SHP2 (PDB ID: 5EHR) upon analysis of their 3D orientation by molecular docking. Consequently, as has been discussed earlier (**Section 1.2.3**), compound **111675** also contained the following "common" pharmacophoric features; (A) a mono/poly-substituted aromatic carbocycle (marked in yellow, **Figure 2.1**), (B) a heteroaromatic ring core like pyrimidinone, pyrazine, indole etc. (marked in blue, **Figure 2.1**), (C) an amine appendage (marked in purple, **Figure 2.1**) and (D) an amino or alkylamino group or analogous fused azacycle on the heterocyclic core (marked in green, **Figure 2.1**) [92, 93]. These unvarying and necessary features, thus, carry the potential to be exploited judiciously and rationally to design and develop newer and better SHP2 inhibitory scaffolds in future.With our current objective to further optimize the virtual lead to enhance its SHP2 inhibitory potential, the fused heterocycle (site A) was replaced with an extended sp^2-sp^2 hybridized moiety (the 5-phenyl-1,3,4-thiadiazole ring in structure-I) by foreseeing better affinity for the enzyme and more flexibility to achieve further active conformation of the ligand within the binding site. However, the distance between site A and site C was shortened and the methyloxy carbonyl side chain (or any such substituent) of **111675** was removed from structure-I as it did not participate in any interactions with SHP2 [110].

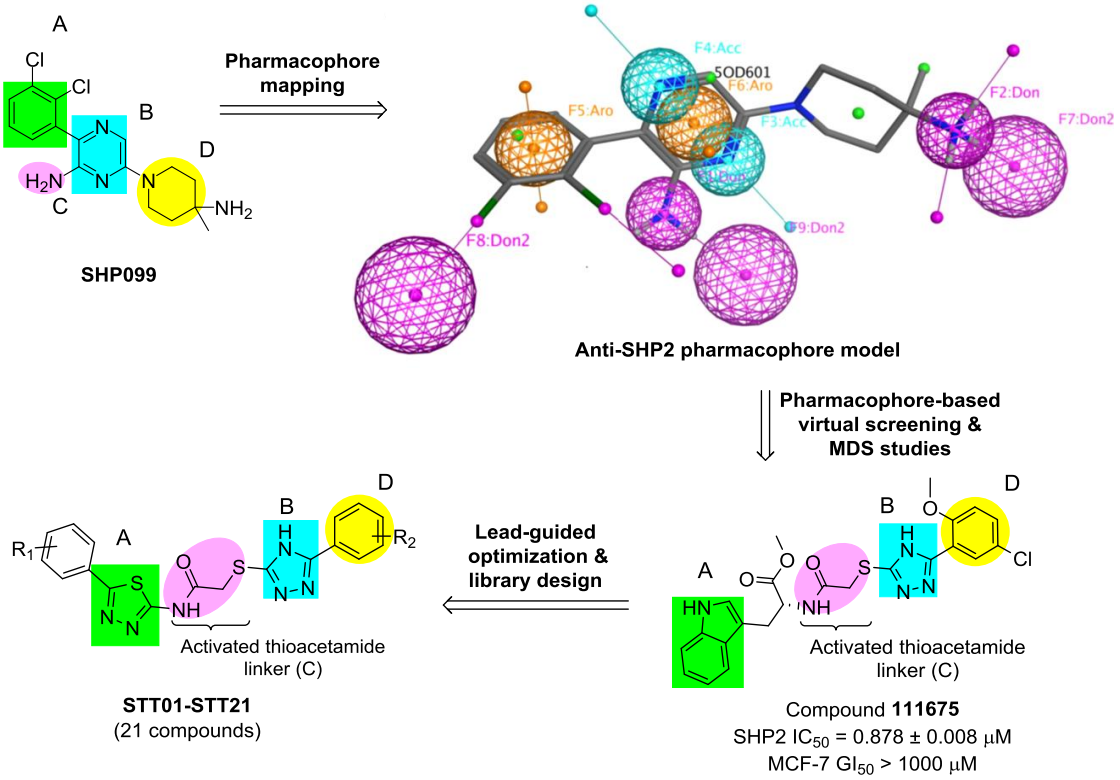

Figure 2.1. Design rationale of compounds **STT01-STT21**

Other parts of compound **111675** were retained *per se* in our designed structure as they contributed suitably to SHP2 inhibitory activity. Thus, the activated amide linker (C) directly tethered site A and site B together (**Figure 2.1**).

2.1.1.1. Lead-based library design

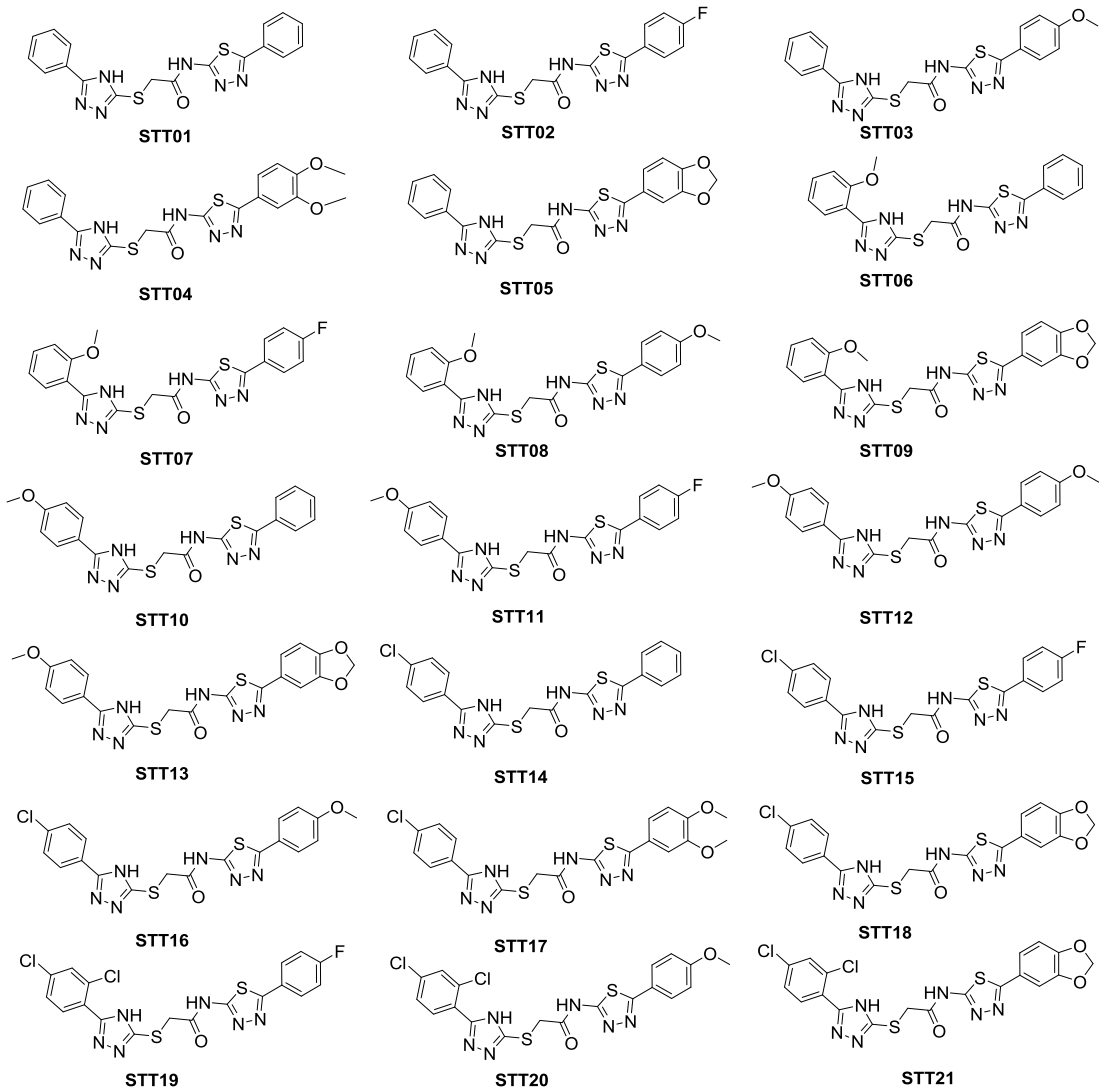

Figure 2.2. Skeletal formulae of rationally designed compounds (**STT01-STT21**)

Validated virtual lead **111675** was synthesized and characterized, and it was further utilized for virtual lead-guided optimization and a library of 21 compounds was designed and synthesized by judicious modifications in the backbone of **111675** and also, by introducing different substituents at the terminal aryl ring (**Figure 2.3**). The 1,3,4-thiadiazole ring is well known for its anticancer and antibacterial property which arises from it being bioisosteric with pyrimidine, the principal component of thymine, cytosine and uracil nucleobases [103, 111, 112]. Also, many thiadiazole bearing

compounds have been shown to inhibit cancerous cells like MCF7 (breast cancer) [113] and tumorigenic enzymes like carbonic anhydrase IX (solid tumor) [114]. In a nutshell, it can be stated that there are reports of many five membered heterocyclic scaffolds as allosteric SHP2 inhibitors and we envisaged evaluating the five membered heterocyclic bis-hybrid backbone connected with an activated linker. The two variable centers were systematically varied and their effects on the activity profile of the final compounds was studied. For this, focused and rational variations were attempted at the 5^{th} position of the five-membered systems (i.e., R_1 and R_2, **Figure 2.1**) to impart varying degree of lipophilicity to the final molecule. For instance, substituents like 4-methoxy, 3,4-dimethoxy and 2,3-dioxo were introduced at R_1 by anticipating a gradual enhancement of lipophilicity and subsequent enhancement of the binding interactions with the enzyme, with increasing number of methoxy substituents. Halogen groups (Cl, F) were incorporated at both the ends to study their effect (e.g., $\pm I$ effect) on the resultant molecules.

2.1.2. Plan of work

The plan of work for the design and development of novel SHP2 inhibitory scaffolds having anticancer potential and acceptable safety profile is represented schematically in **Figure 2.2**. A ligand-based virtual screening approach was strategized by utilizing a prototype inhibitor scaffold to screen a suitable anticancer drug database and subsequently filtering out the hits to generate the virtual lead. Lead-guided optimization was then applied to design and synthesize a set of new analogous molecules which were subsequently evaluated biologically by *in vitro, in cellulo, in vivo* and *ex vivo* studies for desired efficacy and undesired toxicity.

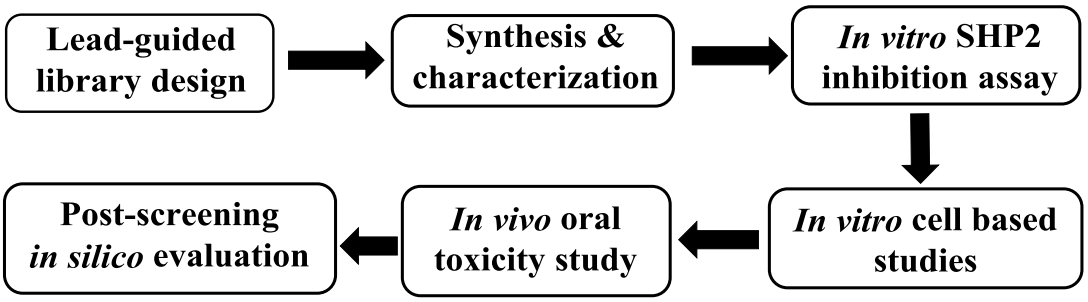

Figure 2.3. Plan of work for this series of compounds

2.2. Experimental work

2.2.1. Pharmacophore-based virtual screening studies

Pharmacophore-based virtual screening (PBVS) is a pharmacoinformatics methodology that employs physicochemical knowhow of the chemical space into the dynamic environs of computational technology to extract novel virtual molecular hits that are precise and promising for a drug target [115]. The term pharmacophore is defined by Gund as "a set of structural features in a molecule that is recognized at a receptor site and is responsible for the molecule's biological activity" [116]. Pharmacophores are actually as sort of conceptual templates where the entire system of protein-ligand interactions can be conveniently delimited by a few conventionally recognized physicochemical features like hydrogen bonding, hydrophilic or hydrophobic interactions etc., that reflect the pharmacological potential of the structure. In PBVS, a model is developed based on conformational sampling of a pharmacologically proven, potent binder of the target i.e. the known ligand and subsequently forming hypothetical spaces consisting of the physicochemical features to identify best features responsible for the pharmacological effects. PBVS utilizes many software tools for this intuitive approximation. Many drug discovery research groups have resorted to structure-based or pharmacophore-based virtual screening

protocols to identify novel structurally distinct and potent SHP2 inhibitors [109, 117, 118].

2.2.1.1. Tools and datasets

Various computational tools were employed in the study for developing pharmacophore model, query search, drug likeness screening, PAINS filter, molecular docking and molecular dynamic simulation studies. Three-dimensional X-ray crystal structure of SHP2 co-crystallized with allosteric inhibitor **SHP099** (ligand PDB ID: 5OD) at a resolution of 1.70Å was acquired from Protein Data Bank (https://www.rcsb.org/structure/5EHR, accessed on 15th November 2022) having PDB ID: 5EHR [119]. The pharmacophore model was generated using pharmacophore query editor module provided in the MOE software. Generated pharmacophore query was used to search Enamine™ Advanced Database [120] through Pharmit web server (http://pharmit.csb.pitt.edu/search.html). The obtained hits were further screened for their drug-likeness (using DruLiTo software developed by NIPER, Mohali) and PAINS interference (https://www.cbligand.org/PAINS/login.php). Additionally, the generated hits were furthered filtered according to their predicted ADMET properties wherein the prediction was carried out by Pre-ADMET online server (https://preadmet.webservice.bmdrc.org/). Molecular docking of filtered molecules was carried out using MOE software [121] while molecular dynamic simulation studies of top two hits was performed by GROMACS [122].

2.2.1.2. Pharmacophore-based virtual screening protocol

Protein structure of SHP2 complexed with **SHP099** with a resolution of 1.70 Å (PDB ID: 5EHR) was obtained from protein data bank (PDB) and utilized for development

of pharmacophore model. Protein was cleaned by removing undesired chains, solvent and ligand molecules using sequence editor module of MOE. Further, the protein structure was prepared using protein preparation option provided into sequence editor module. Before moving to pharmacophore mapping the receptor was disabled from system menu to clear and make ligand more visible. Additionally, the pharmacophoric features present in **SHP099** were mapped by selecting features then adding them using features option from pharmacophore query editor module. Several pharmacophoric features, i.e., hydrogen acceptor, hydrogen donor, aromatic centre, were used to create the pharmacophore query. The generated pharmacophore query was exported in .php format.

2.2.2. Chemistry

2.2.2.1. Synthesis of compound 111675 (virtual lead SHP2 inhibitor)

D-tryptophan methyl ester hydrochloride (CAS No.: 14907-27- 8) and 5-chloro-2-anisic acid (CAS No.: 3438-16-2) were procured from TCI Chemicals. Both the reactants were used as such without further purification. All other laboratory grade synthetic reagents were procured from Sigma-Aldrich Chemical Private Ltd., India, Merck India, Fischer Scientific Ltd., Central Drug House (P) Ltd. India, Loba Chemie India, Sisco Research Laboratories Pvt Ltd., India etc. and used as such without further purification. In general, reaction was monitored by TLC with the help of pre-coated silica gel plates (Merck, Kieselgel 60F-254, 0.20 mm).

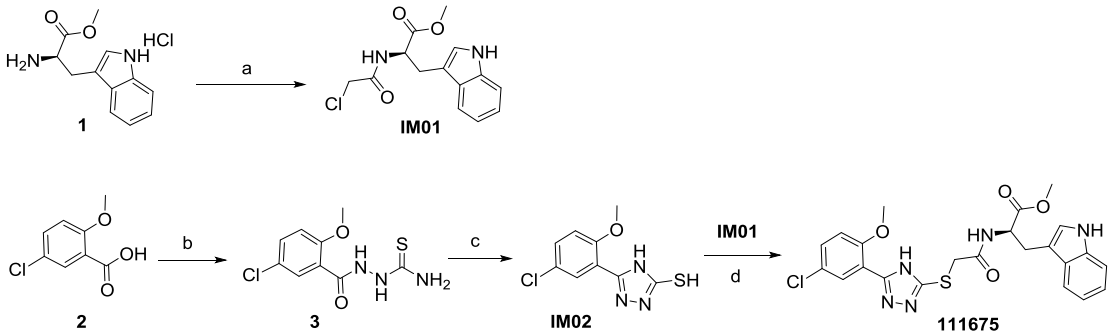

Scheme 2.1. Synthetic scheme for compound **111675.** *Reagents & conditions*: (a) chloroacetyl chloride, K_2CO_3, DMF, 0-5°C to RT, 1-2 h; 79% yield (b) i) oxalyl chloride, dry DCM, 0-5°C to RT, 2-3 h, ii) thiosemicarbazide, ACN, RT, 3-4 h; (c) i) KOH, water, reflux, 3-4 h, ii) dil. HCl, pH 5-6; 74% yield (2 steps) (d) K_2CO_3, DMF, RT, 0.5-1 h, 87% yield.

Step 1: Synthesis of methyl (2-chloroacetyl)-D-tryptophanate (IM01)

To a suspension of D-tryptophan methyl ester hydrochloride (**1**) (0.3 g, 1.18 mmol) in DMF (10 mL) was added powdered potassium carbonate (0.33 g, 2.35 mmol) and cooled to 0-5 ºC. Chloroacetyl chloride (0.17 g, 1.41 mmol) was added to the suspension dropwise and stirred at 0-5 ºC following which the reaction mass was allowed to heat up to room temperature and further stirred for 1-2 h. Progress of the reaction was monitored by TLC and on completion of reaction, it was poured into iced brine (100 mL), stirred briefly, extracted with ethyl acetate (2×50 mL) and washed with brine. After drying over anhydrous sodium sulphate, the organic layer was evaporated to give crude product as a viscous oil. The crude product was purified using preparative TLC with the desired product eluting at 30% ethyl acetate in hexane to give methyl (2-chloroacetyl)-D-tryptophanate (**IM01**) (0.27 g, 79% yield) as a sticky solid.

Step 2: Synthesis of 5-(5-chloro-2-methoxyphenyl)- 4*H*-1,2,4-triazole-3-thiol (IM02)

A solution of 5-chloro-2-anisic acid (**2**) (1 g, 5.35 mmol), oxalyl chloride (0.7 mL, 8.03 mmol) and dichloromethane (DCM, 20 mL) was stirred at RT for a period of 3-4 h after

which solvent was evaporated from the reaction mass and the residue was suspended in dry acetonitrile (ACN, 10 mL). This was added to a stirred suspension of thiosemicarbazide (0.5 g, 5.35 mmol) in dry ACN (20 mL) and stirred at RT for 3-4 h. The resultant white precipitate was filtered under reduced pressure, washed with ACN (2×5 mL) and sucked dry. After drying in a vacuum tray drier for 2-3 h, the obtained thiosemicarbazate salt (**3**) was suspended in deionised water (40 mL) and KOH pellets (3 g, 53.5 mmol) were added to it. Upon brief stirring, the white suspension turned into a clear solution and was refluxed for 3-4 h. Then it was cooled to RT and the pH was adjusted to 5-6 by addition of dil. HCl. Immediately, there was formation of white precipitate which was filtered under reduced pressure and sucked dry. On drying the product in a vacuum tray drier overnight, the desired product 5-(5-chloro-2-methoxyphenyl)-4*H*-1,2,4-triazole-3-thiol (**IM02**) was obtained as a white powder (1.12 g, 74% yield).

Step 3: Synthesis of methyl (2-((5-(5-chloro-2-methoxyphenyl)-4*H*-1,2,4-triazol-3-yl)thio)acetyl)-D-tryptophanate (111675)

To a stirred solution of methyl (2-chloroacetyl)-D-tryptophanate (**IM01**) (0.12 g, 0.41 mmol) and 5-(5-chloro-2-methoxyphenyl)-4*H*-1,2,4-triazole-3-thiol (**IM02**) (0.1 g, 0.41 mmol) in dry DMF (5 mL) was added finely powdered potassium carbonate (0.12 g, 0.82 mmol) and stirred at ambient temperature for 30 min. On completion of reaction as monitored by TLC, the reaction mass was poured into iced brine (50 mL) and stirred briefly after which the resultant white precipitate was filtered under reduced pressure, washed with water (2×25 mL) and sucked dry for 15-20 mins. Drying overnight at 60 ºC in a tray drier oven afforded the final compound methyl (2-((5-(5-chloro-2-

methoxyphenyl)-4*H*-1,2,4-triazol-3-yl)thio)acetyl)-D-tryptophanate (**111675**) as a creamy solid (0.176 g, 0.35 mmol).

2.2.2.2. Synthesis of compounds STT01-STT21

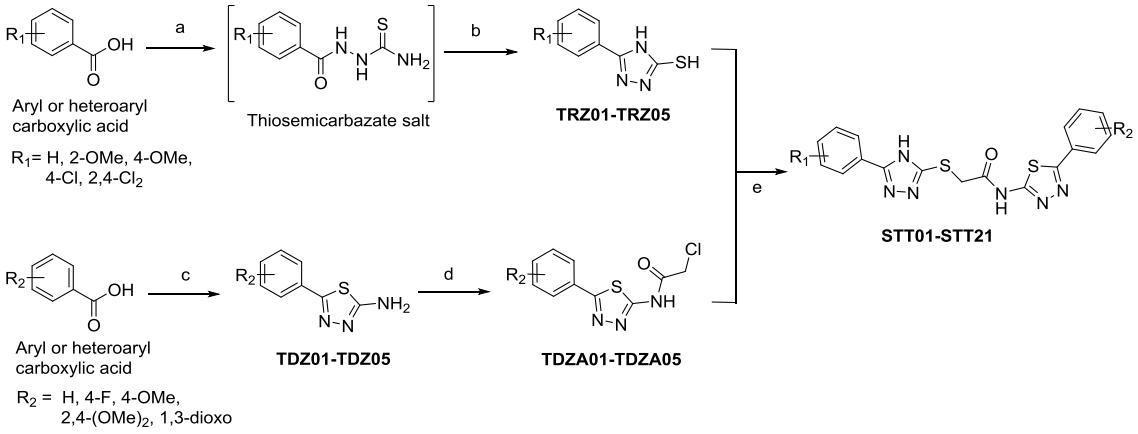

Scheme 2.2. Synthetic scheme for final compounds **STT01-STT21.** *Reagents and conditions*: (a) i) oxalyl chloride, dry DCM, 0-5 ºC to RT, 2-3 h, ii) thiosemicarbazide, ACN, RT, 3-4 h; (b) i) KOH, water, reflux, 3-4 h, ii) 1N HCl, pH 5-6, 65-87% yield (2 steps); (c) i) thiosemicarbazide, $POCl_3$, 75-80 ºC, 0.5-1 h ii) water, reflux, 3-4 h, iii) 40% aq. NaOH solution, pH 8, 76-92% yield; (d) chloroacetyl chloride, K_2CO_3, DMF, 0-5 ºC to RT, 1-2 h, 77-95% yield; (e) K_2CO_3, DMF, RT, 0.5-1 h, 62-96% yield.

Step 1: Synthesis of 5-(substituted phenyl)-4*H*-1,2,4-triazole-3-thiols (TRZ01-TRZ05)

A solution of substituted benzoic acid (5.35 mmol), oxalyl chloride (8.03 mmol) and DCM (20 mL) was stirred at RT for a period of 3-4 h after which solvent was evaporated from the reaction mass and the residue was suspended in dry ACN (10 mL). This was added to a stirred suspension of thiosemicarbazide (5.35 mmol) in dry ACN (20 mL) and stirred at RT for 3-4 h. The resultant white precipitate was filtered under reduced pressure, washed with ACN (2 x 5 mL) and sucked dry. After drying in a vacuum tray drier for 2-3 h, the obtained thiosemicarbazate salt was suspended in deionised water (40 mL) and KOH pellets (53.5 mmol) were added to it. Upon brief stirring the white suspension turned into a clear solution and was refluxed for 3-4 h. then it was cooled to

RT and the pH was adjusted to 5-6 by addition of dil. HCl. Immediately, there was formation of white precipitate which was filtered under reduced pressure and sucked dry. On drying the product in a vacuum tray drier overnight, the desired product (**TRZ01-TRZ05**) was obtained as a powdery solid.

Step 2: Synthesis of 5-(substituted phenyl)-1,3,4-thiadiazole-2-amines (TDZ01-TDZ05)

An equimolar amount of aryl/heteroaryl carboxylic acid (0.04 mol) and thiosemicarbazide (0.04 mol) in $POCl_3$ (0.075 mol) was heated at 75-80°C for half an hour, cooled to ambient temperature and water (90-100 mL) was added slowly and reaction mixture was refluxed for another 3-4 h. Reaction was monitored by TLC and after completion of reaction, it was cooled to room temperature and basified to pH 8 by the dropwise addition of 40% NaOH solution under stirring. The precipitate thus obtained was filtered under reduced pressure, dried and recrystallized from suitable solvent to obtain **TDZ01-TDZ05** in good yields.

Step 3: Procedure for the synthesis of *N*-(5-phenyl-1,3,4-thiadiazol-2-yl)-2-((5-phenyl-4*H*-1,2,4-triazol-3-yl)thio)acetamides (STT01-STT21)

To a stirred suspension of **TDZ01-TDZ05** (3.6 mmol) in DMF (10 mL) was added potassium carbonate (7.2 mmol) and chloroacetyl chloride (4.0 mmol) at 0-5°C. The resulting reaction mixture was stirred at ambient temperature for a period of 30 min (completion of reaction was monitored by TLC), the reaction mixture was poured into iced saturated brine (100 mL) and vigorously stirred for 15-20 min, followed by filtration of the obtained precipitate under reduced pressure. and drying the residue to obtain the desired intermediates **TDZA01-TDZA05**. These products were taken for the next step without further purification and characterization.

The final compounds **STT01-STT21** were synthesized by the condensation reaction of 5-(substituted phenyl)-1,3,4-thiadiazole-2-yl chloroacetamides (**TDZA01-TDZA05**) with the 1,2,4-triazole-3-thiol derived fragments (**TRZ01-TRZ05**). Each of the two key intermediates were dissolved in 1:1 stoichiometric ratio in dry DMF (5-10 mL) and finely powdered potassium carbonate (2 mol. equiv.) was added and stirred at ambient temperature for 30 min. On completion of reaction as monitored by TLC, the reaction mass was poured into iced brine (50 mL) and stirred briefly after which the resultant white precipitate was filtered under reduced pressure, washed with water (2 x 25 mL) and sucked dry for 15-20 mins. Drying overnight at 60 ºC in a tray drier oven afforded the desired final compounds.

2.2.2.3. Physicochemical characterization

The physicochemical characterizations of all the synthesized compounds were performed for melting range, solubility, retardation factor (R_f), calculated logP (ClogP), experimental logP by partitioning in *n*-octanol/water and appearance of the compounds (**STT01-STT21**).

A. TLC and R_f calculation

TLC was carried out to determine the retardation factor (R_f) value of each compound. A mobile phase of 60 % ethyl acetate and 40 % *n*-hexane was used to monitor the progress of the reaction as well as for R_f determination of final compounds. R_f is defined as the distance travelled by solute divided by distance travelled by solvent.

$$R_f = \text{Distance travelled by solute/Distance travelled by solvent}$$

The appearance of the single spot in TLC of final compound indicated the purity of the compounds.

B. Melting point and solubility determination

The melting point ranges were determined in digital melting point apparatus model IIC327 by using one end open capillary tubes. The solubility of the final compounds was determined in number of polar and non-polar organic solvents at ambient temperature. All the final compounds were soluble in DMF and DMSO.

C. Determination of Log P

The λ_{max} of compounds **STT01-STT21** was determined at a concentration of 10 µg/mL in HPLC grade methanol. The standard calibration curve of absorbance vs. concentration of each compound at its λ_{max} was obtained by preparing 6 different concentrations viz. 1, 2, 4, 6, 8, 10 µg/mL in methanol to determine the linearity range and sensitivity of the method. This was subsequently used to calculate unknown concentration of compound in n-octanol and water (maintained at pH 7.4 by phosphate buffer), respectively. For Log P, n-octanol and water (pH 7.4, phosphate buffer) were pre-saturated with distilled water and n-octanol, respectively. About 1 mg of each compound was then weighed and added to a bilayer of 10 mL of 1:1 pre-saturated n-octanol and buffered water (pH 7.4) and shaken vigorously for 15-20 min and kept overnight to separate. The two layers were collected separately and absorbance of compound in each layer was determined at its λ_{max} and the concentration was deduced from the calibration curve. Partition coefficient and Log P are calculated as follows: Partition coefficient (P) = $conc_{octanol}$ / $conc_{water}$, Log P = $\log_{10}$ (partition coefficient).

2.2.2.4. Spectral characterization

The chemical structure of intermediates and final compounds was evaluated by using several spectroscopic techniques like UV-Vis spectroscopy, vibrational spectroscopy

(FTIR), rotational spectroscopy (NMR) and high-resolution mass spectrometry (HRMS). The wavelength of maximum absorbance (λ_{max}) of final compounds was recorded on Agilent Cary 60 spectrophotometer. The absorption spectra of infrared radiation were determined for all the synthesized compounds using Shimadzu FTIR-8400S instrument through KBr pressed pellet method.

^{1}H, ^{13}C and ^{19}F NMR spectroscopic characterization was performed for all the synthesized compounds using Bruker 500 MHz FT-NMR spectrophotometer and deuterated chloroform ($CDCl_3$) or deuterated dimethyl sulfoxide (DMSO-d_6) was used as solvent. The analysis was carried out at the central instrument facility (CIF), IIT (BHU), Varanasi and SATHI facility in Central Discovery Centre (CDC), Banaras Hindu University (BHU). The values of chemical shift are presented in δ ppm (parts per million) downfield from tetramethylsilane (TMS, internal standard) for ^{1}H & ^{13}C NMR and trichlorofluoromethane ($CFCl_3$, internal standard) for ^{19}F NMR. In ^{1}H NMR the peaks of spectra are reported as: *s* - singlet, *d*- doublet, *dd* – doublet of doublet, *dt* – doublet of triplet, *ddd* – doublet of doublet of doublet, *t* – triplet and *m* – multiplet. The obtained spectral features/signatures of the compounds are discussed in the 'Results and Discussion' section (**Section 2.3**). Mass spectrometry of the intermediates was performed in the Central Analytical Laboratory of Birla Institute of Technology & Science Pilani, Hyderabad Campus (model: Shimadzu Model: LCMS 8040, Triple Quadrupole up to 2000 m/z value; modes: ESI and APCI). High-resolution mass spectrometry (HRMS) characterization was performed using X500R QTOF system in +IDA TOF mode available in the Analytical Laboratory of Department of Chemistry, Institute of Science, Banaras Hindu University (ISc-BHU), Varanasi.

2.2.3. Biological studies

2.2.3.1. *In vitro* SHP2 enzyme inhibition and enzyme kinetics assay

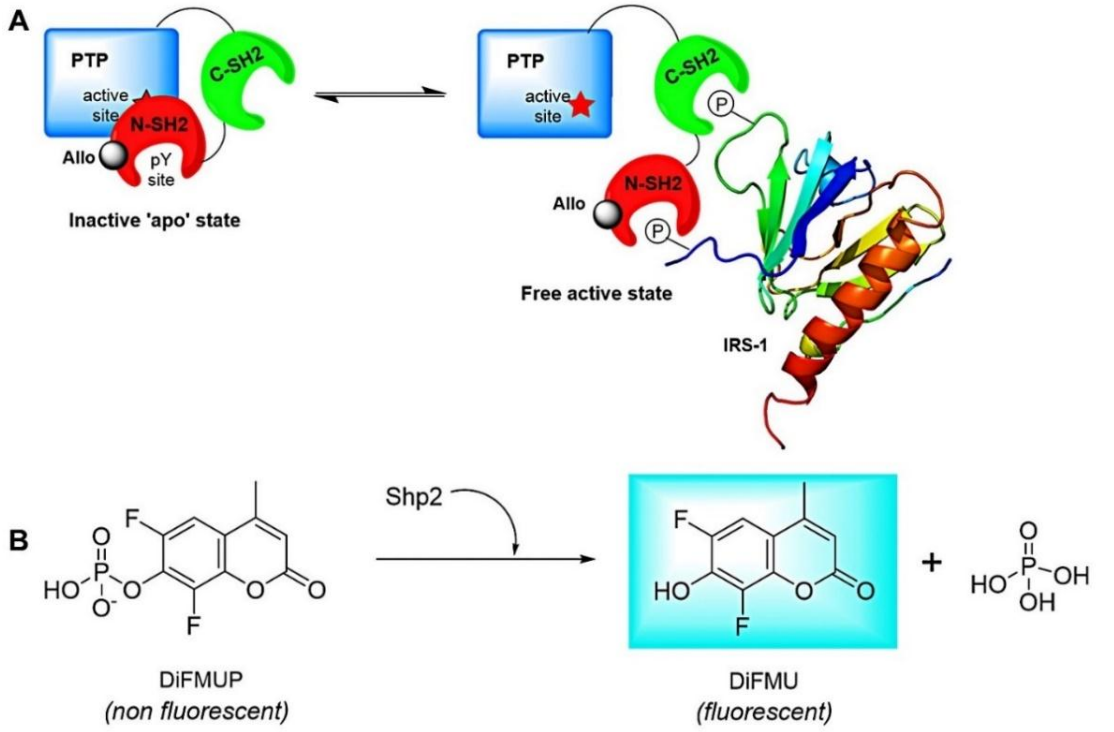

Figure 2.4. A) Allosteric activation of SHP2 by binding to a bis-tyrosyl-phosphorylated peptide (IRS-1). B) Dephosphorylation of 6,8-difluoro-4-methylumbelliferyl phosphate (DiFMUP) to 6,8-difluoro-4-methylumbelliferone (DiFMU).

The biochemical *in vitro* assay to evaluate SHP2 inhibition activity of the compounds **111675** and **STT01-STT21** was done using a homogeneous full-length SHP-2 assay kit (Catalog No.: 79330), which was obtained from BPS Bioscience, San Diego, CA. The assay was performed in a 96-well, black, flat bottom, low-binding polystyrene plate (Genaxy Scientific, Catalog No.: GEN-0263) at room temperature as per the protocol mentioned for the kit. Each test compound was assayed in three concentrations viz. 10 µM, 1 µM and 0.1 µM (prepared in 60 mM HEPES buffer, pH 7.2) in duplicate. The final reaction volume per well was 100 µL. SHP2 enzyme was allosterically activated prior to the assay by the addition of the bis-tyrosyl-phosphorylated IRS-1 protein (IRS1_pY1172(dPEG8)pY1222 (Sequence: H_2N-LN(pY)IDLDLV(dPEG8)LST(pY)

ASINFQK-amide) wherein 0.2 ng/µL of SHP2 was incubated with 0.5 µM of IRS-1 for an hour (**Figure 2.4**). Upon addition of the surrogate fluorogenic substrate, 1 mM DiFMUP (at a final concentration of 10 µM per well), its dephosphorylation to DiFMU was measured [123] fluorometrically with a multimode plate reader (BioTek Cytation 5 Imaging Reader, Agilent Technologies) at excitation wavelength of 360 nm and emission wavelength of 460 nm. Two independent experiments were conducted and the IC_{50} value was calculated using GraphPad Prism 8.0.1 software as a mean of both the experiments along with the standard error of mean (SEM). The % inhibition and dose-response curve were calculated using control-based normalization for both the experiments.

Subsequently, the mechanism of inhibition of fl-SHP2 by lead compound of this series was determined by an enzyme kinetics study where three fixed concentrations of the compound (1.0, 0.5 and 0.1 µM), pre-incubated with fl-SHP2 (at 2 ng/µL final concentration) were incubated with five different concentrations of the substrate i.e., DiFMUP (0.25, 0.5, 1.0, 1.5 and 2.0 µM) at ambient temperature for an hour in presence of DTT (500 µM) and fluorescence measured with a multimode plate reader (BioTek Cytation 5 Imaging Reader, Agilent Technologies) at excitation wavelength of 360 nm and emission wavelength of 460 nm. No inhibitor was added in the control wells. All assays were done in duplicate in 60 mM HEPES buffer, pH 7.2 in 96-well plates. Based on the mean fluorescence values, the non-linear plot of [S] vs. [V] through Michaelis-Menten kinetics and a double-reciprocal plot of 1/[S] vs. 1/[V] through Lineweaver Burk method were done for each inhibitor concentration.

2.2.3.2. *In vitro* DPPH assay for antioxidant property evaluation

The antioxidant and free radical scavenging potential of few potent SHP2 inhibitory compounds of this series was estimated using the well-established DPPH assay [124] with slight modification. DPPH (2,2-diphenyl-1-picrylhydrazyl hydrate, TCI, cat no. D4313) is reduced in the assay conditions to diphenyl picryl hydrazine (DPPHH) by a free-radical scavenging (FRS) antioxidant thereby changing the color from deep purple (DPPH) to pale yellow (DPPHH), due to the lower amount of hydrogen and this is measured at 510-530 nm [125]. Briefly, five different concentrations (10, 20, 40, 80 and 160 μM) of each test compound and ascorbic acid (as the negative control) were prepared in HPLC grade methanol and 75 μL of each was added to a 96-well plate followed by 75 μL of methanolic DPPH solution (at a final concentration of 100 μM per well). Upon incubation for 20-30 min, the absorbance of the plate was read in a multimode plate reader (BioTek Cytation 5 Imaging Reader, Agilent Technologies) at 520 nm. Each compound was assayed in triplicate in two independent experiments and the IC_{50} value was calculated using GraphPad Prism 8.0.1 software as a mean of both the experiments along with the standard error of mean (SEM). Control-based normalization was done to calculate the percent free-radical scavenging activity of each tested compound using the following formula:

$$\% \text{ FRS} = [(\text{Absorbance}_{\text{control}} - \text{Absorbance}_{\text{test}}) / \text{Absorbance}_{\text{control}}] \times 100$$

2.2.3.3. *In vitro* blood-brain barrier permeability assay (PAMPA-BBB) of compound STT13

Compound **STT13** was evaluated for its *in vitro* blood-brain barrier permeability to assess its potential to pass the brain. This was done by a parallel artificial membrane permeability assay (PAMPA) by the following protocol [126]. In separate centrifuge

tubes, 1000 μL of 500 μM compound **STT13** was prepared by mixing 50 μL of 10 mM of the compound in DMSO with 950 μL 1N PBS. For the permeability controls, 500 μM of each was prepared. In separate tubes, 200 μM equilibrium standards for compound **STT13** and control were prepared followed by preparation of the blank control by mixing 5 μL DMSO with 245 μL 1N PBS. 200 μL 1N PBS was added to wells in the acceptor plate and with the acceptor plate still in its tray, 5 μL of 20 mg/mL porcine brain lipid (CAS No.: 86088-88-2, Brain Polar Lipid Extract (Porcine), Avanti Polar Lipids, Inc., Cat: 141101P-100MG) was added in dodecane directly to the well membranes of the acceptor plate. Next, 300 μL of 500 μM compound **STT13** and 500 μM permeability controls were added to duplicate wells of the donor plate. The acceptor plates were carefully placed into the donor plate wells and incubated at RT or 37°C for 18 h or the desired incubation time period (e.g.16 – 24 h). The donor plates were carefully removed and the liquid in acceptor plate i.e., the acceptor solution was collected for analysis. 100 μL each of acceptor solution and equilibrium standard for compound **STT13** and all permeability controls were added to separate wells of a 96-well plate (Cat # 980040) along with 100 μL blank control to designated wells. Absorbance spectrum was read from 200 nm to 500 nm in 10 nm intervals to determine peak absorbance of test compound **STT13**.

Using the determined peak absorbance for the test compound and permeability controls, the permeability rate (P_e) was determined using the following calculation:

$$P_e = \mathrm{C} \times -ln\left(1 - \frac{ODA}{ODe}\right) \text{ cm/s}$$

Where ODA is the absorbance of acceptor solution minus blank, ODE is the absorbance of the equilibrium standard minus blank, and, using an 18 h incubation, $C = 7.72 \times 10^{-6}$.

2.2.3.4. Cell-based assays

2.2.3.4.1. Cell conditioning and culture

MCF-7 breast cancer cell lines, PC12 rat pheochromocytoma neural cell lines, U87MG human glioblastoma cell lines and human neuroblastoma SH-SY5Y cells were procured from the National Centre for Cell Science (NCCS), Pune, India. MCF-7, U87MG and SH-SY5Y cells were cultured in 96-well plates for 24 h in DMEM (Dulbecco's Modified Eagle's Medium, Himedia, cat no. AL007A-500ML), supplemented with 10% FBS (Fetal Bovine Serum, Himedia, cat no. RM 10432) and 1% Pen-Strep anti-biotic anti- mitotic solution (Himedia, Mumbai, India), at 5% CO_2, 95% humidity and 37°C. PC12 cells were cultured in 96-well plate for 24 h in Ham's F12k medium (Nutrient Mixture F-12 Ham, Kaighn's Modification, Himedia, cat no. AL-106-500ML) supplemented with 10% FBS (Fetal Bovine Serum, Himedia, cat no. RM 10432) and 1% antibiotic solution at 37°C with 95% humidity and 5% CO_2. MTT (3-(4,5-dimethyl-2-thiazolyl)-2,5-diphenyl-2*H*-tetrazolium bromide, Himedia, cat no. MB186-100MG) was used in a final concentration of 0.5 mg/mL.

2.2.3.4.2. *In vitro* antiproliferation study in cancer cell lines

The *in vitro* anticancer efficacy of those compounds that displayed submicromolar SHP2 inhibitory activity ($IC_{50} < 1.0$ μM) (compounds **STT05, STT06, STT11, STT13, STT14, STT17, STT20, STT21**) was assessed by an MTT assay on MCF-7 cells. Briefly, MCF-7 cells were seeded in 96-well plates at a density of 10000 cells per well and incubated overnight. After incubation, the media was aspirated and fresh media was added, supplemented with different concentrations (30 – 90 μM) of test compounds in triplicate for 24 h. After the completion of the treatment, 100 μL MTT supplemented culture media (final concentration of MTT = 0.5 mg/mL) was added and incubated for

3 h. After the incubation, the media was aspirated, and 100 µL of molecular grade dimethyl sulfoxide (SRL, cat no. 67685) was added to dissolve the insoluble formazan crystals formed, and the optical density was observed in an ELISA plate reader (iMark, Biorad, USA) at 570 nm.

Furthermore, antiproliferation effect of lead compound **STT13** against PC12, U87MG and SH-SY5Y cell lines (procured from NCCS, Pune) was determined by MTT assay in a similar protocol. Upon culture of cells (10000 cells/well for PC12, 5000 to 8000 cells/ well for U87MG) they were treated with different concentrations (0, 1, 10, 50, 100, 250, 500, 1000 µM) of the test compound in quadruplicates. After incubation for 24 h, MTT solution (5 mg/mL) was added to the cultured and treated cells and further incubated for 2 h. At the end of the experiment, culture supernatant was removed and cell layer matrix was dissolved in 100 µL of molecular grade dimethyl sulfoxide (SRL, cat no. 67685) and read in an ELISA plate reader (iMark, Biorad, USA) at 540 nm and 660 nm. IC_{50} was calculated using GraphPad Prism 8.0.1. Images were captured in grey mode under inverted microscope (Olympus ek2 or Dewinter Victory Plus) using AmScope digital 10 MP Aptima CMOS Camera. Percent cell viability was calculated by using the below formula: % cell viability = $(Absorbance_{sample} / Absorbance_{control}) \times 100$

2.2.3.4.3. Colony formation and scratch wound-healing assay of compound STT13

An investigation of colony development of MCF-7 cells was conducted upon treatment with test compound **STT13**. This assay for *in vitro* cancer cell survival is predicated on the ability of a single cell to proliferate into colonies [127]. Briefly, the MCF-7 cell lines were seeded in 35 mm petri dishes at 2-50 cells per petri dish and incubated

overnight. After that, treatment with compound **STT13** (equivalent to 5 μM concentration) and docetaxel as the standard, was provided and further incubated for 24 h. Then, the media was removed, followed by addition of fresh media, which was changed every day for 7 days. After 7 days, the media was removed and washed with PBS, followed by staining the colonies with 0.5% crystal violet solution. The colonies were subsequently calculated manually by using the following formula: % colony forming = (no. of colonies in the treated petri dish / no. of colonies in the control petri dish) × 100

The scratch wound healing assay [128] was performed to study effect of test compound **STT13** on breast cancer cell migration. MCF-7 cells were seeded and cultured in growth medium until confluence, in 24-well tissue culture plates. The cellular monolayer was scratched and wounded using a sterile 200-μL pipette tip and then rinsed with complete medium. Each well was treated with the test compound **STT13** and reference drug docetaxel. Light microscopy was used to track the wound regions (cell-free areas) at 0 h and 24 h time period at 4x magnification. Microphotographs were obtained at each time point, and Image J software was used to determine the wound areas in each picture quantitatively. The below formula was used to calculate the percent wound closure: [(wound area at 0 h – wound area after 24 h)/wound area at 0 h] × 100

2.2.3.4.4. Annexin binding assay for detection of cellular apoptosis

U87MG cell lines (procured from NCCS, Pune) were cultured and treated with the IC_{50} dose of compound **STT13**. After treatment, cells were washed twice with cold PBS and then resuspended in 1X binding buffer at a concentration of 1×10^6 cells/mL. The cells were divided into groups of unstained cells, control, annexin only, propidium iodide

(PI) only and drug treatment. Annexin V-FITC (1 mL) (Thermo-Fisher Scientific, Invitrogen™, cat no. BMS306FI-20) and PI (at a final concentration of 1.0 μg/mL) (Thermo-Fisher Scientific, Invitrogen™, cat no. P1304MP) were added to respective labeled tubes. After vortexing and incubating for 15 min at room temperature in the dark, 1X Binding buffer was added to each tube and analyzed by Flow Cytometer (BD FACS Lyric™) within 1 h at 488 nm excitation. Green annexin V fluorescence was measured at 530 ± 20 nm and red PI fluorescence was measured above 600 nm by setting gates based on light scatter [129, 130].

2.2.3.4.5. Cell cycle analysis by flow cytometry

U87MG cells were plated and treated with IC_{50} dose of compound **STT13** for 24 h. After incubation period, cells were harvested using trypsin and collected in 1.5 mL tube and washed once with 500 μL chilled PBS. Approx 1×10^6 cells were suspended in 100 μL of PBS, and vortexed gently to obtain a mono-dispersed cell suspension, with minimal cell aggregation. Cells were then fixed by transferring this suspension, with a pipette, into centrifuge tubes containing 900 μL of 70% ethanol on ice and incubated for at least 2 h at 4°C. After fixation, cells were centrifuged and the resultant pellet was suspended in 500 μL of PI staining solution (0.1% v/v Triton X-100, 10 μg/mL PI and 100 μg/mL DNase-free RNase A in PBS) and kept in the dark at room temperature for 30 min, or at 37°C for 10 min. Samples were then acquired on a flow cytometer and cell fluorescence was measured. The maximum excitation of PI bound to DNA is seen at 536 nm, and emission is at 617 nm. Here, emission was measured using the long-pass 600- or 610-nm filter [131].

2.2.3.4.6. Reactive oxygen species (ROS) estimation by flow cytometry

U87MG cells were plated in 6 well plates at a density of 5000 to 10000 cells/well in 1 mL DMEM supplemented with 10% FBS and 1% antibiotic solution and incubated for 24 h at 37°C & 5% CO_2. Cells without treatment were considered as control. After incubation, the old medium was removed and fresh culture medium was added before treatment. Then cells were treated at the IC_{50} dose of compound **STT13** and further incubated for 24 h. After incubation, medium was removed, and cells were harvested with trypsin-EDTA and collected in 1.5 mL tubes and washed once with 500 µL chilled PBS buffer. Finally, cell pellets were dispensed in 100 µL PBS with 2 µM H_2DCFDA (Thermo-Fisher Scientific, Invitrogen™, cat no. D-399) stain and the samples acquired in Flow Cytometer (BD FACS Calibur, USA) within 1 h. The redox state of the sample was measured by detecting the increase in fluorescence at 530 nm when the sample was excited at 485 nm. Acquired data were analyzed by using Flowing software version 2.5.1.

2.2.3.4.7. Mitochondrial membrane potential (MMP) estimation by flow cytometry

U87MG cells were cultured and treated with IC_{50} dose of compound **STT13** and incubated for 24 h. After incubation, medium was removed and cells were harvested with trypsin-EDTA and collected in 1.5 mL tube and washed once with 500 µL chilled PBS buffer. Finally, the cell pellet was dispensed in 400 µL JC-1 staining buffer with 2 µM JC-1 dye (Thermo-Fisher Scientific, Invitrogen™, cat no. T3168) and the samples were acquired in Flow Cytometer (BD FACS Canto II) within 1 h.

2.2.3.5. *In vivo* studies

2.2.3.5.1. *In vivo* acute oral toxicity evaluation of compound STT13

All animal experimentations were conducted in accordance with Committee for Control and Supervision of Experiments on Animals (CCSEA) Guideline vide Institutional Registration Number: 2123/GO/Re/S/21/CPCSEA. The experimental protocols were approved by the Institutional Animals Ethics Committee (IAEC) of Indian Institute of Technology (Banaras Hindu University), Varanasi, India (IAEC Approval Number: IIT(BHU)/IAEC/2024/I/039). Adult female Wistar rats (8-10 week old) weighing 130 ± 8 g were acquired from the Institutional Animal House, IMS-BHU, Varanasi, India and acclimatized for a week in a controlled environment (22 ± 1 ºC, 45-55% RH, 12/12h light/ dark cycle) with food and water *ad libitum*.

The *in vivo* acute oral toxicity of compound **STT13** was performed on adult female Wistar rats in accordance with the OECD Guideline 423 (Acute Toxic Class Method) [132] to determine the median lethal dose i.e., LD_{50} of compound **STT13**. The animals were randomly divided into two groups viz. vehicle control (Group C) and 2000 mg/kg body weight (BW) (Group A) dose with 6 animals in each group (i.e., n = 6). A starting dose of 2000 mg/kg BW of the animals was selected due to the fact that the toxicity profile of our test compound was hitherto unknown. Compound **STT13** was suspended in 0.5% aqueous sodium carboxy methyl cellulose (NaCMC) solution in appropriate dosing calculations and administered in a single dose by oral gavage to relevant groups of mice that were fasted for 2-3 h prior to dosing. Vehicle control groups received 0.5% aqueous NaCMC solution. Each dose volume was not more than 1 mL. All the animals were observed individually for any changes in vital signs and external signs of toxicity in the first 4 h post-dosing and then once every 24 h for 14 days. Various signs of

toxicity like changes in the skin, fur, eyes, and mucous membranes were observed. Additionally, the rats were also monitored for any signs of tremor, convulsions, salivation, lethargy, diarrhoea, sleep, and comatose conditions. Individual body weight of each animal and food intake (in grams of food) was taken prior to dosing and then again on the 7th and 14th day prior to sacrifice and any change whatsoever was noted. On the 14th day, all animals were humanely sacrificed by first, anaesthetizing the animals with 3% v/v isoflurane inhalation (Cat: R620 veterinary anaesthesia machine, RWD life science, San Diego, USA) and then decapitating them. Blood from each animal was collected immediately into two separate vials, one containing an anticoagulant (EDTA) for whole blood analysis (CBC) and another containing a clot activator for biochemical analysis of serum. The following parameters were tested in all groups for CBC examination; hemoglobin, red blood cell count (RBC), hematocrit (HCT), mean corpuscular hemoglobin (MCH), mean corpuscular volume (MCV), mean corpuscular hemoglobin concentration (MCHC), red blood cell distribution width (RDW), platelet count and white blood cell count (WBC). The parameters tested for the biochemical examination of blood for the assessment of hepatotoxicity of all test and control groups were creatinine, alkaline phosphatase (ALP), aspartate aminotransferase (AST) and alanine aminotransferase (ALT). Five organs namely, brain, heart, spleen, liver and kidneys were taken out, weighed individually for each animal and their histopathological study was done to assess any toxicity of the test compound on the tissues of these organs. Organ coefficient of all the organs mentioned above was calculated using the formula: organ coefficient = [weight of the organ (g) / total body weight (g)] × 100 and compared with the vehicle control group. Histopathological study of the perfused organs was done by fixing the harvested organs in 1X PBS solution

containing 5-10% formalin, histological sections were taken from each organ, fixed on a slide, stained with hematoxylin and eosin (H&E) stain and finally, visualized under a microscope and photomicrographs were taken.

2.2.3.5.2. *In vivo* pharmacokinetic studies of compound STT13 in female Wistar rats

A. Calibration curve and linearity in plasma spiked samples

The standard calibration curve of compound **STT13** in plasma spiked samples (plasma obtained from female Wistar rats) was obtained by preparing serial dilutions (viz. 50, 25, 12.5, 6.25, 3.125 and 1.5625 μM) of the test compound **STT13** in plasma (as shown in the table below).

Plasma volume (μL)	STT13 Dilutions (mM)	STT13 volume added (μL)	ACN volume make-up (μL)	Final volume (μL)	Final conc. of STT13 (μM)
100	5	10	890	1000	50
100	2.5	10	890	1000	25
100	1.25	10	890	1000	12.5
100	0.625	10	890	1000	6.25
100	0.3125	10	890	1000	3.125
100	0.15625	10	890	1000	1.5625

Blank sample = 100 μL plasma + 10 μL DMSO + 890 μL ACN

A plot of the AUC obtained in each chromatogram vs. the corresponding concentration of the sample gave a straight line which was the calibration curve. Upon addition of ACN, there will be immediate precipitation of plasma proteins. At this stage, each sample was vortexed for 2-3 mins at 3000 rpm and kept the samples standing for 15 min post-vortexing. Each sample was centrifuged at not less than 6000 rpm for 20 min at 4ºC. The supernatant was collected in HPLC vials after filtering through 0.22 μ filter and HPLC run at the developed and validated method for compound **STT13** i.e., solvent

system: 100% ACN, injection volume: 20 μL, total run time: 10 min, flow rate: 0.7 mL/min, detection signals: 290, 295, 300, 310 nm [133].

The peak AUC of each dilution plotted against the corresponding concentration as a linear function gave a calibration curve which was used to calculate the average regression equation and correlation coefficient by the appropriate linear least-squares regression analysis. The calibration curve and the resultant regression statistics of the developed process were then utilized to determine the PK parameters of compound **STT13** upon administration to a living system like rats.

B. Plasma stability assay of compound STT13

The stability of compound **STT13** in rat plasma was determined by incubating a specific concentration of the compound in plasma for different time periods e.g., 0, 10, 20, 30, 60, 120 min in separate Eppendorf tubes [134]. After the appropriate incubation time, plasma proteins were precipitated from each time-point sample by the addition of ACN. The samples were centrifuged at 6000 rpm or more for 20 min and depletion of test compound was monitored using RP-HPLC by applying the std calibration curve. Compound depletion was monitored by determining the AUC of the respective sample in the HPLC run using the previously validated method. A calibration curve was devised from the concentration vs. AUC obtained from the depletion data. The *in vitro* plasma half-life of the compound ($T_{1/2}$) was calculated from the slope of the curve by the following formula: $T_{1/2}$ (min) = $\frac{ln(2)}{-slope}$

C. *In vivo* pharmacokinetic profiling of compound STT13

Healthy female Wistar rats (160-170 g, n = 4) were used for the estimation of pharmacokinetic parameters of compound **STT13**. Food was withheld from the animals

12-16 h prior to the experiments (water given *ad lib*). The test compound **STT13** was administered orally at a dose of 10 mg/kg BW to each animal as an aqueous suspension in 0.5% NaCMC. At pre-determined time points (viz. 0, 0.5, 1, 2, 4, 8, 12 and 24 h), blood samples were drawn out from the retro-orbital plexus of an anesthetized animal (around 300 μL) in vials pre-treated with Na-heparin to prevent coagulation. The blood samples were centrifuged at not less than 7000 rpm for 6 min at 4ºC to separate plasma. 100 μL of the plasma supernatant was mixed with 400 μL of ACN (the mobile phase, in this case) to precipitate the plasma proteins and extract the compound. The mixture was again centrifuged at not less than 7000 rpm for 10 min at 4ºC to separate the organic layer. The supernatant was collected and filtered through 0.22 μ filter and collected in respective HPLC vials. An Infinity II 1260 High-Performance Liquid Chromatography system (Agilent, USA) was used for the HPLC analysis where 20 μL of each sample was injected using 100% acetonitrile as the mobile phase at a flow rate of 0.7 mL/min. The total run time was kept at 10 min through a Shodex C18-4E column (250 mm x 4.6 mm, 5 μm, 100 Å) and detection at 315 nm was done with a 1260 Infinity II DAD WR 120-Hz detector.

Further, from the plasma concentration (Cp) vs. time data, the PK parameters were calculated by extravascular non-compartment model using PKSolver add-in feature of MS Excel (downloaded from https://www.jasonsumma.com/s/PKSolver-for-Microsoft-Excel.zip, accessed on 20th August, 2024) [135].

2.2.4. Computational studies

A Hewlett-Packard Z230 Tower workstation Intel® Xeon® CPU E3-1240 v3at 3.40 GHz processor, RAM 12.0 GB running on Windows 7 Professional 64-bit operating system

was used for most of the computational processes including molecular docking. All skeletal formulae of compounds are rendered in 'ACS Document 1996' setting in ChemDraw® Professional v15.0.0.106. AutoDockTools 4.2 was obtained from http://www.scripps.edu. Discovery Studio Visualizer v21.1.0.20298 and PyMOL 1.3 were obtained from http://www.accelrys.com and http://www.pymol.org, respectively. The *in silico* ADMET prediction was performed using the Pre-ADMET online server (https://preadmet.webservice.bmdrc.org/).

2.2.4.1. Molecular docking studies

The molecular docking study of synthesized compounds (**STT01-STT21**) was done by AutoDockTools 4.2 with SHP2 (PDB ID: 5EHR) in its tunnel allosteric site. The 3D X-ray crystalline structure of SHP2 co-crystallized with allosteric inhibitor **SHP099** (ligand PDB ID: 5OD) at a resolution of 1.70 Å was acquired from Protein Data Bank (https://www.rcsb.org/structure/5EHR) having PDB ID: 5EHR. Next, the protein was prepared by adding polar hydrogen atoms and Gasteiger charges to the 3D receptor structure and all the protein atoms were assigned AD4 type of AutoDock atoms and the protein was saved in .pdbqt format (charge containing PDB file). The skeletal formula of each compound (i.e., the 'ligand') was drawn in ChemDraw Professional 15.0.0.106, imported to Chem3D to generate the corresponding 3D structure, MMFF94 energy minimization was performed on each ligand and saved in .pdb format. Next, the individual 'prepared' ligands were loaded in the ADT workspace, the torsion roots were detected and duly assigned and the molecules were saved as .pdbqt files. The pdbqt file of protein was then loaded and utilized to generate the grid parameter file (.gpf) and a grid box by setting appropriate grid coordinates from the location and orientation of co-crystallized ligand of 5EHR. Finally, the docking parameter file (.dpf) was generated

with the macromolecule and ligand pdbqt files where Genetic Algorithm was used as search parameter and the default docking parameters were left unchanged. Autogrid4.exe was used to calculate grid parameter while autodock4.exe was utilized for docking calculation. The docking results were processed and binding energy (ΔG kcal/mol) and inhibition constant (K_i) were noted for top conformer of each ligand and the docked complex was saved as .pdbqt and .pdb file. Additionally, the PDB file of top conformer of each complex was visualized in Discovery Studio Visualizer v21.1.0.20298 to get the 2D interaction and 3D orientation of the ligand with protein at the docked site.

2.2.4.2. Molecular dynamics simulation studies

Molecular dynamics simulation was performed on compound **STT13** using Desmond module (Schrodinger Release 2021.1). The docked 5EHR-**STT13** complex was placed in a cubic box of 1000 $Å^3$ dimension and solvated by the TIP3P water model. The entire system was optimized with OPLS-2005 force field and the charged system was neutralized by adding counterions. Then, the simulation run was initiated on the complex for 100 ns at 300 K temperature with Brownian Dynamics NVT simulation. Throughout the simulation at different time interval of 100 ps, check points and energy data were recorded. The Maestro graphical user interface (Maestro, Schrodinger, LLC, New York, NY, 2021) was used for the preparation of input files as well as analysis and visualization of the results.

2.2.4.3. Prediction of ADMET properties

The ADMETox properties of the final compounds **STT01-STT21** were predicted by Pre-ADMET online server (https://preadmet.webservice.bmdrc.org/, accessed on 23rd

November 2022) where each molecule was loaded as a .mol text. The conversion from .sdf or .cdx to .mol was done in ChemDraw® Professional v15.0.0.106. Once loaded in the input page of the server, the ADME properties were calculated for the following parameters: human intestinal absorption (HIA), *In-vitro* Caco2 cell permeability, Madin-Darby canine kidney (MDCK) cell permeability, skin permeability, blood brain barrier (BBB) permeability (C_{brain}/C_{blood}) and *in-vitro* plasma protein binding (PPB). Also, the compound's activity towards the important drug metabolizing cytochrome enzymes CYP2C9, CYP2C19 and CYP3A4 was predicted. In an entirely similar protocol, the toxicity data was generated for the 21 compounds by assessing parameters like Ames test for mutagenicity in *Salmonella typhimurium*, 2 year duration carcinogenicity bioassay in mouse, 2 year duration carcinogenicity bioassay in rat and *in-vitro* Human Ether-a-go-go Related Gene channel inhibition (hERG inhibition).

2.2.4.4. Prediction of pharmacokinetic (PK) parameters

Few important PK and bioavailability parameters of our lead compound **STT13** were predicted using Deep-PK, a robust machine learning method based on diverse molecular descriptors and graph neural networks developed by the Biosig Lab at The University of Queensland, and accessible through the following web server, https://biosig.lab.uq.edu.au/deeppk/prediction, accessed on 10th June, 2024. The structure of compound **STT13** was imported into the predictor module in the form of the corresponding SMILES string generated by ChemDraw Professional 15.0.0.106, followed by the predictive calculations which were generated and reported. Some of the parameters were further calculated from the above predicted data using the Pharmacokinetic Simulator accessible via the following web-based server, http://www.vulpinescience.co.uk/uploads/MedChem%20Calculators_Ver3.2/

(accessed on 10th June, 2024), developed by Dr. David Fox of the Vulpine Science and Learning Limited, West Stourmouth, England, UK.

2.2.5. Statistical analysis

All assay values viz. IC_{50}, GI_{50} and % FRS values furnished in this report are the mean of 2-3 independent experiments (n = 2/3) along with ± standard error of mean (SEM). Wherever applicable, comparison between different group means was done by a one-way analysis of variance (ANOVA) with an unpaired t-test in GraphPad Prism 8.0.1 software. Statistical significance was found to be $p<0.05$ versus the corresponding IC_{50} values obtained against the enzyme. In case of cell-based assays, the P-value was at $p < 0.0001$ indicating statistical significance.

2.3. Results and discussion

2.3.1. Pharmacophore-based virtual screening (PBVS) studies

The co-crystallized ligand **SHP099** (ligand PDB ID: 5OD) of SHP2 (5EHR) consists of three rings viz. one aryl ring, one heteroaromatic ring containing two nitrogen atoms and a carbocyclic ring containing a heteroatom. It also contains two primary amine groups one joined to the central heteroaromatic ring and the other joined to the carbocycle *via* tetrahedral carbon.

The identified pharmacophoric features (**Figure 2.5**) include: two primary amine groups (hydrogen bond donors, F1 & F2), two heteroaromatic ring nitrogen (hydrogen bond acceptors, F3 & F4), two aromatic rings (F5 & F6) and finally three features containing secondary donor function (F7, F8 & F9).

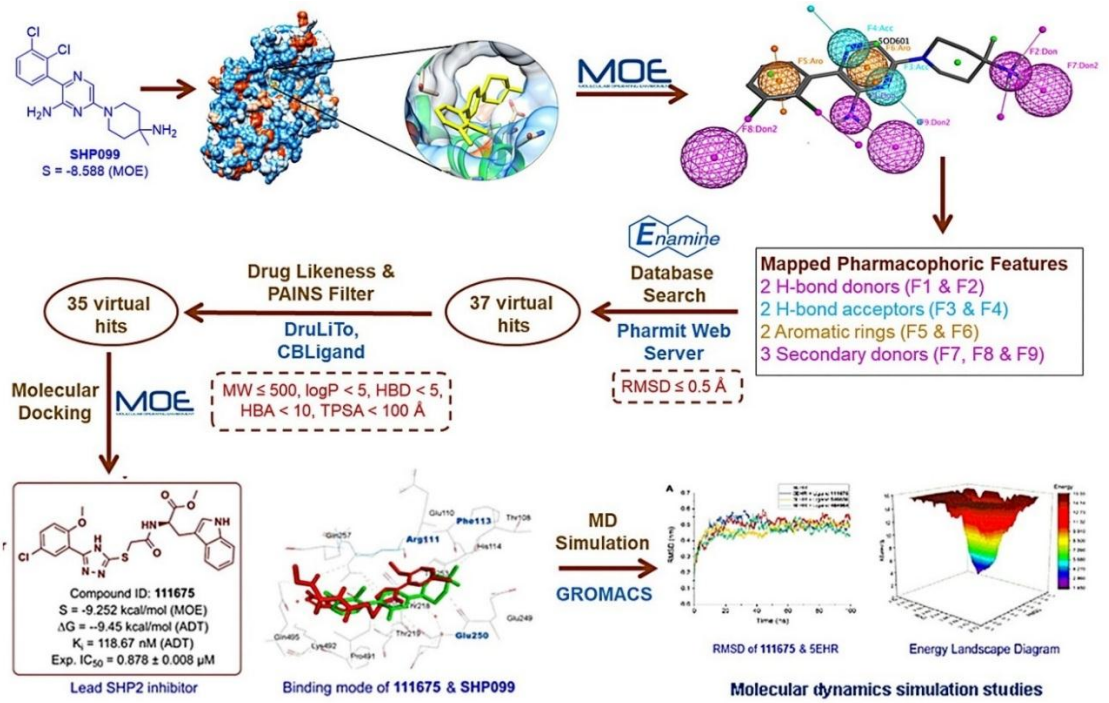

Figure 2.5. Results of pharmacophore-based virtual screening

The pharmacophore query generated using MOE having above discussed features was utilized to screen the Enamine^{TM} Advanced Database through Pharmit web server. The screening search resulted in 37 hits with RMSD ≤ 0.5 which were selected and saved as a structure data file (.sdf) format. The obtained hits belong to several chemical classes namely: triazole (17 hits), quinazoline (9 hits), triazine (4 hits), oxadiazole (4 hits) and pyrimidine (3 hits).

2.3.1.1. Identification of the virtual lead by rule-based screening, molecular docking and MD simulation

Further refinement of the 37 hits by rules-based filters for drug-likeness and PAINS screening gave 35 virtual hits whose molecular docking was done using MOE software. This populated all the ligands as per their binding affinity (S score) for evaluated and prepared SHP2 protein (5EHR). The S score of the 35 molecules ranged from −9.835 to −7.349 kcal/mol with the top 5 molecules **546656**, **80376**, **111675**, **153433** and

546602 having S score of −9.835, −9.655, −9.252, −9.212 and −9.173 kcal/mol, respectively. The next level screening of the 5 topmost ligands to arrive upon one (or two) virtually most active and all-round suitable molecule for SHP2 inhibition was done as per their predicted ADMET properties, toxicity profile and drug-like characteristics of the most and least active hits. The final predicted values for **111675** and **SHP099** are given in **Tables 2.1, 2.2** & **2.3** respectively.

Table 2.1. PreADMET predicted ADME properties of compounds **111675** and **SHP099**

Compd ID	MW	CLogP	HIA (%)	Caco2 (nm/s)	MDCK (nm/s)	SP ($logK_p$, cm/h)	BBB	PPB (%)	CYP2C9 inhibition	CYP2C19 inhibition	CYP3A4 inhibition
111675	499.97	2.86	88.39	8.389	0.090	-4.18	0.223	98.25	Inhibitor	Non-inhibitor	inhibitor
SHP099[#]	352.26	2.95	95.48	20.885	0.170	-3.03	0.039	63.34	Non-Inhibitor	Non-inhibitor	Non-Inhibitor

HIA: Human Intestinal Absorption [0–20 (poor), 20–70 (moderate), 70–100 (well)], Caco2: In-vitro Caco2 cell permeability [<4 (low), 4–70 (moderate), >70 (high)], MDCK: Maden Darby Canine Kidney cell permeability [<25 (low), 25–500 (moderate), >500 (high)], SP: Skin permeability, BBB: Blood brain barrier permeability (C_{brain}/C_{blood}), PPB: In-vitro plasma protein binding. [#]standard inhibitor

Table 2.2. PreADMET predicted toxicity parameters of compounds **111675** and **SHP099**

Compd ID	Ames test	Carcinogenicity (mouse)	Carcinogenicity (rat)	hERG inhibition
111675	Non-mutagen	Negative	Positive	High Risk
SHP099[#]	Mutagen	Positive	Negative	Medium Risk

Ames test-Ames test for mutagenicity in *Salmonella typhimurium*, Carcinogenicity (Mouse)-2 years carcinogenicity bioassay in mouse, Carcinogenicity (Rat)-2 years carcinogenicity bioassay in rat, hERG Inhibition-In Vitro Human Ether-a-go-go Related Gene Channel Inhibition; *least active hit, #standard inhibitor

Table 2.3. Drug-likeness parameters of compounds **111675** and **SHP099**

Compd Code	MW	LogP	HBD	HBA	TPSA	nRB	nAtom	nAcidicGroup	RC	nRigidB	nAromRing	nHB
111675	499.97	3.220	0	9	102.62	11	34	0	4	26	4	9
SHP099	352.26	1.33	0	5	27.96	2	23	0	3	23	2	5

MW = Molecular Weight, HBD = Hydrogen bond donor, HBA = Hydrogen bond acceptor, TPSA = Topological polar surface area, MR = Molecular refractivity, nRB = No. of rotatable bonds, nAtom = No. of atoms, nAcidicGroup = No. of acidic group, RC = Ring count, nRigidB = No. of rigid bond, nAromRing = No. of aromatic ring, nHB = No. of hydrogen bond.

Table 2.4. Binding affinity (S score) from MOE, binding energy (ΔG) and inhibition constant (K_i) values from ADT for compounds **111675** and **SHP099**

Compd ID	Structure	MW	S (kcal/mol) (MOE)	ΔG (kcal/mol) (ADT)	Ki (μM) (ADT)
111675	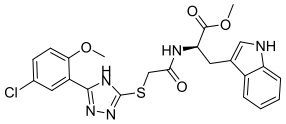	499.97	-9.25	-9.45	0.118
SHP099#	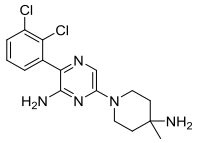	352.26	-8.59	-10.27	0.029

#standard inhibitor

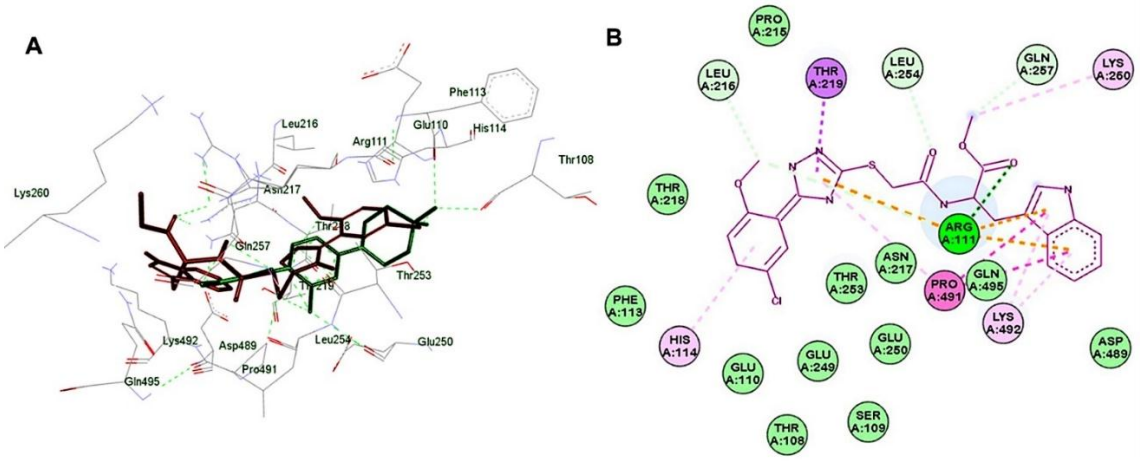

Figure 2.6. A) 3D binding mode of ligand **111675** (red) and **SHP099** (green). B) 2D interaction map of ligand **111675** within the active site of SHP2 (5EHR).

The subsequent molecular docking of the top ligand and comparison with **SHP099** gave us an idea about their probable inhibitory potential. The binding energy (ΔG) of the compounds **111675** and **SHP099** were −9.45 kcal/mol and −10.27 kcal/mol whereas the inhibition constant (Ki) for 5EHR were 0.118 μM and 0.029 μM respectively (**Table 2.4**). It can be mentioned here that the binding energy and the Ki data of both the reference and test compound are in good correlation with the in vitro SHP2 inhibition data (discussed in detail in **Section 2.3.3.1**) The 3D orientation and 2D interaction of compound **111675** in the tunnel allosteric site of SHP2 is shown in **Figure 2.6**. Based on molecular docking score and binding orientation, **111675** was further evaluated by

molecular dynamic simulation studies. It displayed well accommodated stabilization within the active site during simulation. Retention of crucial interactions (viz. conventional H-bonding, pi-cation interactions, pi-pi stacking, van Der Waals forces etc.) from molecular docking and formation of additional hydrophobic and hydrogen bonding interactions validated the binding of the ligand.

2.3.2. Chemistry

2.3.2.1. Synthesis of compound 111675 and designed final compounds STT01-STT21

The lead compound of our pharmacophore-based virtual screening of the Enamine Advanced Database i.e., **111675** was synthesized starting from the two key intermediates, **IM01** and **IM02** (**Scheme 1**) in good yield (~87%) by employing conventional synthetic methodologies. The synthesis process is shown in **Scheme 1**.

Further, the analogs **STT01-STT21** designed from the in house lead compound **111675** were synthesized by following multistep synthesis protocol as shown in **Scheme 2**. At first, five analogs each of the two key heterocyclic cores (**TRZ01-TRZ05** and **TDZ01-TDZ05**, respectively) were made from substituted aryl/heteroaryl carboxylic acids. The thiosemicarbazate salts of the substituted aryl/heteroaryl carboxylic acids were refluxed in an excess of caustic base followed by acidification to pH 5-6 to give the desired triazole-2-yl thiols (**TRZ01-TRZ05**). In a slightly modified protocol [136], the 1,3,4-thiadiazole-2-amines (**TDZ01-TDZ05**) were synthesized from their corresponding thiosemicarbazate salts by the reaction of $POCl_3$ followed by reflux in water and subsequent basification to pH 8 to close the ring. Reaction with chloroacetyl chloride afforded the acetamides **TDZA01-TDZA05** which were used in the next step without further characterization. Final compounds **STT01-STT21** were synthesized by the

reaction of **TDZA** fragments with **TRZ** fragments in DMF with potassium carbonate as the base [137].

2.3.2.2. Physicochemical characterization of final compounds

All the final compounds of **STT** series (**STT01-STT21**) were obtained in good yield ranging from 65-94 % as powdered solid. Physicochemical characteristics of the final compounds like melting point, ClogP and experimental logP (*n*-octanol/water) were determined and are given in **Table 2.5**. Most of the compounds possessed logP values near the acceptable range for an orally and intestinally bioavailable drug candidate i.e., from 1.35-1.80 with few of the most potent inhibitors exhibiting logP around 2 which is the acceptable value for a CNS-targeting drug molecule [138].

Table 2.5. Physicochemical characterization data of compounds **STT01-STT21**

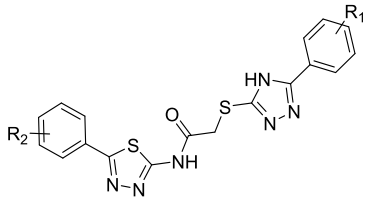

STT01-STT21

Compd Code	R_1	R_2	MW	ClogP[a]	LogP[b]	% yield	Melting range (ºC)	R_f[c]	Appearance
STT01	H	H	394.47	3.18	1.99	65	154-155	0.51	Brown solid
STT02	H	4-F	412.46	3.33	2.08	93	228-230	0.55	Tan solid
STT03	H	4-OCH_3	424.49	3.24	0.99	75	190-192	0.55	White solid
STT04	H	3,4-$(OCH_3)_2$	454.52	2.96	1.78	90	216-218	0.65	Pink solid
STT05	H	1,3-Dioxo	438.48	3.27	1.71	73	191-193	0.60	Brown solid
STT06	2-OCH_3	H	424.43	2.68	0.72	67	181-183	0.67	White solid
STT07	2-OCH_3	4-F	442.45	2.83	1.42	78	211-212	0.60	White solid
STT08	2-OCH_3	4-OCH_3	454.52	2.74	1.13	84	229-231	0.52	Grey solid
STT09	2-OCH_3	1,3-Dioxo	468.56	2.77	1.36	68	183-184	0.63	Grey solid
STT10	4-OCH_3	H	424.48	3.24	1.01	86	128-130	0.52	Tan solid
STT11	4-OCH_3	4-F	442.48	3.39	1.40	71	215-217	0.68	White solid
STT12	4-OCH_3	4-OCH_3	454.52	3.30	1.26	83	201-203	0.70	White solid
STT13	4-OCH_3	1,3-Dioxo	468.50	3.33	1.69	94	230-232	0.60	Grey solid
STT14	4-Cl	H	428.91	3.91	2.03	60	216-218	0.75	Grey solid
STT15	4-Cl	4-F	446.91	4.05	2.31	78	222-224	0.53	Tan solid
STT16	4-Cl	4-OCH_3	458.93	3.97	1.06	62	192-194	0.66	Pink solid

STT17	4-Cl	3,4-$(OCH_3)_2$	488.96	3.69	0.81	59	220-222	0.72	White solid
STT18	4-Cl	1,3-Dioxo	472.92	4.00	1.86	61	209-210	0.55	Grey solid
STT19	2,4-Cl_2	4-F	481.34	4.52	0.96	60	204-206	0.66	White solid
STT20	2,4-Cl_2	4-OCH_3	493.38	4.43	1.46	96	181-183	0.50	White solid
STT21	2,4-Cl_2	1,3-Dioxo	507.36	4.46	1.80	87	168-169	0.50	White solid

[a] Calculated using ChemDraw v15.0.0.106. [b] Experimental LogP data. [c] R_f values in 60% ethyl acetate in hexane.

2.3.2.3. Spectral characterization

All compounds were characterized by FTIR, ^1H, ^{13}C & ^{19}F NMR and HRMS analysis. The obtained spectral data of all synthesized compounds (presented below) are in good agreement with the predicted and/or calculated data, as applicable. The functional group present in the structure of each compound were confirmed by absorption of characteristic band in the specific region. The characteristic IR peaks of compounds are discussed in hereinafter. The residual solvent peak was observed at δ 2.50 ppm while peak due to moisture was observed near δ 3.35 ppm. For **IM01**, conversion of the amine functionality to the corresponding chloroacetamide was confirmed by the appearance of NMR signal of two protons at δ 4.01 ppm and a carbon signal at δ 42.44 ppm.

Methyl (2-chloroacetyl)-D-tryptophanate (**IM01**): ^1H NMR (500 MHz, $CDCl_3$) δ ppm 8.48 (s, 1H), 7.56 (d, *J* = 7.9 Hz, 1H), 7.36 (d, *J* = 8.1 Hz, 1H), 7.21 (t, *J* = 7.6 Hz, 1H), 7.15 (t, *J* = 7.4 Hz, 2H), 7.01 (s, 1H), 4.95 (s, 1H), 4.01 (s, 2H), 3.72 (s, 3H), 3.37 (s, 2H); ^{13}C NMR (126 MHz, $CDCl_3$) δ ppm 171.76, 166.02, 136.24, 127.43, 122.98, 122.31, 119.71, 118.45, 111.42, 109.39, 53.31, 52.56, 42.44, 27.53.

Formation of **IM02** was confirmed spectroscopically by appearance of two signals at δ 13.22 and δ 13.70 ppm corresponding to the -SH and -NH protons; also, appearance of two signals in CMR at δ 147.56 and δ 167.05 ppm corresponding to the 1,2,4-triazole ring carbons.

5-(5-Chloro-2-methoxyphenyl)-4*H*-1,2,4-triazole-3-thiol (**IM02**): ^{1}H NMR (500 MHz, DMSO-d_6) δ ppm 13.70 (s, 1H), 13.22 (s, 1H), 7.67 (d, *J* = 2.7 Hz, 1H), 7.56 (dd, *J* = 9.0, 2.7 Hz, 1H), 7.22 (d, *J* = 9.0 Hz, 1H), 3.87 (s, 3H); ^{13}C NMR (126 MHz, DMSO-d_6) δ ppm 167.05, 156.17, 147.56, 132.14, 128.90, 124.79, 116.51, 114.48, 56.62.

Condensation of **IM01** and **IM02** to form compound **111675** i.e., formation of the final compound was proven by the disappearance of -SH peak from the proton NMR spectrum and appearance of all peaks corresponding to **IM01**.

Methyl (2-((5-(5-chloro-2-methoxyphenyl)-4*H*-1,2,4-triazol-3-yl)thio)acetyl)-D-tryptophanate (**111675**): R_f = 0.52 at 0.5% MeOH in DCM; m.p.: 160-161 ºC; FTIR (*v*, cm^{-1}, KBr): 3282 (N-H str.), 1738 (ester C=O), 1660 (amide C=O), 1533 (1,3,4-triazole ring C-H str.), 824 (C-Cl str.), 743 (N-H str.); ^{1}H NMR (500 MHz, DMSO-d_6) δ ppm 13.90 (s, 1H), 10.94 (s, 1H), 8.73 (d, *J* = 7.5Hz, 1H), 8.01 (d, *J* = 2.8Hz, 1H), 7.52 (dd, *J* = 8.9, 2.8Hz, 1H), 7.46 (d, *J* = 7.8Hz, 1H), 7.33 (d, *J* = 8.1Hz, 1H), 7.24 (d, *J* = 8.9Hz, 1H), 7.14 (d, *J* = 2.4Hz, 1H), 7.05 (t, *J* = 7.5Hz, 1H), 6.97 (t, *J* = 7.4Hz, 1H), 4.54 (q, *J* = 7.1Hz, 1H), 3.95 (s, 3H), 3.94 (s, 2H), 3.55 (s, 3H), 3.19−3.05 (m, 2H); ^{13}C NMR (126 MHz, DMSO-d_6) δ ppm 172.46, 168.05, 155.79, 136.55, 131.46, 128.64, 127.51, 124.99, 124.21, 121.40, 118.86, 118.37, 114.44, 111.92, 109.52, 56.57, 53.98, 52.29, 36.26, 27.68; HRMS calcd for $C_{23}H_{22}ClN_5O_4S$ $[M+H]^+$ 500.1159, found 500.1159.

Ring closing of the carboxylic acid group to form the 1,2,4-triazole-3-thiol system in fragments **TRZ01-TRZ05** was confirmed by appearance of two signals near *δ* 13.50 and *δ* 13.70 ppm corresponding to the -SH and -NH protons; also, appearance of two

signals in CMR near δ 148 and δ 166 ppm corresponding to the 1,2,4-triazole ring carbons. Similarly, formation of fragments **TDZ01-TDZ05** from substituted benzoic acids resulted in signal near δ 160 and δ 169 ppm due to the 1,3,4-thiadiazole ring. The signal due to terminal -NH group of fragments **TDZ01-TDZ05** which was observed near δ 14 ppm disappeared in the NMR spectrum of fragments **TDZA01-TDZA05** that indicates the formation of chloro-acetamides from amine fragments. The signal due to terminal SH group that was observed near δ 14 ppm in fragments **TRZ01-TRZ05** disappeared in the NMR spectrum of final compounds that indicates the formation of thioacetamides (**STT01-STT21**) from the thiol fragments and chloroacetamide fragments. The synthesis of thioacetamides was further confirmed by FTIR spectroscopy where str. vibrations were observed at ν 3400-3300 cm^{-1} due to NH bond in final compounds. Further, the str. vibrations due to amide carbonyl appeared at ν 1700-1680 cm^{-1} while bend. due to -N-H was observed at ν 1590-1600 cm^{-1}. Individual substituents of the R_1 and R_2 groups were specifically confirmed by obtaining FTIR signals corresponding to the functional groups present. For instance, we obtained a peak at ν 1252 cm^{-1} for alkyl aryl ether C-O str. for compounds having R_1 and/or R_2 = 2/4-OCH_3 (e.g., **STT04, STT06, STT10** etc.) or R_2 = 1,3-dioxo (e.g., **STT05, STT10, STT15** etc.), a peak at ν 845 cm^{-1} for C-Cl str. for compounds having R_1 = 4-Cl and/or 2,4-Cl_2 (e.g., **STT14, STT15, STT19** etc.), and a peak at ν 1238 cm^{-1} of C-F str. (range ν 1400-1000 cm^{-1}) for compounds having R_2 = 4-F (e.g., **STT02, STT07, STT11** etc.).

In ^{1}H NMR spectra, the obtained proton signals were consistent with the general structure of the compounds. Peaks due to methylene protons of the thioacetamide linker [-S-C**H**$_2$-C(O)-] were observed at δ 4.25-4.01 ppm in ^{1}H NMR. The specific substitutions in the various homologues of the series were individually confirmed by

corresponding distinct signals obtained in ^{1}H and ^{13}C NMR. For instance, the R_1 substitutions were categorically confirmed by obtaining signals for 2-OCH_3 and 4-OCH_3 substitutions at δ 3.94 ppm (3 protons) and δ 3.80 ppm (3 protons). The R_2 substitutions i.e. 4-OCH_3, 3,4-$(OCH_3)_2$ and 1,3-dioxo were confirmed by obtaining signals at δ 3.80 ppm (3 protons), two signals at δ 3.85 and δ 3.81 ppm (3+3 protons) and δ 6.08 ppm (corresponding to the methylene protons of the 1,3,-dioxo ring) respectively. For the clusters of any one R_1 derivative and analogous R_2 substituent, e.g., **STT02** having R_1 = H and R_2 = 4-F, the presence of the individual substituents was confirmed by specific signals received for each set of protons or carbons as stated above. Also, the thioether carbon at the thioacetamide linker [-S-**C**H_2-C(O)-] was confirmed by a signal at δ 35.54-39.43 ppm. The fluorine-bearing intermediate (**TDZ02**) and analogues (**STT02, STT07, STT11** and **STT15**) were further analysed by ^{19}F NMR to confirm the presence of fluorobenzene moiety in the compounds. A single strong signal at around δ -110 ppm in all the compounds indicated the presence of the fluorine atom attached to an aryl ring (i.e., C_6H_5F) [139]. The obtained HRMS spectra of compounds **STT01-STT21** showed an accuracy of the range of 0.0000 ppm to 0.0010 ppm from calculated $(M+H)^+$ mass of the compounds. The obtained physicochemical and spectral data of intermediates and final compounds are summarized below.

5-Phenyl-4*H*-1,2,4-triazole-3-thiol (**TRZ01**): White solid; yield = 87%, ^{1}H NMR (500 MHz, DMSO-d_6) δ ppm 13.83 (s, 1H), 13.67 (s, 1H), 7.93 – 7.90 (m, 2H), 7.52 (dd, *J* = 5.0, 1.9 Hz, 3H); ^{13}C NMR (126 MHz, DMSO-d_6) δ ppm 167.52, 150.66, 131.07, 129.57, 126.12, 125.92.

5-(2-Methoxyphenyl)-4*H*-1,2,4-triazole-3-thiol (**TRZ02**): White solid; yield = 82%, ^{1}H NMR (600 MHz, DMSO-d_6) δ ppm 13.62 (s, 1H), 13.11 (s, 1H), 7.64 (dd, *J* = 7.7, 1.8 Hz, 1H), 7.51 (ddd, *J* = 8.4, 7.4, 1.8 Hz, 1H), 7.18 (dd, *J* = 8.6, 1.0 Hz, 1H), 7.06 (td, *J* = 7.5, 1.0 Hz, 1H), 3.85 (s, 3H); ^{13}C NMR (126 MHz, DMSO-d_6) δ ppm 166.67, 157.26, 148.84, 132.73, 129.73, 121.10, 114.88, 112.40, 56.10.

5-(4-Methoxyphenyl)-4*H*-1,2,4-triazole-3-thiol (**TRZ03**): White solid; yield = 65%, ^{1}H NMR (500 MHz, DMSO-d_6) δ ppm 13.67 (s, 1H), 13.54 (s, 1H), 7.87 – 7.84 (m, 2H), 7.09 – 7.05 (m, 2H), 3.82 (s, 3H); ^{13}C NMR (126 MHz, DMSO-d_6) δ ppm 167.15, 161.46, 150.58, 127.79, 118.36, 115.00, 55.86.

5-(4-Chlorophenyl)-4*H*-1,2,4-triazole-3-thiol (TRZ04): White solid; yield = 76%, ^{1}H NMR (500 MHz, DMSO-d_6) δ ppm 13.74 (s, 1H), 7.92 (s, 2H), 7.63 – 7.54 (m, 2H).

5-(2,4-Dichlorophenyl)-4*H*-1,2,4-triazole-3-thiol (**TRZ05**): White solid; yield = 68%, ^{1}H NMR (500 MHz, DMSO-d_6) δ ppm 13.81 (s, 1H), 10.66 (s, 2H), 7.85 (d, *J* = 2.1 Hz, 1H), 7.75 (t, *J* = 1.2 Hz, 2H), 7.75 – 7.67 (m, 2H), 7.66 – 7.58 (m, 2H), 7.57 (d, *J* = 1.4 Hz, 3H); ^{13}C NMR (126 MHz, DMSO-d_6) δ ppm 164.99, 136.55, 135.85, 133.73, 133.62, 133.12, 132.23, 131.23, 130.48, 129.99, 129.29, 128.32, 127.93, 124.60.

5-Phenyl-1,3,4-thiadiazol-2-amine (**TDZ01**): Off-white solid; yield = 76%, m.p.: 213-214 ºC; ^{1}H NMR (500 MHz, DMSO-d_6) δ ppm 7.74 – 7.76 (m, 2H), 7.42 – 7.48 (m, 5H); ^{13}C NMR (126 MHz, DMSO-d_6) δ ppm 169.98, 156.82, 131.44, 130.05, 129.60, 126.77; MS (ESI$^-$): calculated for $C_8H_7N_3S$ $[M-H]^-$, 176.01; found, 175.85.

5-(4-Fluorophenyl)-1,3,4-thiadiazol-2-amine (**TDZ02**): Pink solid; yield = 92%, m.p.: 211-213 ºC; ^{1}H NMR (500 MHz, DMSO-d_6) δ ppm 7.85 – 7.75 (m, 2H), 7.43 (s,

2H, amine -NH), 7.34 – 7.27 (m, 2H); ^{13}C NMR (126 MHz, DMSO-d_6) δ ppm 169.09, 164.10, 162.14, 155.71, 128.97, 128.90, 128.09, 128.07, 116.70, 116.53; ^{19}F NMR (471 MHz, DMSO-d_6) δ ppm -111.58; MS (ESI$^-$): calculated for $C_8H_6FN_3S$ [M-H]$^-$, 194.02; found, 193.85.

5-(4-Methoxyphenyl)-1,3,4-thiadiazol-2-amine (**TDZ03**): White solid; yield = 84%, m.p.: 185-187 ºC; ^{1}H NMR (500 MHz, DMSO-d_6) δ ppm 7.68 – 7.69 (d, *J* = 5.0 Hz, 5H), 7.30 (s, 2H), 7.02 – 7.03 (d, *J* = 5.0 Hz, 5H), 3.81 (s, 3H); ^{13}C NMR (126 MHz, DMSO-d_6) δ ppm 168.34, 160.75, 156.73, 128.29, 124.10, 114.98, 55.80; MS (ESI$^-$): calculated for $C_9H_9N_3OS$ [M-H]$^-$, 206.04; found, 205.90.

5-(3,4-Dimethoxyphenyl)-1,3,4-thiadiazol-2-amine (**TDZ04**): White solid; yield = 89%, m.p.: 166-168 ºC; ^{1}H NMR (500 MHz, DMSO-d_6) δ ppm 7.37 (d, *J* = 2.1 Hz, 1H), 7.20 (dd, *J* = 8.2, 2.1 Hz, 1H), 7.01 (d, *J* = 8.4 Hz, 1H), 3.82 (s, 3H), 3.80 (s, 3H); ^{13}C NMR (126 MHz, DMSO-d_6) δ ppm 168.44, 156.93, 150.54, 149.43, 124.17, 120.31, 112.28, 109.10, 56.06, 55.97; MS (ESI$^-$): calculated for $C_9H_9N_3OS$ [M-H]$^-$, 236.05; found, 235.90.

5-(Benzo[*d*][1,3]dioxol-5-yl)-1,3,4-thiadiazol-2-amine (**TDZ05**): Light pink solid; yield = 90%, m.p.: 184-185 ºC; ^{1}H NMR (500 MHz, DMSO-d_6) δ ppm 7.33 (t, *J* = 1.7 Hz, 3H), 7.20 (dd, *J* = 8.1, 1.8 Hz, 1H), 6.99 (d, *J* = 8.1 Hz, 1H), 6.09 (s, 2H); ^{13}C NMR (126 MHz, DMSO-d_6) δ ppm 168.51, 156.62, 148.91, 148.39, 125.63, 121.61, 109.20, 106.31, 102.07.

***N*-(5-Phenyl-1,3,4-thiadiazol-2-yl)-2-((5-phenyl-4*H*-1,2,4-triazol-3-yl)thio)acetamide** (**STT01**): White solid; yield = 65%, m.p.: 154-155 ºC; FTIR (*v*, cm^{-1}, KBr): 3430 (amide N-H str.), 2937 (alkene C-H str.), 1702 (amide C=O str.), 1542

(N-H bend.), 1304 (aromatic amine C-N str.), 688 (C=C bend.); ^{1}H NMR (500 MHz, DMSO-d_6) δ ppm 7.96 – 7.91 (m, 4H), 7.54 – 7.47 (m, 6H), 4.28 (s, 2H); ^{13}C NMR (126 MHz, DMSO-d_6) δ ppm 167.90, 162.39, 159.15, 131.09, 130.65, 130.60, 129.84, 129.46, 127.40, 126.41, 35.54; HRMS calcd for $C_{18}H_{14}N_6OS_2$ $[M+H]^+$ 395.0749, found 395.0715.

***N*-(5-(4-Fluorophenyl)-1,3,4-thiadiazol-2-yl)-2-((5-phenyl-4*H*-1,2,4-triazol-3-yl)thio)acetamide** (**STT02**): Tan solid; yield = 93%, m.p.: 228-230 ºC; FTIR (ν, cm^{-1}, KBr) 3353 (amide N-H str.), 2925 (alkene C-H str.), 1671 (amide C=O str.), 1595 (N-H bend.), 1339 (aromatic amine C-N str.), 1252 (C-F str.), 697 (C=C bend.); ^{1}H NMR (500 MHz, DMSO-d_6) δ ppm 8.04 – 7.98 (m, 2H), 7.93 – 7.85 (m, 2H), 7.48 (dd, *J* = 8.3, 6.6 Hz, 2H), 7.42 (dd, *J* = 8.5, 6.1 Hz, 1H), 7.30 (t, *J* = 8.8 Hz, 2H), 3.99 (s, 2H); ^{13}C NMR (126 MHz, DMSO-d_6) δ ppm 172.34, 168.79, 163.80, 161.84, 159.49, 157.44, 156.65, 130.45, 129.83, 129.80, 129.60, 129.22, 128.65, 128.58, 126.26, 116.51, 116.34, 39.92; ^{19}F NMR (471 MHz, DMSO) δ ppm -110.02; HRMS calcd for $C_{18}H_{13}FN_6OS_2$ $[M+H]^+$ 413.0654, found 413.0687.

***N*-(5-(4-Methoxyphenyl)-1,3,4-thiadiazol-2-yl)-2-((5-phenyl-4*H*-1,2,4-triazol-3-yl)thio)acetamide** (**STT03**): White solid; yield = 75%, m.p.: 190-192 ºC; FTIR (*v*, cm^{-1}, KBr) 3405 (amide N-H str.), 2915 (alkene C-H str.), 1678 (amide C=O str.), 1588 (N-H bend.), 1312 (aromatic amine C-N str.), 1256 (alkyl aryl ether C=O str.), 696 (C=C bend.); ^{1}H NMR (500 MHz, DMSO-d_6) δ ppm 13.33 (s, 1H), 7.97 – 7.91 (m, 2H), 7.90 – 7.83 (m, 2H), 7.53 – 7.45 (m, 3H), 7.10 – 7.04 (m, 2H), 4.25 (s, 2H), 3.82 (s, 3H); ^{13}C NMR (126 MHz, DMSO-d_6) δ ppm 168.02, 161.99, 161.48, 159.02, 158.80, 130.51, 129.44, 128.90, 128.32, 126.40, 123.34, 115.21, 55.87, 35.78; HRMS calcd for $C_{19}H_{16}N_6O_2S_2$ $[M+H]^+$ 425.0854, found 425.0874.

***N*-(5-(3,4-Dimethoxyphenyl)-1,3,4-thiadiazol-2-yl)-2-((5-phenyl-4*H*-1,2,4-triazol-3-yl)thio)acetamide** (**STT04**): Pink solid; yield = 90%, m.p.: 216-218 ºC; FTIR (*v*, cm^{-1}, KBr) 3251 (amide N-H str.), 2938 (alkene C-H str.), 1647 (amide C=O str.), 1535 (N-H bend.), 1340 (aromatic amine C-N str.), 1271 (alkyl aryl ether C=O str.), 695 (C=C bend.); ^{1}H NMR (500 MHz, DMSO-d_6) δ ppm 8.00 (d, *J* = 7.6 Hz, 2H), 7.47 (d, *J* = 8.5 Hz, 3H), 7.43 (d, *J* = 7.3 Hz, 1H), 7.35 (d, *J* = 8.4 Hz, 1H), 7.04 (d, *J* = 8.4 Hz, 1H), 4.01 (s, 2H), 3.85 (s, 3H), 3.81 (s, 3H); ^{13}C NMR (126 MHz, DMSO-d_6) δ ppm 171.35, 166.28, 159.33, 150.27, 149.45, 130.33, 129.63, 129.22, 126.25, 125.50, 119.97, 112.46, 109.43, 56.08, 55.96, 38.86; HRMS calcd for $C_{20}H_{18}N_6O_3S_2$ $[M+H]^+$ 455.0960, found 455.0978.

***N*-(5-(Benzo[*d*][1,3]dioxol-5-yl)-1,3,4-thiadiazol-2-yl)-2-((5-phenyl-4*H*-1,2,4-triazol-3-yl)thio)acetamide** (**STT05**): Brown solid; yield = 73%, m.p.: 191-193 ºC; FTIR (*v*, cm^{-1}, KBr) 3384 (amide N-H str.), 2923 (alkene C-H str.), 1660 (amide C=O str.), 1560 (N-H bend.), 1335 (aromatic amine C-N str.), 1259 (alkyl aryl ether C=O str.), 693 (C=C bend.); ^{1}H NMR (500 MHz, DMSO-d_6) δ ppm 8.05 – 7.99 (m, 2H), 7.51 – 7.45 (m, 2H), 7.45 – 7.38 (m, 2H), 7.30 (dd, *J* = 8.1, 1.7 Hz, 1H), 6.99 (d, *J* = 8.0 Hz, 1H), 6.08 (s, 2H), 4.01 (s, 2H); ^{13}C NMR (126 MHz, DMSO-d_6) δ ppm 171.98, 167.76, 162.83, 159.26, 158.56, 156.75, 148.45, 148.31, 130.31, 129.62, 129.21, 127.23, 126.29, 121.21, 109.20, 106.26, 101.88, 39.43; HRMS calcd for $C_{19}H_{14}N_6O_3S_2$ $[M+H]^+$ 439.0647, found 439.0663.

2-((5-(2-Methoxyphenyl)-4*H*-1,2,4-triazol-3-yl)thio)-*N*-(5-phenyl-1,3,4-thiadiazol-2-yl)acetamide (**STT06**): White solid; yield = 67%, m.p.: 181-183 ºC; FTIR (*v*, cm^{-1}, KBr) 3302 (amide N-H str.), 2940 (alkene C-H str.), 1692 (amide C=O str.), 1569 (N-H bend.), 1311 (aromatic amine C-N str.), 1252 (alkyl aryl ether C-O str.), 689 (C=C

bend.); ^{1}H NMR (500 MHz, DMSO-d_6) δ ppm 8.02 (d, *J* = 7.8 Hz, 1H), 7.89 (d, *J* = 7.5 Hz, 2H), 7.48 (dt, *J* = 14.3, 7.3 Hz, 4H), 7.19 (d, *J* = 8.3 Hz, 1H), 7.06 (t, *J* = 7.5 Hz, 1H), 4.16 (s, 2H), 3.94 (s, 3H); ^{13}C NMR (126 MHz, DMSO-d_6) δ ppm 169.88, 160.40, 158.65, 156.97, 153.04, 132.14, 131.87, 130.19, 129.64, 129.53, 127.00, 121.20, 115.73, 112.29, 56.00, 37.33; HRMS calcd for $C_{19}H_{16}N_6O_2S_2$ $[M+H]^+$ 425.0854, found 425.0883.

***N*-(5-(4-Fluorophenyl)-1,3,4-thiadiazol-2-yl)-2-((5-(2-methoxyphenyl)-4*H*-1,2,4-triazol-3-yl)thio)acetamide** (**STT07**): White solid; yield = 78%, m.p.: 211-212 ºC; FTIR (*v*, cm^{-1}, KBr) 3394 (amide N-H str.), 2947 (alkene C-H str.), 1591 (amide C=O str.), 1569 (N-H bend.), 1317 (aromatic amine C-N str.), 1259 (alkyl aryl ether C=O str.), 1231 (C-F str.), 677 (C=C bend.); ^{1}H NMR (500 MHz, DMSO-d_6) δ ppm 13.69 (s, 1H), 8.04 (dd, *J* = 7.8, 1.8 Hz, 1H), 7.90 – 7.86 (m, 2H), 7.49 – 7.45 (m, 1H), 7.29 (t, *J* = 8.9 Hz, 2H), 7.19 (d, *J* = 8.5 Hz, 1H), 7.08 (t, *J* = 7.4 Hz, 1H), 4.05 (s, 2H), 3.95 (s, 3H); ^{13}C NMR (126 MHz, DMSO-d_6) δ ppm 168.31, 165.56, 163.78, 163.07, 161.82, 157.29, 156.97, 153.72, 131.98, 129.77, 129.55, 128.63, 128.56, 121.22, 116.51, 116.34, 112.28, 56.01, 39.37; ^{19}F NMR (471 MHz, DMSO-d_6) δ ppm -112.55; HRMS calcd for $C_{19}H_{15}FN_6O_2S_2$ $[M+H]^+$ 443.0760, found 443.0780.

***N*-(5-(4-Methoxyphenyl)-1,3,4-thiadiazol-2-yl)-2-((5-(2-methoxyphenyl)-4*H*-1,2,4-triazol-3-yl)thio)acetamide** (**STT08**): Gray solid; yield = 84%, m.p.: 229-231 ºC; FTIR (*v*, cm^{-1}, KBr) 3447 (amide N-H str.), 2917 (alkene C-H str.), 1702 (amide C=O str.), 1580 (N-H bend.), 1342 (aromatic amine C-N str.), 1254 (alkyl aryl ether C=O str.), 676 (C=C bend.); ^{1}H NMR (500 MHz, DMSO-d_6) δ ppm 13.77 (s, 1H), 8.00 (dd, *J* = 7.8, 1.8 Hz, 1H), 7.90 – 7.84 (m, 2H), 7.47 (ddd, *J* = 8.8, 7.4, 1.8 Hz, 1H), 7.18 (d, *J* = 8.3 Hz, 1H), 7.12 – 7.01 (m, 3H), 4.25 (s, 2H), 3.93 (s, 3H), 3.82 (s, 3H); ^{13}C NMR

(126 MHz, DMSO-d_6) δ ppm 167.83, 162.18, 161.55, 158.45, 156.97, 153.05, 132.29, 129.51, 128.95, 123.17, 121.19, 115.45, 115.23, 112.29, 55.99, 55.88, 35.32; HRMS calcd for $C_{20}H_{18}N_6O_3S_2$ $[M+H]^+$ 455.0960, found 455.0995.

***N*-(5-(Benzo[*d*][1,3]dioxol-5-yl)-1,3,4-thiadiazol-2-yl)-2-((5-(2-methoxyphenyl)-4*H*-1,2,4-triazol-3-yl)thio)acetamide** (**STT09**): Gray solid; yield = 68%, m.p.: 183-184 ºC; FTIR (*ν*, cm^{-1}, KBr) 3393 (amide N-H str.), 2900 (alkene C-H str.), 1606 (amide C=O str.), 1583 (N-H bend.), 1388 (aromatic amine C-N str.), 1258 (alkyl aryl ether C=O str.), 676 (C=C bend.); ^{1}H NMR (500 MHz, DMSO-d_6) δ ppm 13.69 (s, 1H), 8.05 – 8.02 (m, 1H), 7.49 – 7.45 (m, 1H), 7.43 – 7.41 (m, 1H), 7.32 – 7.29 (m, 1H), 7.19 (d, *J* = 8.4 Hz, 1H), 7.07 (t, *J* = 7.5 Hz, 1H), 7.00 (d, *J* = 8.1 Hz, 1H), 6.09 (s, 2H), 4.07 (s, 2H), 3.95 (s, 3H); ^{13}C NMR (126 MHz, DMSO-d_6) δ ppm 171.06, 158.82, 156.97, 148.58, 148.33, 132.02, 129.54, 126.97, 121.33, 121.21, 115.94, 112.29, 109.22, 106.33, 101.89, 56.01, 38.72; HRMS calcd for $C_{20}H_{16}N_6O_4S_2$ $[M+H]^+$ 469.0752, found 469.0795.

2-((5-(4-Methoxyphenyl)-4*H*-1,2,4-triazol-3-yl)thio)-*N*-(5-phenyl-1,3,4-thiadiazol-2-yl)acetamide (**STT10**): Tan solid; yield = 86%, m.p.: 128-130 ºC; FTIR (*ν*, cm^{-1}, KBr) 3362 (amide N-H str.), 2932 (alkene C-H str.), 1700 (amide C=O str.), 1569 (N-H bend.), 1337 (aromatic amine C-N str.), 1253 (alkyl aryl ether C=O str.), 686 (C=C bend.); ^{1}H NMR (500 MHz, DMSO-d_6) δ ppm 13.68 (s, 1H), 7.94 (dt, *J* = 6.8, 2.3 Hz, 2H), 7.90 – 7.83 (m, 2H), 7.57 – 7.50 (m, 3H), 7.08 – 7.02 (m, 2H), 4.25 (s, 2H), 3.80 (s, 3H); ^{13}C NMR (126 MHz, DMSO-d_6) δ ppm 168.03, 162.34, 161.18, 159.26, 131.07, 130.68, 129.83, 128.05, 127.38, 114.89, 55.80, 35.51; HRMS calcd for $C_{19}H_{16}N_6O_2S_2$ $[M+H]^+$ 425.0854, found 425.0887.

***N*-(5-(4-Fluorophenyl)-1,3,4-thiadiazol-2-yl)-2-((5-(4-methoxyphenyl)-4*H*-1,2,4-triazol-3-yl)thio)acetamide** (**STT11**): White solid; yield = 71%, m.p.: 215-217 ºC; FTIR (*v*, cm^{-1}, KBr) 3383 (amide N-H str.), 2933 (alkene C-H str.), 1696 (amide C=O str.), 1569 (N-H bend.), 1336 (aromatic amine C-N str.), 1254 (alkyl aryl ether C=O str.), 1239 (C-F str.), 623 (C=C bend.); ^{1}H NMR (500 MHz, DMSO-d_6) δ ppm 7.96 – 7.92 (m, 2H), 7.89 (d, *J* = 8.5 Hz, 2H), 7.33 (t, *J* = 8.8 Hz, 2H), 7.04 (d, *J* = 8.5 Hz, 2H), 4.14 (s, 2H), 3.81 (s, 3H); ^{13}C NMR (126 MHz, DMSO-d_6) δ ppm 169.98, 164.31, 163.67, 162.35, 160.94, 159.45, 157.69, 157.31, 129.23, 129.16, 128.49, 127.96, 121.32, 116.76, 116.58, 114.79, 55.75, 37.39; ^{19}F NMR (471 MHz, DMSO-d_6) δ -112.55; HRMS calcd for $C_{19}H_{15}FN_6O_2S_2$ $[M+H]^+$ 443.0760, found 443.0795.

***N*-(5-(4-Methoxyphenyl)-1,3,4-thiadiazol-2-yl)-2-((5-(4-methoxyphenyl)-4*H*-1,2,4-triazol-3-yl)thio)acetamide** (**STT12**): White solid; yield = 83%, m.p.: 128-130 ºC; FTIR (*v*, cm^{-1}, KBr) 3163 (amide N-H str.), 2940 (alkene C-H str.), 1613 (amide C=O str.), 1579 (N-H bend.), 1333 (aromatic amine C-N str.), 1254 (alkyl aryl ether C=O str.), 624 (C=C bend.); ^{1}H NMR (500 MHz, DMSO-d_6) δ ppm 7.93 (d, *J* = 8.3 Hz, 2H), 7.81 (d, *J* = 8.3 Hz, 2H), 7.04 (d, *J* = 8.4 Hz, 4H), 4.06 (s, 2H), 3.81 (s, 6H); ^{13}C NMR (126 MHz, DMSO-d_6) δ ppm 170.87, 165.36, 160.75, 160.66, 159.52, 158.26, 157.12, 128.28, 127.91, 125.08, 122.00, 114.97, 114.71, 55.77, 55.73, 38.44; HRMS calcd for $C_{20}H_{18}N_6O_3S_2$ $[M+H]^+$ 455.0960, found 455.0963.

***N*-(5-(Benzo[*d*][1,3]dioxol-5-yl)-1,3,4-thiadiazol-2-yl)-2-((5-(4-methoxyphenyl)-4*H*-1,2,4-triazol-3-yl)thio)acetamide** (**STT13**): Gray solid; yield = 94%, m.p.: 230-232 ºC; FTIR (*v*, cm^{-1}, KBr) 3403 (amide N-H str.), 2916 (alkene C-H str.), 1615 (amide C=O str.), 1558 (N-H bend.), 1336 (aromatic amine C-N str.), 1257 (alkyl aryl ether C=O str.), 668 (C=C bend.); ^{1}H NMR (600 MHz, DMSO-d_6) δ ppm 7.95 (d, *J* = 8.3 Hz,

2H), 7.47 (s, 1H), 7.37 (d, *J* = 8.1 Hz, 1H), 7.09 (d, *J* = 8.3 Hz, 2H), 7.05 (d, *J* = 8.1 Hz, 1H), 6.13 (s, 2H), 4.09 (s, 2H), 3.85 (s, 3H); ^{13}C NMR (151 MHz, DMSO-d_6) δ ppm 171.12, 165.67, 160.78, 159.52, 158.26, 157.16, 148.79, 148.35, 127.93, 126.49, 121.78, 121.57, 114.73, 109.28, 106.38, 101.95, 55.72, 38.36; HRMS calcd for $C_{20}H_{16}N_6O_4S_2$ $[M+H]^+$ 469.0752, found 469.0790.

2-((5-(4-Chlorophenyl)-4*H*-1,2,4-triazol-3-yl)thio)-*N*-(5-phenyl-1,3,4-thiadiazol-2-yl)acetamide (**STT14**): Gray solid; yield = 60%, m.p.: 216-218 ºC; FTIR (*v*, cm^{-1}, KBr) 3313 (amide N-H str.), 2920 (alkene C-H str.), 1697 (amide C=O str.), 1525 (N-H bend.), 1381 (aromatic amine C-N str.), 845 (C-Cl str.), 684 (C=C bend.); ^{1}H NMR (500 MHz, DMSO-d_6) δ ppm 7.99 (d, *J* = 8.2 Hz, 2H), 7.89 (d, *J* = 7.5 Hz, 2H), 7.54 (d, *J* = 8.2 Hz, 2H), 7.49 (q, *J* = 7.3 Hz, 3H), 4.12 (s, 2H); ^{13}C NMR (126 MHz, DMSO-d_6) δ ppm 170.22, 164.02, 160.44, 158.37, 156.44, 134.36, 131.94, 130.15, 129.63, 129.38, 128.93, 127.99, 127.00, 37.70; HRMS calcd for $C_{18}H_{13}ClN_6OS_2$ $[M+H]^+$ 429.0359, found 429.0390.

2-((5-(4-Chlorophenyl)-4*H*-1,2,4-triazol-3-yl)thio)-*N*-(5-(4-fluorophenyl)-1,3,4-thiadiazol-2-yl)acetamide (**STT15**): Tan solid; yield = 78%, m.p.: 222-224 ºC; FTIR (*v*, cm^{-1}, KBr) 3179 (amide N-H str.), 2934 (alkene C-H str.), 1603 (amide C=O str.), 1542 (N-H bend.), 1334 (aromatic amine C-N str.), 1238 (C-F str.), 831 (C-Cl str.), 616 (C=C bend.); ^{1}H NMR (500 MHz, DMSO-d_6) δ ppm 8.01 – 7.92 (m, 4H), 7.56 (d, *J* = 8.2 Hz, 2H), 7.36 (t, *J* = 8.7 Hz, 2H), 4.25 (s, 2H); ^{13}C NMR (126 MHz, DMSO-d_6) δ ppm 168.33, 164.69, 162.71, 160.92, 160.47 – 160.02 (m), 134.94, 129.65, 129.58, 129.53, 128.09, 127.72, 127.55, 116.94, 116.76, 36.05; ^{19}F NMR (471 MHz, DMSO-d_6) δ -109.69; HRMS calcd for $C_{18}H_{12}ClFN_6OS_2$ $[M+H]^+$ 447.0265, found 447.0290.

2-((5-(4-Chlorophenyl)-4*H*-1,2,4-triazol-3-yl)thio)-*N*-(5-(4-methoxyphenyl)-1,3,4-thiadiazol-2-yl)acetamide (**STT16**): Pink solid; yield = 62%, m.p.: 192-194 ºC; FTIR (*v*, cm^{-1}, KBr) 3325 (amide N-H str.), 2941 (alkene C-H str.), 1610 (amide C=O str.), 1525 (N-H bend.), 1315 (aromatic amine C-N str.), 1258 (alkyl aryl ether C=O str.), 842 (C-Cl str.), 606 (C=C bend.); ^{1}H NMR (500 MHz, DMSO-d_6) δ ppm 8.01 (d, *J* = 8.2 Hz, 2H), 7.82 (d, *J* = 8.4 Hz, 2H), 7.52 (d, *J* = 8.2 Hz, 2H), 7.05 (d, *J* = 8.4 Hz, 2H), 4.06 (s, 2H), 3.81 (s, 3H); ^{13}C NMR (126 MHz, DMSO-d_6) δ ppm 170.41, 163.83, 160.85, 160.16, 158.74, 156.32, 134.05, 129.46, 129.30, 128.44, 127.92, 124.68, 115.02, 55.80, 37.91; HRMS calcd for $C_{19}H_{15}ClN_6O_2S_2$ $[M+H]^+$ 459.0464, found 459.0499.

2-((5-(4-Chlorophenyl)-4*H*-1,2,4-triazol-3-yl)thio)-*N*-(5-(3,4-dimethoxyphenyl)-1,3,4-thiadiazol-2-yl)acetamide (**STT17**): White solid; yield = 62%, m.p.: 192-194 ºC; FTIR (*v*, cm^{-1}, KBr) 3307 (amide N-H str.), 2903 (alkene C-H str.), 1606 (amide C=O str.), 1529 (N-H bend.), 1314 (aromatic amine C-N str.), 1271 (alkyl aryl ether C=O str.), 845 (C-Cl str.), 646 (C=C bend.); ^{1}H NMR (500 MHz, DMSO-d_6) δ ppm 7.94 (d, *J* = 8.2 Hz, 2H), 7.55 (d, *J* = 8.3 Hz, 2H), 7.49 (s, 1H), 7.43 (d, *J* = 8.4 Hz, 1H), 7.06 (d, *J* = 8.5 Hz, 1H), 4.27 (s, 2H), 3.83 (d, *J* = 15.7 Hz, 6H); ^{13}C NMR (126 MHz, DMSO-d_6) δ ppm 167.69, 162.39, 158.60, 157.09, 151.34, 149.60, 135.05, 129.54, 128.11, 127.49, 123.25, 120.84, 112.50, 109.82, 56.13, 56.07, 35.66; HRMS calcd for $C_{20}H_{17}ClN_6O_3S_2$ $[M+H]^+$ 489.0570, found 489.0602.

***N*-(5-(Benzo[*d*][1,3]dioxol-5-yl)-1,3,4-thiadiazol-2-yl)-2-((5-(4-chlorophenyl)-4*H*-1,2,4-triazol-3-yl)thio)acetamide** (**STT18**): Gray solid; yield = 62%, m.p.: 192-194 ºC; FTIR (*v*, cm^{-1}, KBr) 3176 (amide N-H str.), 2912 (alkene C-H str.), 1607 (amide C=O str.), 1543 (N-H bend.), 1332 (aromatic amine C-N str.), 1259 (alkyl aryl ether

C=O str.), 835 (C-Cl str.), 640 (C=C bend.); ^{1}H NMR (500 MHz, DMSO-d_6) δ ppm 8.01 (d, *J* = 8.2 Hz, 2H), 7.52 (d, *J* = 8.2 Hz, 2H), 7.44 (s, 1H), 7.34 (d, *J* = 8.3 Hz, 1H), 7.01 (d, *J* = 8.3 Hz, 1H), 6.10 (s, 2H), 4.04 (s, 2H); ^{13}C NMR (126 MHz, DMSO-d_6) δ ppm 170.84, 164.89, 159.71, 158.87, 156.30, 148.87, 148.40, 134.03, 129.56, 129.29, 127.92, 126.46, 121.58, 109.26, 106.49, 101.98, 38.25; HRMS calcd for $C_{19}H_{13}ClN_6O_3S_2$ $[M+H]^+$ 473.0257, found 473.0257.

2-((5-(2,4-Dichlorophenyl)-4*H*-1,2,4-triazol-3-yl)thio)-*N*-(5-(4-fluorophenyl)-1,3,4-thiadiazol-2-yl)acetamide (**STT19**): White solid; yield = 60%, m.p.: 204-206 ºC; FTIR (*v*, cm^{-1}, KBr) 3425 (amide N-H str.), 2923 (alkene C-H str.), 1687 (amide C=O str.), 1591 (N-H bend.), 1331 (aromatic amine C-N str.), 1236 (C-F str.), 838 (C-Cl str.), 653 (C=C bend.); ^{1}H NMR (500 MHz, DMSO-d_6) δ ppm (500 MHz, DMSO-d_6) δ 14.47 (s, 1H), 12.99 (s, 1H), 8.08 – 7.90 (m, 3H), 7.83 – 7.75 (m, 2H), 7.57 (d, *J* = 1.7 Hz, 1H), 7.37 (d, *J* = 8.9 Hz, 2H), 4.30 (s, 2H); ^{13}C NMR (126 MHz, DMSO-d_6) δ ppm 167.80, 162.85, 158.82, 154.88, 152.97, 132.98, 131.22, 130.50, 129.81, 129.79, 129.73, 128.38, 127.44, 117.03, 116.85, 29.47; HRMS calcd for $C_{18}H_{11}Cl_2FN_6OS_2$ $[M+H]^+$ 480.9875, found 480.9898.

2-((5-(2,4-Dichlorophenyl)-4*H*-1,2,4-triazol-3-yl)thio)-*N*-(5-(4-methoxyphenyl)-1,3,4-thiadiazol-2-yl)acetamide (**STT20**): White solid; yield = 96%, m.p.: 181-183 ºC; FTIR (*v*, cm^{-1}, KBr) 3156 (amide N-H str.), 2925 (alkene C-H str.), 1610 (amide C=O str.), 1588 (N-H bend.), 1316 (aromatic amine C-N str.), 1245 (alkyl aryl ether C=O str.), 824 (C-Cl str.), 615 (C=C bend.); ^{1}H NMR (500 MHz, DMSO-d_6) δ ppm 10.65 (d, *J* = 11.0 Hz, 1H), 7.90 – 7.84 (m, 2H), 7.84 – 7.74 (m, 3H), 7.57 (d, *J* = 2.0 Hz, 2H), 7.12 – 7.06 (m, 2H), 4.29 (s, 2H), 3.83 (s, 3H); ^{13}C NMR (126 MHz, DMSO-d_6) δ ppm 173.26, 165.40, 161.59, 158.38, 156.68, 148.34, 132.98, 132.38, 131.13,

130.50, 130.06, 128.98, 127.79, 115.25, 55.90, 29.47; HRMS calcd for $C_{19}H_{14}Cl_2N_6O_2S_2$ $[M+H]^+$ 493.0075, found 493.0102.

***N*-(5-(Benzo[*d*][1,3]dioxol-5-yl)-1,3,4-thiadiazol-2-yl)-2-((5-(2,4-dichlorophenyl)-4*H*-1,2,4-triazol-3-yl)thio)acetamide** (**STT21**): White solid; yield = 87%, m.p.: 168-169 ºC; FTIR (ν, cm^{-1}, KBr) 3311 (amide N-H str.), 2899 (alkene C-H str.), 1630 (amide C=O str.), 1530 (N-H bend.), 1340 (aromatic amine C-N str.), 1260 (alkyl aryl ether C=O str.), 862 (C-Cl str.), 641 (C=C bend.); ^{1}H NMR (500 MHz, DMSO-d_6) δ ppm 12.91 (s, 1H), 7.79 (d, J = 8.4 Hz, 1H), 7.77 (dd, J = 7.0, 1.9 Hz, 1H), 7.57 – 7.53 (m, 1H), 7.50 (d, J = 1.8 Hz, 1H), 7.43 (dd, J = 8.1, 1.8 Hz, 1H), 7.05 (d, J = 8.1 Hz, 1H), 6.13 (s, 2H), 4.29 (s, 2H); ^{13}C NMR (126 MHz, DMSO-d_6) δ ppm 167.40, 162.22, 159.03, 158.38, 149.83, 148.60, 132.98, 132.87, 130.49, 130.06, 129.99, 128.13, 124.57, 122.44, 109.47, 106.93, 102.28, 29.47; HRMS calcd for $C_{19}H_{12}Cl_2N_6O_3S_2$ $[M+H]^+$ 506.9867, found 506.9911.

2.3.3. Biological studies

2.3.3.1. *In vitro* SHP2 inhibition and enzyme kinetics assay

Table 2.6. *In vitro* enzyme inhibition results of compounds **111675** and **STT01-STT21**

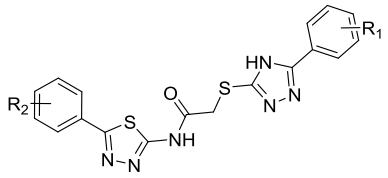

STT01-STT21

Compd Code	R_1	R_2	SHP2 IC_{50} (μM)[a]	Compd Code	R_1	R_2	SHP2 IC_{50} (μM)[a]
111675	--	--	0.878 ± 0.008	**STT12**	4-OCH_3	4-OCH_3	1.053 ± 0.021
STT01	H	H	1.365 ± 0.065	**STT13**	4-OCH_3	1,3-dioxo	0.318 ± 0.001
STT02	H	4-F	3.144 ± 0.001	**STT14**	4-Cl	H	0.917 ± 0.057
STT03	H	4-OCH_3	1.012 ± 0.008	**STT15**	4-Cl	4-F	1.325 ± 0.076
STT04	H	3,4-$(OCH_3)_2$	1.044 ± 0.015	**STT16**	4-Cl	4-OCH_3	3.146 ± 0.005

STT05	H	1,3-dioxo	0.457 ± 0.029	**STT17**	4-Cl	3,4-$(OCH_3)_2$	0.985 ± 0.062
STT06	2-OCH_3	H	0.724 ± 0.076	**STT18**	4-Cl	1,3-dioxo	1.687 ± 0.019
STT07	2-OCH_3	4-F	2.945 ± 1.668	**STT19**	2,4-Cl_2	4-F	2.317 ± 0.838
STT08	2-OCH_3	4-OCH_3	1.176 ± 0.034	**STT20**	2,4-Cl_2	4-OCH_3	0.913 ± 0.157
STT09	2-OCH_3	1,3-dioxo	1.476 ± 0.239	**STT21**	2,4-Cl_2	1,3-dioxo	0.484 ± 0.167
STT10	4-OCH_3	H	1.029 ± 0.003	**SHP099**	--	--	0.070[b]
STT11	4-OCH_3	4-F	0.857 ± 0.070				

[a] Values represent the assay drug concentration that give 50% inhibition of SHP2 activity and are the mean ± SEM of two independent experiments done in duplicate; statistical significance: $p<0.05$ versus the corresponding IC_{50} values obtained against SHP2, as determined by ANOVA/Dunnett's test; [b] Reported IC_{50} value against SHP2 in a similar DiFMUP assay protocol using fl-SHP2 enzyme and a bis-tyrosyl phosphorylated peptide activator [94].

The SHP2 inhibitory activity of initial virtual lead compound **111675** and subsequently, lead-inspired analogues **STT01**-**STT21** was determined using BPS Bioscience Kit No.: 72330 wherein full-length SHP2 enzyme (fl-SHP2, His-Tag recombinant) was allosterically activated by the binding of a bis-tyrosyl-phosphorylated peptide (IRS-1) and the inhibition was measured by the dephosphorylation of 6,8-difluoro-4-methylumbelliferyl phosphate (DiFMUP) to 6,8-difluoro-4-methylumbelliferone (DiFMU) (**Figure 2.4**) [140]. The SHP2 IC_{50} values of all the compounds are given in **Table 2.6** along with that of the reference inhibitor **SHP099** (reported data) [94]. Compound **111675** showed submicromolar IC_{50} against SHP2 (0.878 ± 0.008 μM). All final compounds of the **STT series** showed SHP2 inhibition in micromolar to submicromolar range; IC_{50} values ranged from 0.318 ± 0.001 μM for compound **STT13** to 3.146 ± 0.005 μM for compound **STT16.** Thus, compound **STT13** emerged as the lead compound as per the SHP2 inhibitory potency.

SAR of SHP2 inhibition for compounds STT01-STT21

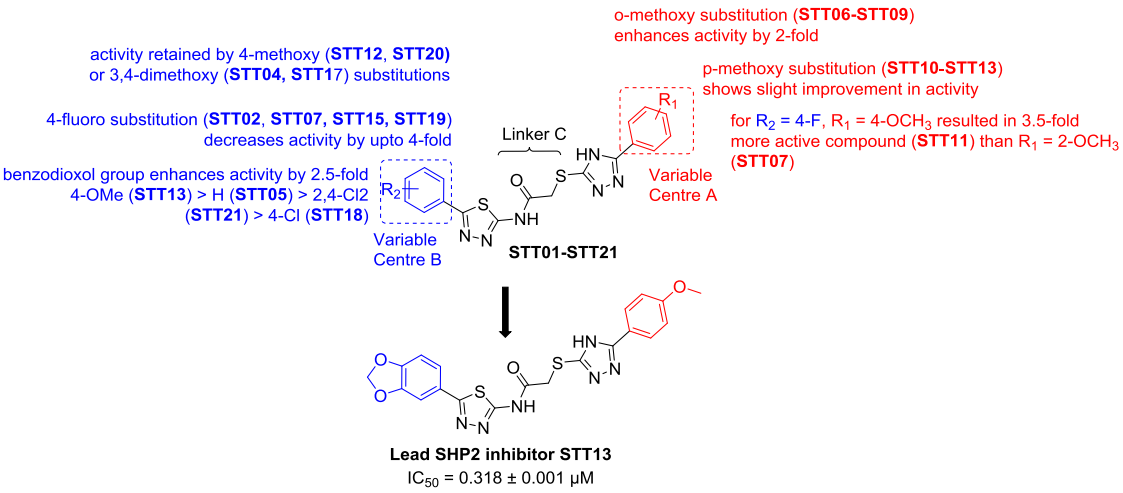

Figure 2.7. Structure-activity relationship (SAR) of the synthesized compounds **STT01-STT21** along with the structure of most potent compound **STT13**. All correlating statements in the figure are with reference to the corresponding unsubstituted analogue i.e. R_1 = H and R_2 = H wherever applicable.

The current library of 21 compounds consists of analogous members containing two variable centres A and B (**Figure 2.7**), one at the phenyl ring attached to the triazole moiety (centre A) and other at the phenyl ring attached to the thiadiazole moiety (centre B). Combinative structural modifications at both the centres display appreciable effect on the IC_{50} values of the compounds of the series. A study of the IC_{50} values of all the tested compounds gives us an idea regarding the correlation between the various structural modifications we did on our designed scaffold and their activity against SHP2 and are listed below.

- Most notable among the structure-activity relationship analysis is the effect of introducing the 1,3-benzodioxo ring in place of mono-substitution or di-substitution at centre B. The three topmost SHP2 inhibitors, compound **STT13** (IC_{50} = 0.318 ± 0.001 μM), **STT05** (IC_{50} = 0.457 ± 0.029 μM) and **STT21** (IC_{50} = 0.484 ± 0.167 μM) contain the benzodioxole group in their structure. Indeed, the benzodioxole moiety is a highly

privileged scaffold in drug discovery due to its lipophilic nature as well as presence of the acidic methylene protons that easily form the reactive benzodioxolium ions, homolytic radicals and carbanions by oxidation at the methylenic carbon. For this reason, the benzodioxole appendage can be seen in a large number of bioactive molecules including anticancer [141, 142] and anti-infective agents [143] and psychoactive drugs [144].

- All these compounds have moderate Log P (**STT13**: Log P = 1.69, **STT05**: Log P = 1.71, **STT21**: Log P = 1.80) within the acceptable range for a CNS targeting drug candidate (i.e., around 2.0) [138].

- Among the three inhibitors containing the benzodioxole moiety, the *para*-methoxy substitution (**STT13**) resulted in the highest potency against SHP2 whereas the other two compounds (unsubstituted, **STT05** and 2,4-dichloro substituted, **STT21**) were almost 1.5-fold less potent.

- A comparison based on the substitutions at the centre A revealed many salient correlations. *Ortho*-methoxy substitution at the centre A increased anti-SHP2 activity by almost 2-folds from the unsubstituted one (**STT01** and **STT06**, IC_{50} = 1.365 ± 0.065 µM and 0.724 ± 0.076 µM, respectively).

- The positional isomer of the 2-methoxy derivatives i.e., 4-methoxy substitutions resulted in slight improvement in activity (compare **STT06** and **STT10**, **STT08** and **STT12**).

- For the 4-fluoro substitution at centre B, the corresponding 4-methoxy derivative (**STT11**, IC_{50} = 0.857 ± 0.070 µM) displayed 3.5-fold better activity than the 2-methoxy derivative (**STT07**, IC_{50} = 2.945 ± 1.668 µM).

- All the 4-chloro and 2,4-dichloro substitutions at centre A resulted in somewhat less potent molecules than the other substitutions (**STT14**-**STT20**).

- In case of effect of substitutions at centre B, in general, introduction of 4-fluoro group drastically reduced activity compared to the unsubstituted derivative (compare compounds **STT01** and **STT02**; 2.3-fold decrease in activity, **STT06** and **STT07**; 4-fold decrease in activity, **STT14** and **STT15**; 1.5-fold decrease in activity, vide **Table 2.6**).

- The SHP2 inhibitory activity was somewhat retained by the para substitution at centre B phenyl ring with methoxy group (compare compounds **STT01** and **STT03**, **STT06** and **STT08**, **STT10** and **STT12**).

- Similarly, no substitution vs. 3,4-dimethoxy substitution (compare compounds **STT01** and **STT04**, **STT14** and **STT17**) or 4-monomethoxy substitution vs. 3,4-dimethoxy substitution (compare compounds **STT03** and **STT04**, **STT16** and **STT17**) did not impede activity against SHP2.

Based on the SHP2 inhibition data of our series, the lead compound **STT13** was chosen for enzyme kinetics studies to understand the putative mechanism of inhibition. The rate of inhibition of SHP2 [V] via hydrolysis of DiFMUP to DiFMU was measured at three fixed concentrations of compound **STT13** taken at five different concentrations of the substrate [S]. A non-linear plot of [S] vs. [V] through Michaelis-Menten kinetics and a double-reciprocal plot of 1/[S] vs. 1/[V] through Lineweaver Burk method were done for each inhibitor concentration (**Figure 2.8**). Analysis of the Lineweaver Burk plot (**Figure 2.8B**) showed that compound **STT13** inhibited SHP2 by mixed to non-competitive type inhibition. In the plot, there was change in V_{max} with a change in

concentration which indicates non-competitive or mixed mode of inhibition. This is significant in the current scenario, as compound **STT13** was designed to target the allosteric site of SHP2 and mixed to non-competitive inhibition does not rule out the possibility of it being an allosteric inhibitor of the enzyme albeit in an *in vitro* study. Further corroboration of the allosteric mode of action of compound **STT13** for SHP2 would require other relevant studies like using truncated SHP2 constructs for *in vitro* assays and development and analysis of X-ray co-crystal structure of the protein with ligand compound **STT13**.

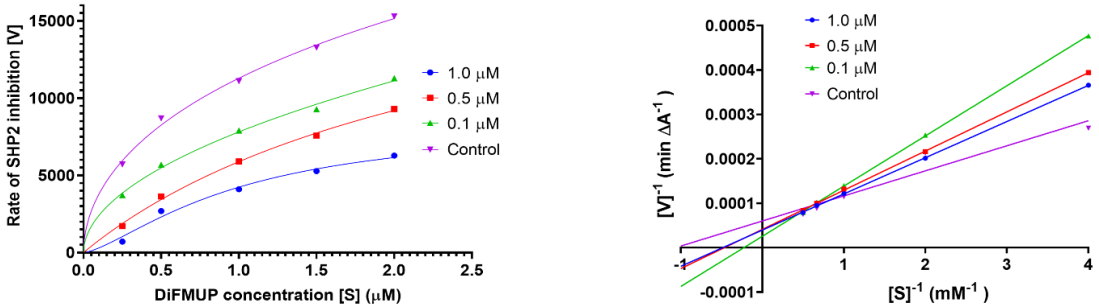

Figure 2.8. Enzyme kinetics graphs on the mode of fl-SHP2 inhibition by compound **STT13**. (A) Michaelis-Menten plot for increasing concentrations of substrate i.e., DiFMUP (0.25, 0.5, 1.0, 1.5 and 2.0 μM) ([S], in μM) vs. rate of SHP2 inhibition [V] in the absence (control) and presence of compound **STT13** (1.0, 0.5 and 0.1 μM). B) Lineweaver Burk reciprocal plot of 1/[S] vs. 1/[V] at increasing concentrations of DiFMUP.

2.3.3.2. *In vitro* antioxidant assay

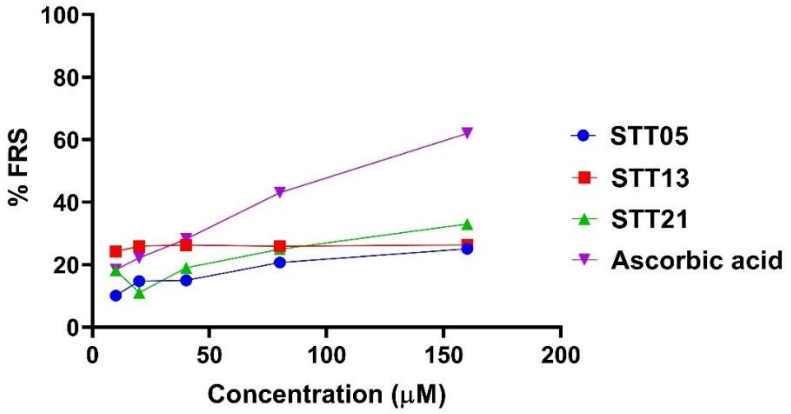

Figure 2.9. Percent free radical scavenging (% FRS) activity of compounds **STT05**, **STT13**, **STT21** and ascorbic acid plotted against the various concentrations of each compound used in the assay. The individual plot points represent the % FRS value obtained from two independent experiments in triplicate, expressed as mean ± SEM.

Reactive oxygen species (ROS) generated due to exogenous or endogenous stimuli, is a major perpetrator in the development and progression of carcinoma [145]. An overexpression of ROS in the tumor microenvironment (TME) and subsequent imbalance in the inherent redox equilibrium has been correlated with enhanced proliferation, migration, genotoxicity and inhibition of cell apoptosis leading to increased cell survival. Thus, therapeutic intervention in the form of antioxidants has been a route of choice for cancer chemotherapy [146]. The foremost three molecules that exhibited the best anti-SHP2 activity i.e., compounds **STT13**, **STT05** and **STT21** were subjected to an antioxidant activity assay using the 2,2-diphenyl-1-picrylhydrazyl (DPPH) protocol to correlate their *in vitro* anti-SHP2 & anticancer potential with their antioxidant property. Ascorbic acid (AA) was used as the positive control. The antioxidant activity of the compounds is reported as IC_{50} value and percent free radical scavenging (% FRS) activity in **Table 2.7** and the % FRS is also given in **Figure 2.9** as a plot vs. concentration of the respective compound in μM. All the tested compounds

demonstrated potent antioxidant activity as compared to ascorbic acid (DPPH IC_{50} = 67.23 ± 0.824 μM) with compound **STT13** being the most potent one (DPPH IC_{50} = 17.58 ± 0.337 μM). This may be attributed to the presence of the benzodioxol group and the thiadiazole ring which are bioisosteric to the radical scavenging carboxylic acid moiety of ascorbic acid.

Table 2.7. Antioxidant activity of compounds **STT05, STT13** and **STT21** by DPPH assay

Compd	Antioxidant activity (DPPH assay)	
	% FRS[a]	**IC_{50} (μM)[b]**
STT05	20.58 ± 3.711	46.81 ± 0.611
STT13	26.04 ± 0.100	17.58 ± 0.337
STT21	25.98 ± 4.716	40.33 ± 0.525
Ascorbic acid[c]	66.89 ± 2.070	67.23 ± 0.824

[a] % Free radical scavenging (FRS) activity at 100 μM compound concentration ± SEM.

[b] Mean IC_{50} of two independent experiments assayed in triplicate each ± SEM.

[c] Used as positive control.

2.3.3.3. *In vitro* blood-brain barrier permeability assay (PAMPA-BBB) of compound STT13

PAMPA-BBB assay is based on the permeability of compound through porcine brain lipid (PBL) coated porous membrane which mimics the blood-brain-barrier [147]. Drugs often need to cross blood-brain-barrier in order to reach the brain and this makes a compound's ability to passively cross the BBB an important characteristic to evaluate. Parallel Artificial Membrane Permeability Assay (PAMPA) is a quick, inexpensive and high-throughput method of evaluating the permeability of test compounds. As we were trying to establish the efficacy of compound **STT13** in the management of CNS cancer like GBM, the compound was evaluated for its *in vitro* blood-brain barrier permeability to assess its potential to pass the brain. Docetaxel was used as the reference standard and imipramine & tenoxicam were used as the positive and negative permeability

controls respectively. The effective permeability (P_e) value obtained from the assay is given in **Table 2.8**. Compound **STT13** displayed a P_e value of (4.461 ± 0.327) $\times 10^{-6}$ cm/s after an incubation of 18 h. According to Di et.al., any molecule is CNS+ if its $P_e > 4.0 \times 10^{-6}$ cm/s, is CNS± if its $P_e > 2.0 \times 10^{-6}$ cm/s $< 4.0 \times 10^{-6}$ cm/s and is CNS- when $P_e < 2.0 \times 10^{-6}$ cm/s [147]. Thus, this indicates a positive CNS permeability index i.e., compound **STT13** is a probable CNS+ molecule. In other words, it has the potential to cross the BBB as shown by the corresponding *in vitro* experiment.

Table 2.8 PAMPA-BBB assay data

Compd	P_e ($\times 10^{-6}$ cm/s)[a]	Reference P_e ($\times 10^{-6}$ cm/s)[b]	Predicted BBB[c]	CNS Category[d]	Reported CNS[b]
STT13	4.461 ± 0.327	NA	0.111	CNS+	NA
Docetaxel	2.687 ± 0.320	NA	0.025	CNS±	NA
Imipramine[e]	14.922 ± 0.131	13	2.920	CNS+	CNS+
Tenoxicam[e]	1.267 ± 0.168	0.1	0.095	CNS-	CNS-

[a] P_e values as mean ± SD of two independent experiments in duplicate.

[b] Values are cited from Di *et.al.*, 2003[147].

[c] BBB permeability using PreADMET web-based server (accessed on 08.08.2024).

[d] CNS+ ($P_e > 4.0 \times 10^{-6}$ cm/s), CNS± ($P_e > 2.0 \times 10^{-6}$ cm/s $< 4.0 \times 10^{-6}$ cm/s), CNS- ($P_e < 2.0 \times 10^{-6}$ cm/s)[b]

[e] Used as positive and negative permeability controls respectively

NA: not applicable

2.3.3.4. Cell-based study

2.3.3.4.1. Cell proliferation assay using MTT

The most active compounds of the **STT** series that exhibited submicromolar SHP2 inhibitory activity ($IC_{50} < 1.0$ μM) in *in vitro* experiments were evaluated along with compound **111675** and screened according to their effect on cancer cell viability via a cell proliferation/cytotoxicity assay in MCF-7 cell lines (human breast cancer) using MTT (3-(4,5-dimethylthiazol-2-yl)-2,5-diphenyl tetrazolium bromide) and docetaxel as the reference standard. It is a well-known fact, that SHP2 promotes MCF-7 cells to

become more invasive and metastasize to remote regions like kidney by synergizing with protein kinases, and cell surface adhesion molecules [148]. This study, too afforded compound **STT13** as the most potent cytotoxic molecule (MCF-7 GI_{50} = 37.02 ± 0.25 μM) among the ones tested (vide **Table 2.9**). Accordingly, with an aim to evaluate the potential of compound **STT13** in neurological cancers and to understand the relevance of our designed scaffold in CNS cancer therapy, its cytotoxic evaluation was performed in rat-derived PC12 neural cells (rat phaeochromocytoma cells), in SHP2-driven U87MG human glioblastoma cells and in human neuroblastoma cells (SH-SY5Y) via a similar MTT assay protocol (**Table 2.9**) [149-151]. PC12 cells are a model of choice to study non-receptor phosphatases like SHP2 as these neural cells have a persistent Ras-ERK cascade regulated by SHP2 [152] and are dependent on the enzyme for effective cell differentiation [153]. SHP2 is also essential for the crucial oncogenic transformation in U87MG GBM cells and thus are an important experimental model to study the effect of SHP2 inhibition for GBM therapy [149]. Also, there is evidence that SHP2 actively regulates growth factor signaling pathways in neuronal cells and its dysregulation leads to apoptotic activation [154].

Table 2.9. Growth inhibition data (GI_{50}) of tested compounds

	GI_{50} (μM)			
	MCF-7	**PC12**	**U87MG**	**SH-SY5Y**
111675	>1000	NT	NT	NT
STT05	91.82 ± 0.45	NT	NT	NT
STT06	146.1 ± 9.31	NT	NT	NT
STT11	72.91 ± 2.17	NT	NT	NT
STT13	37.02 ± 0.25	99.83 ± 0.04	68.69 ± 0.21	23.72 ± 0.89
STT14	106.5 ± 6.75	NT	NT	NT
STT17	111.5 ± 1.51	NT	NT	NT
STT20	261.2 ± 10.8	NT	NT	NT
STT21	79.3 ± 0.68	NT	NT	NT
Docetaxel[a]	4.84 ± 0.16	NT	NT	NT

[a] Reference standard for MTT assay on MCF-7 cells; NT: Not tested

It can be seen from **Table 2.9** that compound **STT13** is a weaker cytotoxic agent for MCF-7 cells (GI_{50} = 37.02 ± 0.25 μM) as compared to docetaxel (GI_{50} = 4.84 ± 0.16 μM); **Figure 2.10A** reveals the nature of cytotoxicity of compound **STT13** on MCF-7 cells which apparently is not dose-dependent. This is because the % viability of the cells remained below 50% through a very narrow change with increasing dose (from 30 μM to 90 μM). The compound also demonstrated weak cytotoxicity in the other two cell lines indicating lack of appreciable anti-proliferative activity.

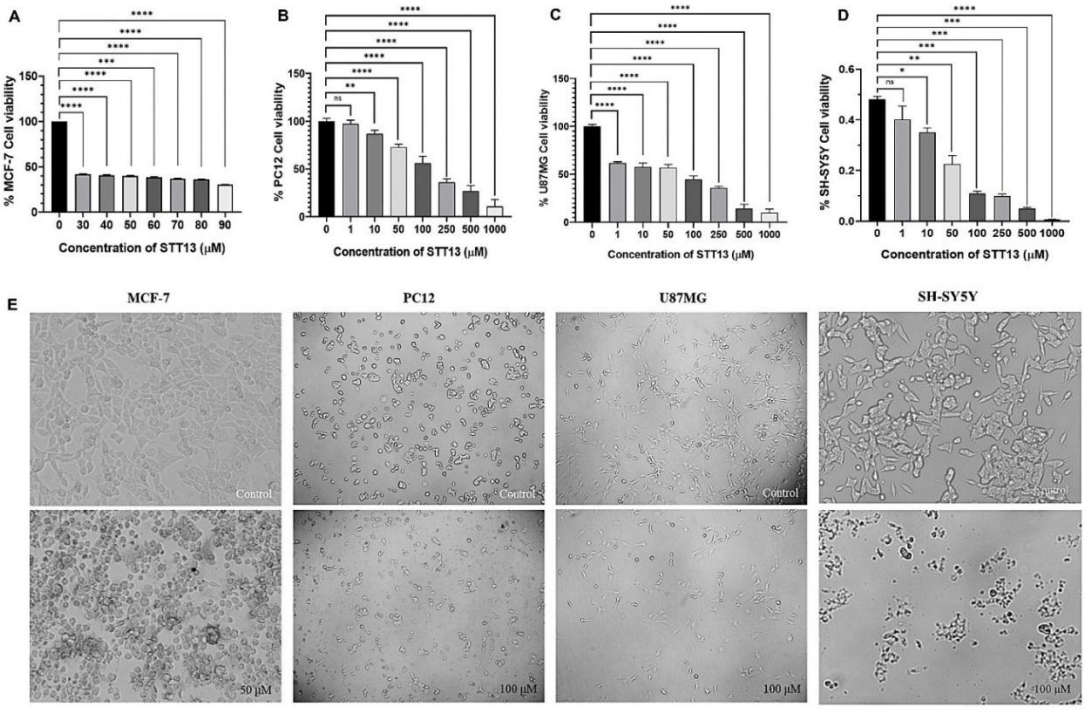

Figure 2.10. *In vitro* cytotoxicity of compound **STT13** on human breast cancer cells (MCF-7), rat-derived neural phaeochromocytoma cells (PC12), human glioblastoma cells (U87MG) and human neuroblastoma cells (SH-SY5Y) after 24 h. A) Percent cell viability vs. concentration graph of compound **STT13** for MCF-7 cells. Data are expressed as mean ± SEM (n = 3). Statistical significance: *** P < 0.001, **** P < 0.0001 vs. control. B) Percent cell viability vs. concentration graph of compound **STT13** for PC12 cells. Data are expressed as mean ± SEM (n = 4). Statistical significance: ns not significant, ** P < 0.01, **** P < 0.0001 vs. control. C) Percent cell viability vs. concentration graph of compound **STT13** for U87MG cells. Data are expressed as mean ± SEM (n = 4). Statistical significance: **** P < 0.0001 vs. control. D) Percent cell viability vs. concentration graph of compound **STT13** for SH-SY5Y cells. Data are expressed as mean ± SEM (n = 3). Statistical significance: **** P <

0.0001 vs. control. E) Inverted microscopic image of MCF-7, PC12, U87MG and SH-SY5Y cells treated with compound **STT13** at 0 μM (control) and 100 μM concentrations (50 μM in case of MCF-7).

However, visual inspection of the cellular morphology showed that the MCF-7 cells were lysed with appreciable loss of morphology (with the appearance of apoptotic bundles) on treatment with compound **STT13** at a concentration of 50 μM for 24 h (Figure 2.10D, first panel). On the contrary, as shown in Figure 2.10B and 2.10C, though the cytotoxicity of compound **STT13** against PC12 cells (GI_{50} = 99.83 ± 0.04 μM) and U87MG cells (GI_{50} = 68.69 ± 0.21 μM) was low to moderate, it showed some dose-dependence; interestingly, 50% or less viability of the cells was achieved between concentrations of 100 μM and 250 μM. Comparative analysis of untreated and compound **STT13**-treated PC12 cells and U87MG astrocytes by inverted microscopy (Figure 2.10D, second and third panel) showed decrease in morphologically intact viable cells and astrocytes on treating the cells with compound **STT13**. At concentrations above 250 μM, it resulted in augmented cell death and complete damage of cell morphology and behavior. It can be inferred from this fact that the SHP2 inhibitory effect of compound **STT13** has correlation with the mortality of SHP2-driven GBM cells like U87MG as well as neural cells like PC12, though further investigation is warranted. Incidentally, compound **111675** did not show any antiproliferative activity up to a test concentration of 130 μM.

2.3.3.4.2. Colony formation and scratch wound healing assay of compound STT13

Compound **STT13** was evaluated for its effect on the proliferation capacity of MCF-7 cells through a colony formation assay [155]. It showed appreciable inhibition of colony growth of U87MG cells as seen by crystal violet staining of the cells upon an incubation of 7 days (**Figure 2.11A**). Docetaxel was used as the internal standard. Treatment with

5 μM of compound **STT13** resulted in a significant decrease in the clonogenic number and formation rate of U87MG cells (**Figure 2.11C** and **Table 2.10**).

Scratch wound healing assay is done to evaluate the effect of any compound on the migration capability of tumor cells [128]. Cell migration is one of the major causes for invasion and metastasis [156] and antimigratory property is desirable in cancer chemotherapeutic agents. Moreover, SHP2 is known to promote growth factor-induced cell migration via downregulation of focal adhesion kinase (FAK) [157]. Compound **STT13** was found to potentially inhibit migration of MCF-7 cells as shown in **Figure 2.11B**. Treatment with 5 μM of compound **STT13** caused 44.2% closure of the scratch wound after a period of 24 h hence indicating its anti-migratory effect in sub-GI_{50} dose (**Figure 2.11D** and **Table 2.10**).

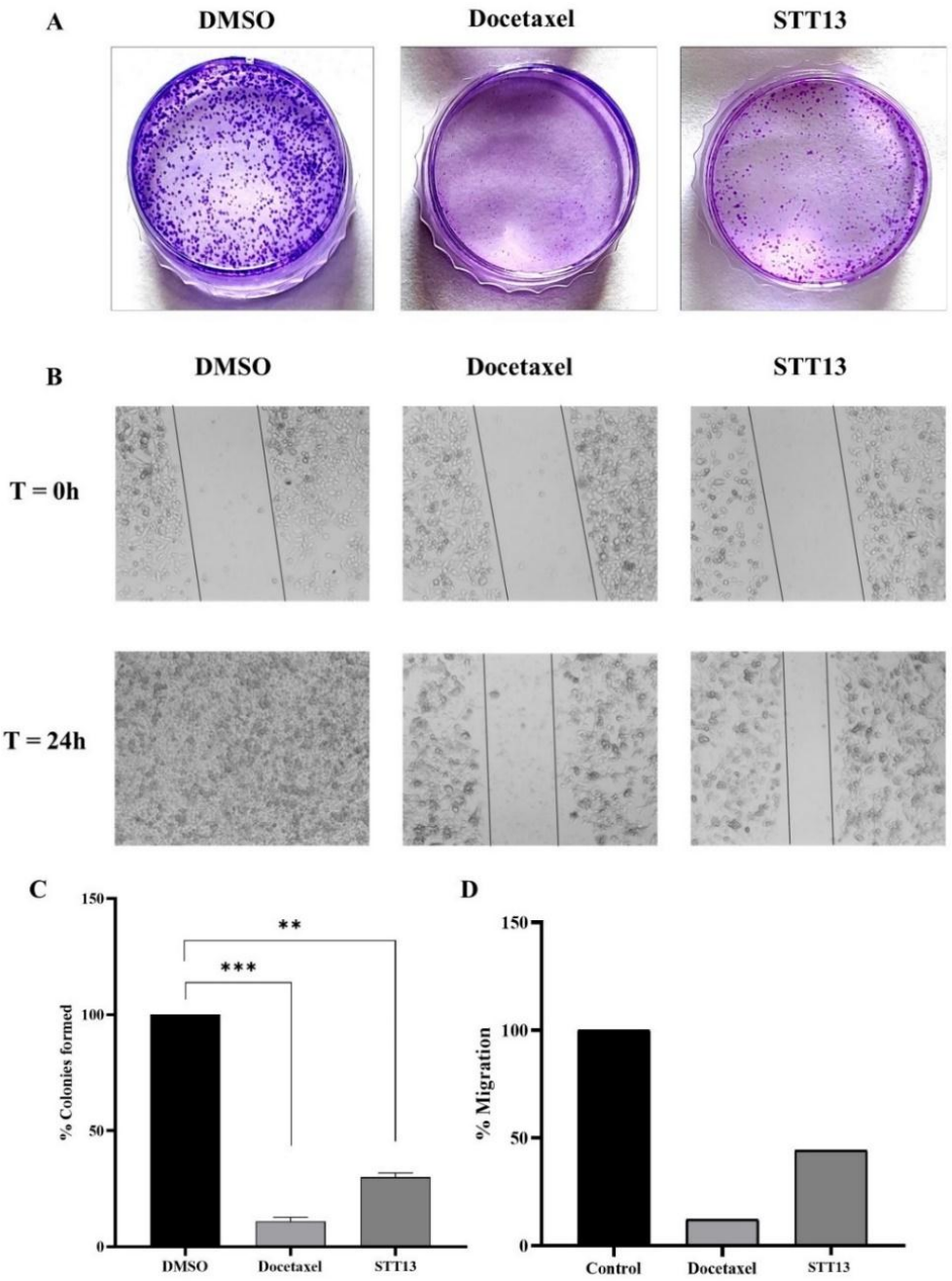

Figure 2.11. A) Inhibition of colony formation of MCF-7 cells by compound **STT13** and docetaxel (reference standard) as compared to untreated cells (DMSO control) after an incubation of 7 days. B) Inhibition of migration of MCF-7 cells by compound **STT13** and docetaxel (reference standard) as compared to untreated cells (DMSO control) at 0 h and 24 h (magnification, 4x). C) Histogram quantifying the % colony formed (n = 3). ** $P < 0.01$, *** $P < 0.001$ versus DMSO. D) Histogram quantifying the % migration.

Table 2.10. Colony formation and wound closure data of compound **STT13** and docetaxel

	DMSO	**Docetaxel[c]**	**STT13**
% Colony formation[a]	100	10	28
% Wound closure[b]	100	12.2	44.2

[a] After 7 day incubation; [b] 24 h after creating scratch wound; [c] Used as reference standard

2.3.3.4.3. Annexin binding assay for detection of cellular apoptosis

In order to derive some mechanistic understanding for the antiproliferative effect of compound **STT13** in cancer cells, few estimations were done by flow cytometry in U87MG cells. Cell apoptosis was detected by Annexin V-FITC and Propidium Iodide (PI) staining [130] of U87MG cells upon treatment with compound **STT13** and detecting cellular apoptotic events at different stages viz. live (Q1), early apoptotic (Q2), late apoptotic (Q3) and necrotic (Q4) phases (**Figure 2.12A** and **2.12B**) [129]. It was observed that after 15 min of incubation post-treatment with compound **STT13**, there were 40.6% viable cells, 43.8% cells in Q2 phase, 15.0% cells in Q3 phase and 0.6% cells in Q4 phase (**Figure 2.12C**). Treatment with compound **STT13** increased the early apoptotic arrest of U87MG cells and decreased the percentage of live cells when compared to untreated ones (25.2% and 59.1% respectively).

2.3.3.4.4. Cell cycle analysis by flow cytometry

The effect of the compound on the cell cycle of U87MG cells was studied via a univariate analysis of the DNA content of the treated and untreated cells at a single time-point (i.e., 'snapshot' measurement) using PI, to estimate which phase of the cell proliferation cycle i.e., G1, S, and G2/M phase is being targeted by the test compound [131, 158]. The treatment with compound **STT13** induced significant changes in the cell cycle distribution of the U87MG cells (**Figure 2.12E-2.12H**). Compared to the control group (32.22% in G1 phase, 15.85% in S phase, and 31.03 % in G2/M phase), the treated group showed a higher proportion of cells in G1 (54.84%) & S (26.84%)

phases and less proportion in G2/M phase (14.95%). This indicates a direct inhibition of DNA synthesis and a possible loss of aneuploidy, which is essential for tumorigenesis and tumor progression [159, 160].

2.3.3.4.5. Reactive oxygen species (ROS) estimation by flow cytometry

Reactive oxygen species (ROS) generated due to exogenous or endogenous stimuli, is a major perpetrator in the development and progression of carcinoma [145]. High levels of ROS are detrimental to cancer cells and ultimately lead to tumor cell death [161-163]. Many chemotherapeutic agents that induce apoptosis of the cancer cells are known to increase the production of ROS within the tumor microenvironment (TME) [164]. In the present study, extent of ROS generation was estimated using the cell-permeable redox-sensitive dye H_2DCFDA. The analysis of ROS levels of U87MG cells treated with an IC_{50} dose of compound **STT13** revealed a 6.55% increase in DCFDA-positive cells in comparison with control. Likewise, increased mean fluorescence intensity (MFI)-positive cells were observed in compound **STT13** (10.36%) with respect to control (6.45%) (**Figure 2.13A-2.13D**).

2.3.3.4.6. Mitochondrial membrane potential (MMP) estimation by flow cytometry

Mitochondrial membrane potential (MMP, $\Delta\psi_m$) is an important marker for cancer cell health via an operational mitochondrial electron transport. Many anticancer drugs induce early apoptosis of cancer cells through a loss of the mitochondrial membrane integrity. We have investigated the effect of compound **STT13** on the $\Delta\psi_m$ of U87MG cells by using the cationic mitochondria-permeant dye JC-1 which is known to accumulate in the mitochondria and form J-aggregates at high MMP. Treatment of U8MG cells with IC_{50} dose of compound **STT13** lead to loss of mitochondrial integrity as seen by the decreased fluorescence intensity (91.80%) with respect to untreated

control group (100%). Further, a direct increase (~22%) in the relative percentage of low MMP mitochondria was also observed (**Figure 2.13E-2.13H**).

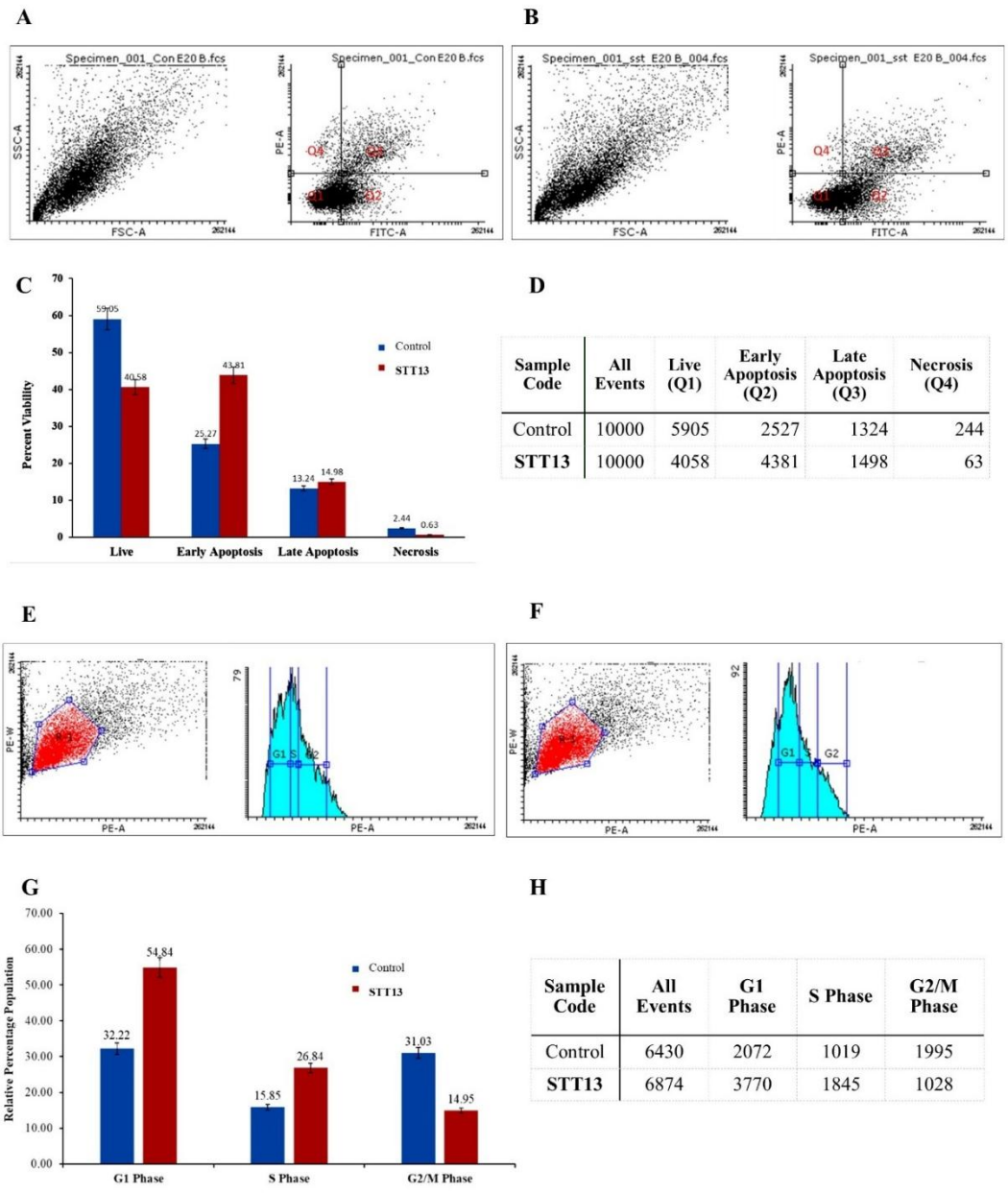

Sample Code	All Events	Live (Q1)	Early Apoptosis (Q2)	Late Apoptosis (Q3)	Necrosis (Q4)
Control	10000	5905	2527	1324	244
STT13	10000	4058	4381	1498	63

Sample Code	All Events	G1 Phase	S Phase	G2/M Phase
Control	6430	2072	1019	1995
STT13	6874	3770	1845	1028

Figure 2.12. Flow cytometric analysis of apoptosis and cell cycle of U87MG cells upon treatment with the IC_{50} dose of compound **STT13**. A) Cell scatter plot (left panel) indicating side scatter (SSC) parameter versus forward scatter (FSC) parameter and propidium iodide (PI) fluorescence versus Annexin V-FITC fluorescence dot plot (right panel) for untreated U87MG cells (control) showing live (Q1), early apoptotic (Q2), late apoptotic (Q3) and necrotic (Q4) cell populations. B) Cell scatter plot (left panel) indicating side scatter (SSC) parameter versus forward scatter (FSC) parameter and propidium iodide (PI) fluorescence versus Annexin V-FITC fluorescence dot plot (right panel) for U87MG cells treated with compound **STT13**. C) Percent viability histogram

showing different phases of apoptosis as induced by compound **STT13** with respect to untreated cells (control). D) Cellular events at different stages of apoptosis measured by flow cytometry. E) Histogram of untreated U87MG cells (control) stained with PI showing distribution of DNA content at the various cell cycle phases. F) Histogram of U87MG cells treated with IC_{50} dose of compound **STT13** and stained with PI showing distribution of DNA content at the various cell cycle phases. G) Relative percentage of viable population of U87MG cells at G1, S and G2/M phases upon treatment with IC_{50} dose of compound **STT13** with respect to untreated cells (control). H) Cellular events at different phases of cell cycle measured by flow cytometry.

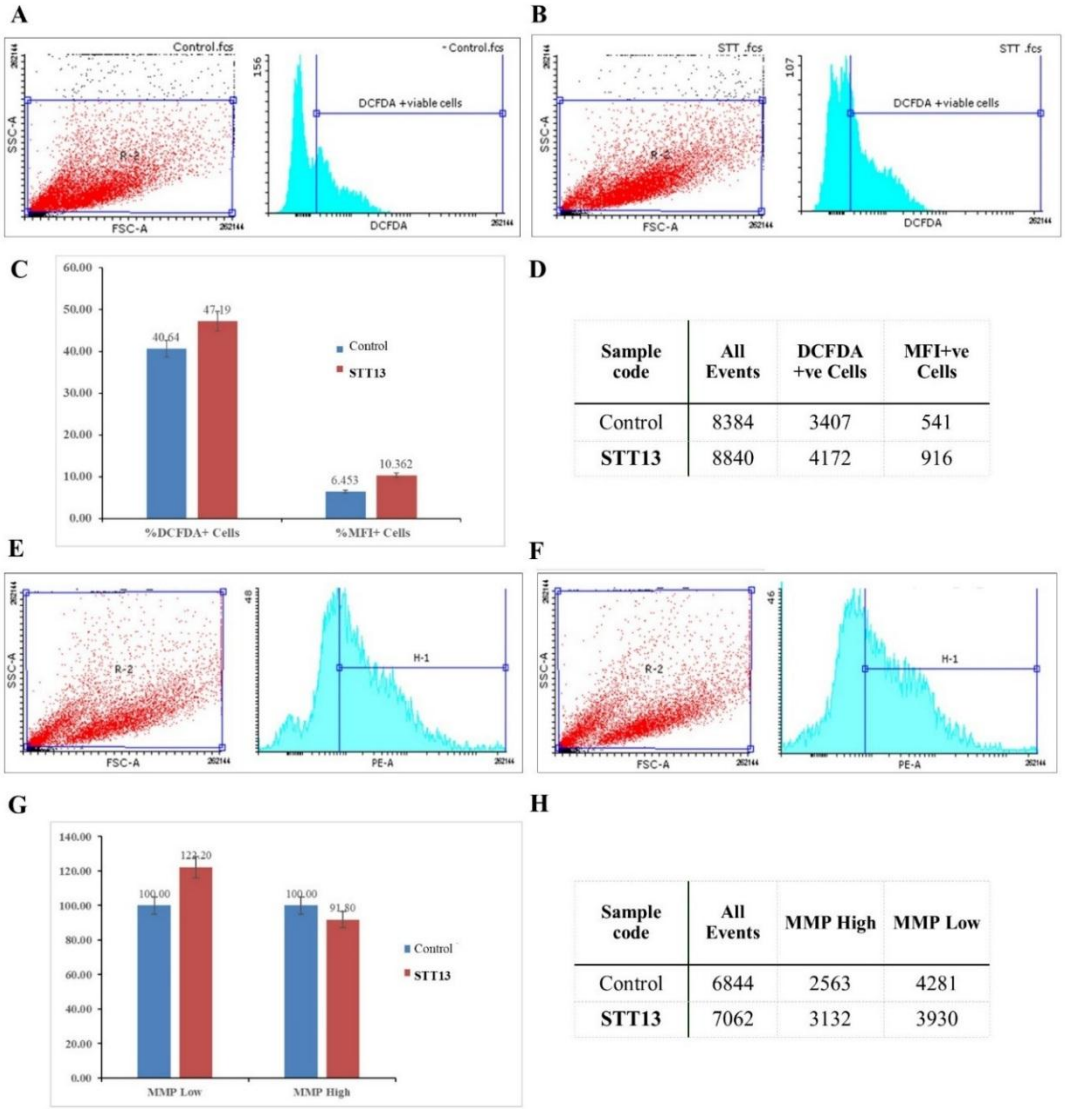

Sample code	All Events	DCFDA +ve Cells	MFI+ve Cells
Control	8384	3407	541
STT13	8840	4172	916

Sample code	All Events	MMP High	MMP Low
Control	6844	2563	4281
STT13	7062	3132	3930

Figure 2.13. Flow cytometric estimation of reactive oxygen species (ROS) and mitochondrial membrane potential (MMP) of U87MG cells upon treatment with the IC_{50} dose of compound **STT13**. A) Cell scatter plot (red) indicating side scatter (SSC) parameter versus forward scatter (FSC) parameter and histogram (blue) of untreated U87MG cells (control) stained with H_2DCFDA showing the cell counts in Y-axis versus the H_2DCFDA intensity in X-axis. B) Cell scatter plot (red) indicating side scatter (SSC) parameter versus forward scatter (FSC) parameter and histogram (blue)

of U87MG cells treated with IC_{50} dose of compound **STT13** stained with H_2DCFDA showing the cell counts in Y-axis versus the H_2DCFDA intensity in X-axis. C) Histogram of %DCFDA+ cells and %MFI+ cells upon treatment with compound **STT13** with respect to untreated cells (control). D) Cellular events at different stages of ROS generation measured by flow cytometry. E) Cell scatter plot (red) indicating side scatter (SSC) parameter versus forward scatter (FSC) parameter and histogram (blue) of untreated U87MG cells (control) stained with JC-1 dye showing the cell counts in Y-axis versus the J-aggregate intensity in X-axis. F) Cell scatter plot (red) indicating side scatter (SSC) parameter versus forward scatter (FSC) parameter and histogram (blue) of U87MG cells treated with IC_{50} dose of compound **STT13** stained with JC-1 dye showing the cell counts in Y-axis versus the J-aggregate intensity in X-axis. G) Relative population of U87MG cells having different extent of mitochondrial depolarization i.e., 'MMP Low' and 'MMP High' upon treatment with IC_{50} dose of compound **STT13** with respect to untreated cells (control). H) Cellular events at different extent of mitochondrial depolarization measured by flow cytometry. R-2 indicates the gate on the main cell population that was analysed here.

It can be inferred from the flow cytometric analysis of compound **STT13** in U87MG cells, that the compound is an inducer of apoptosis by promoting the early apoptotic phase of cell death and simultaneously causing a decrease in the percentage of live cells. At a single time point, it caused an appreciable delay in the G1 and S phases of U87 cells as compared to untreated control cells indicating direct inhibition of DNA synthesis and a possible loss of aneuploidy, which is essential for tumorigenesis and tumor progression [159, 160]. An increase in ROS in the U87 cells treated with compound **STT13** implied enhancement in oxidative stress in the cells ultimately leading to cell death via apoptosis. Finally, apoptosis of the U87MG cells was enhanced by compound **STT13** via a reduction in the $\Delta\psi_m$. as seen by the decrease in the red/green fluorescence intensity ratio.

2.3.3.5. *In vivo* studies

2.3.3.5.1. Acute oral toxicity study in female Wistar rats

Encouraged by the acceptable *in vitro* efficacy of compound **STT13** against SHP2 enzyme and MCF-7 cells, it's *in vivo* safety was evaluated by conducting an acute oral

toxicity study on adult female Wistar rats in accordance with the OECD Guideline 423 (Acute Toxic Class Method) [132] to determine its median lethal dose i.e., LD_{50}. No animal was found dead or in moribund state within or after 14 days at the highest dose of 2000 mg/kg body weight (BW) indicating compound **STT13** was safe for all the animals with its LD_{50} being >2000 mg/kg. Further, no external signs of toxicity were observed in any animal nor in the first 4 h post dosing neither in the subsequent 14 days; the vital signs and behavioural pattern of all groups were also normal (**Table 2.11**). The body weight is the primary index of the general well-being of an animal and any changes in this parameter upon exposure to a foreign substance may be construed as a sign of plausible toxicological effects [165, 166]. Accordingly, this parameter of the animals in the test and control groups were determined and statistical analysis by two-way ANOVA revealed no significant differences in the body weight among the groups ($[F(2,30) = 8.848; p > 0.05]$), time ($[F(2,30) = 0.0602; p > 0.05]$) and their interaction ($[F(2,30) = 0.01858; p > 0.05]$).

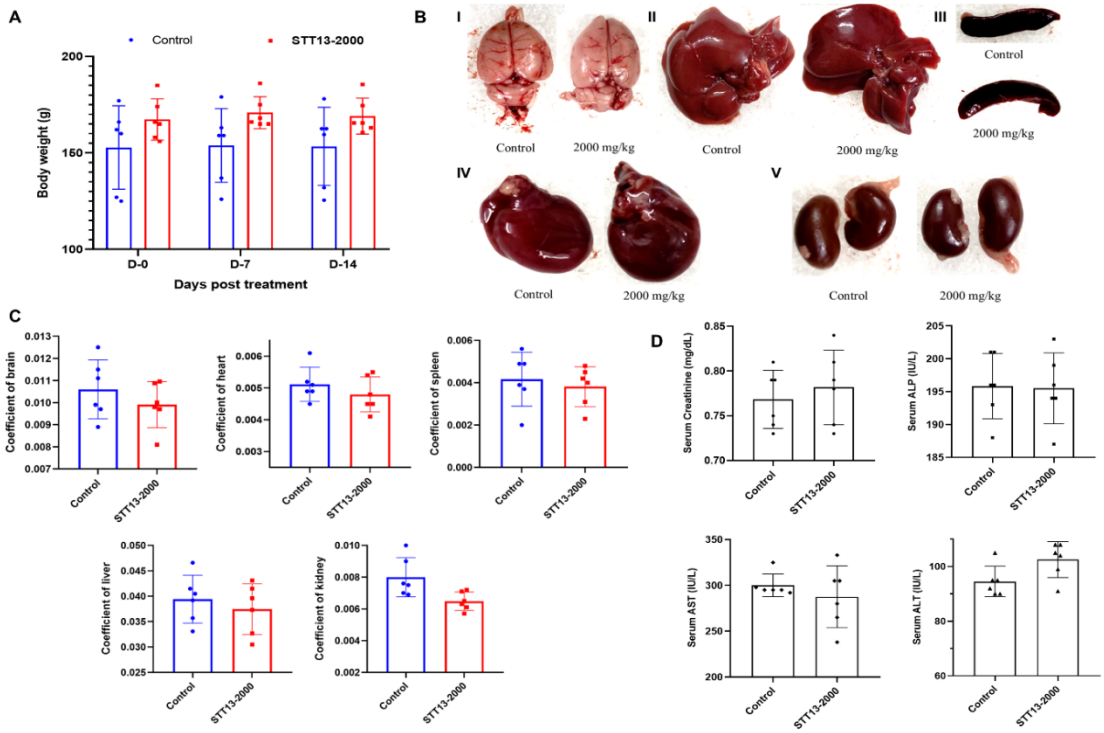

Figure 2.14. Acute oral toxicity study of compound **STT13** in adult female Wistar rats (in accordance with OECD Guidelines 423). A) Effect of single-dose oral administration of compound **STT13** (at dose of 2000 mg/kg BW) on body weight rats at pre-treatment, Day-7 and Day-14. (Two-way ANOVA followed by Bonferroni post hoc test). B) Representative macroscopic photographs showing normal morphology of brain (I), liver (II), spleen (III), heart (IV) and kidneys (V) of animals after single-dose administration of vehicle (control) and 2000 mg/kg BW of compound **STT13** at the end of day 14. C) Effect of single-dose oral administration of compound **STT13** 2000 mg/kg BW on organ coefficient of the brain, heart, liver, kidneys, and spleen at the end of the experiment. D) Effect of single-dose oral administration of compound **STT13** (2000 mg/kg BW) on serum concentration of creatinine, ALP, AST and ALT at the end of the experiment. All values are in mean ± SD (n = 6 female rats/group). (Paired parametric t-test).

Table 2.11. General observation and behavioural analysis during the first 4 h and 24 h after single-dose administration of compound **STT13** (2000 mg/kg BW) in female Wistar rats (n = 6 female rats/group).

Observations	Control		STT13 (2000 mg/kg BW)	
	4 h	24 h	4 h	24 h
Skin and fur	NC	NC	NC	NC
Eyes	NC	NC	NC	NC
Mucous membrane	NC	NC	NC	NC
Salivation	NC	NC	NC	NC
Diarrhoea	NO	NO	NO	NO
Lethargy	NO	NO	NO	NO
Sleep	N	N	N	N
Coma	NO	NO	NO	NO
Tremors and convulsions	NO	NO	NO	NO
Behaviours pattern & somatosensory activity	N	N	N	N

Note: N-Normal, NO-Not observed, and NC-No change.

In addition to body weight, the organ weight of animals is an important test parameter in *in vivo* toxicological studies; changes in the weight of most vital and highly perfused organs in the animal after treatment with a test substance indicates possible and subsequent morphological changes in the organs and the vitals of the animal leading to systemic toxicity [167]. Hence it is important to measure this parameter during the toxicological screening of any test compounds. Organ coefficient is an accurate way of determining any changes in the organ weight of a test animal with respect to any changes in its body weight throughout the course of the toxicological experiments [168]. The effect of single-dose oral administration of compound **STT13** (2000 mg/kg BW) on the organ coefficient of vital organs i.e., brain, heart, liver, kidneys and spleen were determined post sacrifice of the animals and is depicted in **Figure 2.14C**. From the figure we can see that compound **STT13** does not cause any significant changes in the organ coefficient of these highly perfused organs in any of the groups (statistical analysis by unpaired parametric t-test revealed no significant changes in the organ coefficient of brain, heart, liver, kidneys, and spleen among the groups; [F(5,5) = 1.646;

$p > 0.05$], [$F(5,5) = 1.049$; $p > 0.05$], [$F(5,5) = 1.117$; $p > 0.05$], [$F(5,5) = 4.513$; $p > 0.05$], and [$F(5,5) = 1.832$; $p > 0.05$] respectively) indicating that compound **STT13** is safe for the organs even at the highest test dose of 2000 mg/kg BW. Furthermore, the macroscopic evaluation of the said organs of all groups was done and we found no apparent signs of morphological damage or abnormalities in the organs of the test groups when compared to the vehicle control. **Figure 2.14B** shows the perfused organs of all three groups where the highest dose of 2000 mg/kg BW did not show any toxicological effects.

As per the OECD 423 guidelines, we also checked for any tissue damage caused by our test compound to the above mentioned organs through a histopathological study [169]. As can be seen from the photomicrographs shown in **Figure 2.15**, a single oral administration of a dose 2000 mg/kg BW of compound **STT13** exhibited no damage to the tissue architecture of the brain, liver, heart, spleen and the kidneys with no histopathological changes in any of these highly perfused organs at the end of the experiment i.e., on the 14^{th} day. There were presence of normal neurons in the brain cortex, normal hepatocytes with acidophilic cytoplasm, intact vesicular nucleus radiating from the central vein surrounding the portal tract and proper sinusoids in the liver sections, normal myocardial muscle bundles with thin fibro collagenous stroma in the heart sections, normal lymphatic nodules of white pulp, splenic cords of red pulp, and the spleen trabecula in the spleen sections and finally, normal renal tubules in the kidney sections in all the study groups.

Next, we evaluated the toxicological effect of our test compound **STT13** on the biochemical and haematological parameters of the animals by estimating any changes in the serum measurement and whole blood collected from the animals at the end of the

experiments on day 14. Serum creatinine is a measure of kidney health and normal renal function [170], whereas alkaline phosphatases (ALP), aspartate transaminase (AST) and alanine transaminase, aka alanine aminotransferase (ALT) are crucial enzymes secreted by the liver which have been used clinically to screen the proper functioning of the liver [171]. Any alteration in the level of serum AST and ALT is correlated clinically to hepatic necrosis and possible hypertrophy of hepatocytes or any other disease conditions of the liver. ALP, on the other hand, are a group of related phosphatase isoenzymes and abnormal serum levels are generally due to liver conditions or obstruction in the bile ducts. All measurements and statistical data of the biochemical measurements for serum creatinine (mg/dL), ALP (IU/L), AST (IU/L) and ALT (IU/L) are shown in **Figure 2.14D**. We can observe from the figure that there were no substantial changes in the serum level of the enzymes in any of the groups when compared to control (statistical analysis by paired parametric t-test revealed no significant changes in the serum level of creatinine, AST, ALT, and ALP among the groups; $p > 0.05$ in all cases.

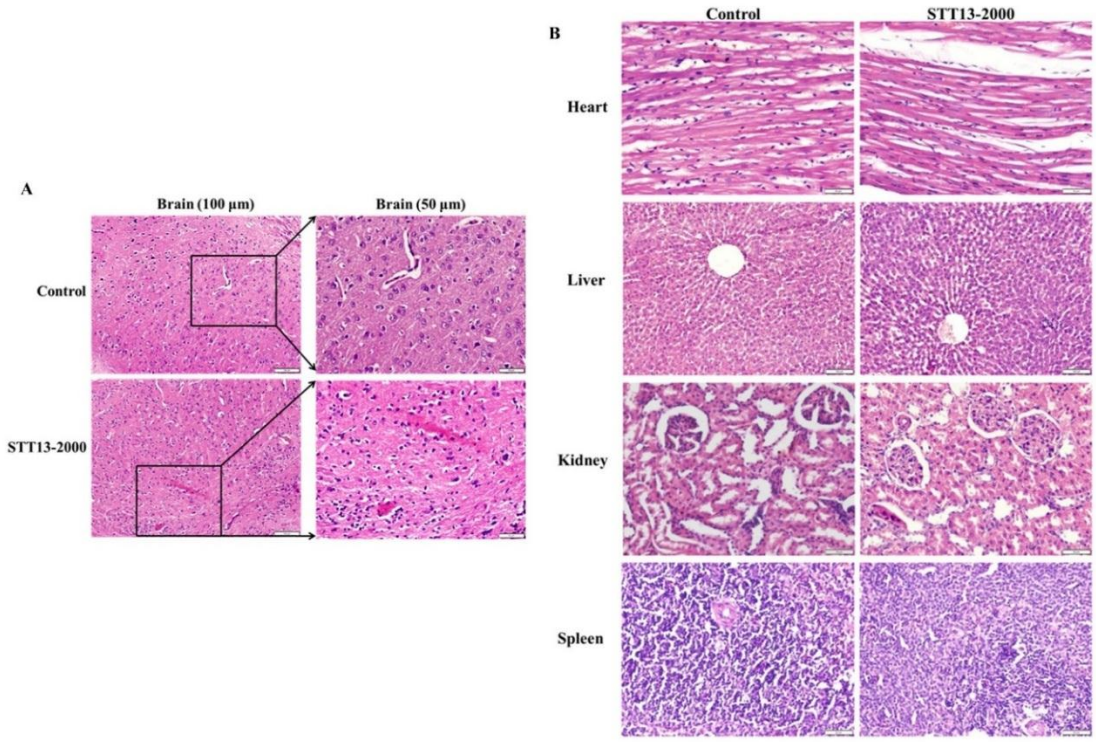

Figure 2.15. A) Effect of single-dose oral administration of compound **STT13** (at a dose of 2000 mg/kg BW) along with vehicle control on brain of female Wistar rats and B) on other highly perfused organs viz. heart, liver, kidney, and spleen tissue stained with hematoxylin and eosin (H&E) dye at the end of 14 days.

Lastly, complete blood count (CBC) of all the test groups was done to check for any toxicological effect of compound **STT13** on the haematology of the animals. The estimated values of the haematological parameters (hemoglobin, red blood cell count (RBC), hematocrit (HCT), mean corpuscular hemoglobin (MCH), mean corpuscular volume (MCV), mean corpuscular hemoglobin concentration (MCHC), red blood cell distribution width (RDW), platelet count and white blood cell count (WBC), **Figure 2.16**) after single-dose oral administration of compound **STT13** showed no significant changes or deviations from the control group. From the above findings of the toxicological study, we inferred that the compound is nontoxic and safe at the high oral dose of 2000 mg/kg BW.

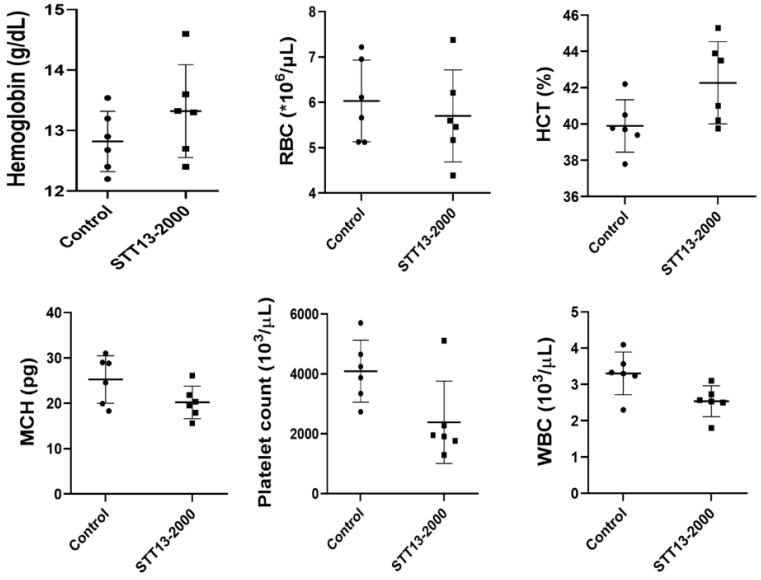

Figure 2.16. Effect of single-dose oral administration of compound **STT13** (2000 mg/kg BW) on CBC of female Wistar rats at the end of 14-day experimental protocol. All values are in mean ± SD (n=6 female mice/ group). (Paired parametric t-test).

2.3.3.5.2. *In vivo* pharmacokinetic studies of compound STT13 in female Wistar rats

A. Calibration curve and linearity in plasma spiked samples

The standard calibration curve of compound **STT13** in plasma spiked samples (obtained from female Wistar rats) was done by preparing serial dilutions (viz. 50, 25, 12.5, 6.25, 3.125 and 1.5625 µM) of the test compound **STT13** in plasma in triplicate. These were run in RP-HPLC system using a previously developed and validated method having the following process parameters: mobile phase: 100% acetonitrile, flow rate: 0.7 mL/min, injection volume: 20 µL, total runtime: 10 min. The peak AUC of each dilution plotted against the corresponding concentration as a linear function gave a calibration curve (**Figure 2.17**) obtained as a straight line which was used to calculate the average regression equation and correlation coefficient (**Table 2.12**) by the appropriate linear least-squares regression analysis. The averaged regression equation for the calibration curve was y = 22850x + 37549 with a regression coefficient

i.e., R^2 of 0.9991. These equations and values were used to calculate any unknown concentration of compound **STT13** in subsequent HPLC experiments.

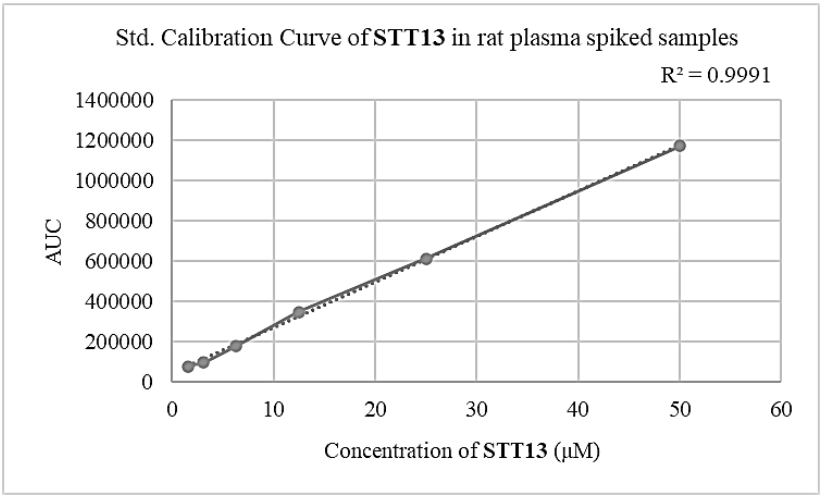

Figure 2.17. Calibration curve of compound **STT13** in rat plasma spiked samples obtained by serial dilution method.

Table 2.12. Regression statistics of compound **STT13** calculated from the calibration curve in plasma spiked samples

Regression statistics	**STT13**
Average regression equation	y = 22850x + 37549
Linearity range (µM)	1.5625 to 50
Observations	6
LOQ (µM)	6.4 (RSD ± 0.16%)
LOD (µM)	2.1 (RSD ± 0.11%)
Intercept	37549
Slope	22850
Correlation coefficient (R^2)	0.9991
Adjusted R^2	0.9989
%RSD of R^2	0.020
$SD_{y/x}$	14534

LOQ: limit of quantification; LOD: limit of detection; SD: standard deviation; RSD: relative standard deviation. %RSD = (SD/Mean) × 100

B. Plasma stability assay of compound STT13

The stability of compound **STT13** in rat plasma was determined by incubating a specific concentration of the compound in plasma for different time periods e.g., 0, 10, 20, 30, 60, 120 min in separate Eppendorf tubes. After the appropriate incubation time,

plasma proteins were precipitated from each sample by the addition of ACN. The samples were centrifuged at 6000 rpm or more for 20 mins and depletion of test compound was monitored using RP-HPLC by applying the std calibration curve as detailed above. The natural logarithm of % compound **STT13** remaining at each time point was determined (**Table 2.13**) and plotted in a graph (**Figure 2.18**).

Table 2.13. Plasma stability data for compound **STT13** in rat plasma

Incubation time (min)	AUC	% Remaining[a]	ln (%rem)[b]
0	548850	100.00	4.60517
10	532569	97.00	4.57471
20	417365	76.00	4.33073
30	409640	74.63	4.31254
60	409537	74.61	4.31227
120	406991	74.10	4.30542

[a] % remaining = $100\times(AUC_{Tn}/AUC_{T0})$, T_n=any incubation time, T_0=0 min incubation; [b] natural logarithm of % **STT13** remaining

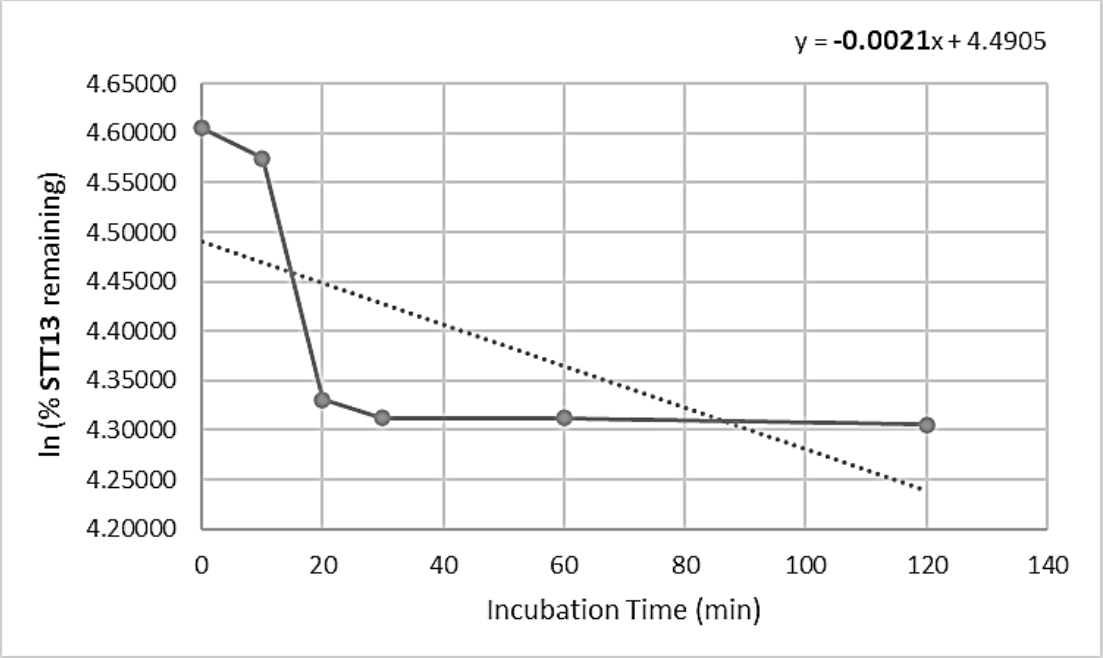

Figure 2.18. Natural logarithm of % compound **STT13** remaining vs. incubation time (min) graph

The *in vitro* plasma half-life ($T_{1/2}$) was calculated using the expression:

$$T_{1/2}\ (\text{min}) = \frac{ln(2)}{-slope} = \frac{0.693}{-slope}$$

where 'slope' is the slope found in the linear fit of the natural logarithm of the % remaining of the parent compound vs. incubation time (i.e., the graph shown in **Figure 2.18**).

Here, slope = -0.0021 (refer, **Figure 2.18**). So, $T_{1/2}$ = 0.693/0.0021 = 330 min = 5.5 h.

Thus, the *in vitro* plasma half-life of compound **STT13** is 5.5 h.

C. *In vivo* PK study of compound STT13

The in vivo pharmacokinetic study of compound **STT13** was performed based on the developed and validated RP-HPLC method and by utilizing the standard calibration curve as devised from the plasma spiked samples. The plasma drug concentration (Cp) at various time intervals was determined by the standard calibration curve (as described above) and is furnished in **Table 2.14**. From this data, a dose-response curve was obtained (**Figure 2.19**) which displays oral absorption kinetics with a prominent absorption phase, a post-absorption phase and an elimination phase.

Table 2.14. Plasma concentration (Cp, in μM) of compound **STT13** at different time points (h) as determined by std. calibration curve

Time (h)	Cp (μM)
0	0
0.5	0.22949
1	0.58328
2	0.59321
4	0.53032
8	0.33768
12	0.3403
24	0.30118

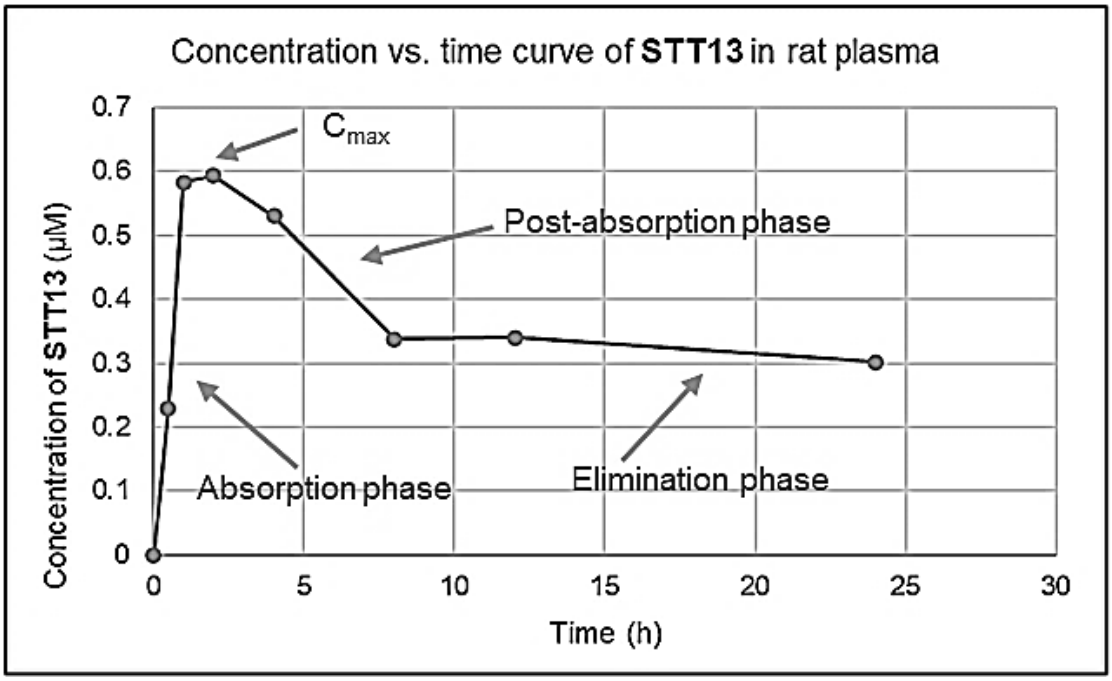

Figure 2.19. Plasma concentration (μM) of compound **STT13** vs. time curve

Further, from the Cp vs. time data, the PK parameters were calculated by extravascular non-compartment model using PKSolver add-in feature of MS Excel. The parameters and their respective values are summarized in **Table 2.15**.

Table 2.15. PK parameters after oral administration of compound **STT13** (10 mg/kg, p.o.)

Parameter	Unit	Actual Value	Predicted value[a]	TNO155[b]
$t_{1/2}$	h	88.32	10.8	34
T_{max}	h	2	0.9	1.1
C_{max}	μmol/L (μM)	0.59321	3.88	NA
AUC_{0-24}	(μmol/L)*h	8.9132	NA	1.09
MRT	h	124.9	NA	NA

[a] PK values were predicted for oral administration using online server Deep-PK, developed by the Biosig Lab (https://biosig.lab.uq.edu.au/deeppk/prediction, accessed on 10th June, 2024) and Pharmacokinetic Simulator (http://www.vulpinescience.co.uk/uploads/MedChem%20Calculators_Ver3.2/MedChem%20Calculators.htm, accessed on 10th June, 2024), [b] Experimental PK parameters of **TNO155** as determined after 14 days by a variable oral dose schedule in 118 patients for various advanced solid tumors (Clinical Trial No.: NCT03114319) [172]

From the PK parameters we could infer that compound **STT13** showed quite rapid absorption to the systemic circulation upon oral administration as seen by the relatively short T_{max} of 2 h though the peak plasma concentration achieved with a dose of 10

mg/kg BW was only 0.59 μM. The high elimination half-life i.e., $t_{1/2}$ of 88 h and a MRT of almost 125 h indicates slow removal of the compound from the body which ultimately means more time for the unmetabolized drug to exert its effect on the living system thereby requiring a relaxed dosing interval. A comparison with the predicted PK values of compound **STT13** revealed a similar correlation between the T_{max} and $t_{1/2}$ of the compound, though the predicted values were lower. Further, the experimental PK parameters of compound **TNO155** (aka batoprotafib)**,** a selective, allosteric, oral inhibitor of SHP2 (IC_{50} = 0.011 μM) were compared with those of compound **STT13**. The comparison was done owing to the fact that **TNO155** is a clinically advanced SHP2 inhibitor and it shares few structural attributes with our lead compound **STT13** (viz., presence of a thioether linkage and a central heterocyclic ring). The PK values of compound **TNO155** were determined in a 14 day study by a variable oral dose schedule in 118 patients for various advanced solid tumors (Clinical Trial No.: NCT03114319) [172]. Compound **TNO155** showed a median $t_{1/2}$ of 34 h and a T_{max} of 1.1 h indicating a similar relationship between these two crucial parameters like compound **STT13**. Thus, it can be largely inferred that our lead compound **STT13** displays pharmacokinetic profile closely comparable to the clinical SHP2 inhibitors.

2.3.4. Computational studies

2.3.4.1. Molecular docking of compounds STT01-STT21 within the tunnel allosteric site of SHP2 (PDB ID: 5EHR)

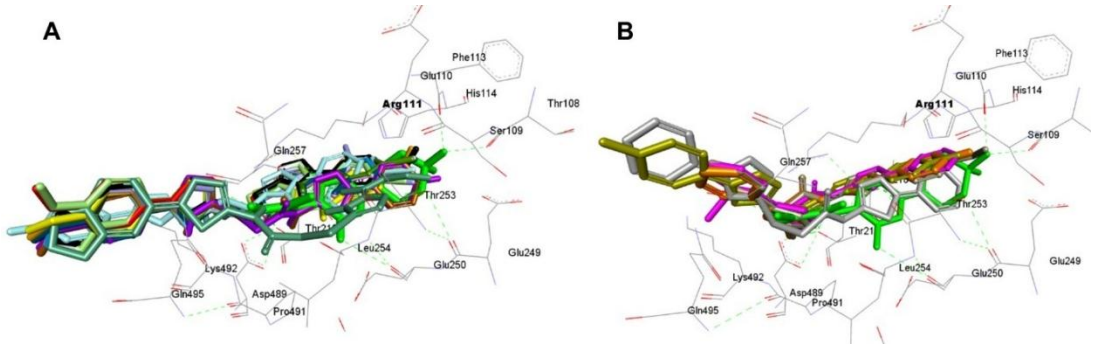

Figure 2.20. Superimposed image of compounds **STT01-STT21** with **SHP099** within the tunnel allosteric site of SHP2 (PDB ID: 5EHR). A) Cluster image of compounds **STT04** (red), **STT05** (blue), **STT07** (light blue), **STT08** (yellow), **STT09** (cyan), **STT10** (brown), **STT11** (purple), **STT12** (orange), **STT13** (black), **STT14** (light blue), **STT16** (deep green), **STT17** (light green), **STT18** (white), **STT19** (light purple), **STT20** (dark blue), **STT21** (light red) and **SHP099** (green). B) Cluster image of compounds **STT01** (light grey), **STT02** (light brown), **STT03** (grey), **STT06** (pink) and **STT15** (bottle green) with **SHP099** (green).

Molecular docking studies of compounds **STT01-STT21** in the tunnel allosteric site of SHP2 (PDB ID: 5EHR) was performed by AutoDockTools 4.2 software using a validated protocol wherein **SHP099** (6-(4-amino-4-methylpiperidin-1-yl)-3-(2,3-dichlorophenyl)pyrazin-2-amine) was the co-crystallized ligand (ligand PDB ID: 5OD) and the reference standard. Validation of the docking protocol was achieved through a gold standard pose (GSP) of **SHP099** by its superimposition with the pose of the native co-crystallized ligand i.e., 5OD (RMSD = 1.42 Å). The free energies of binding (in kcal/mol) and the calculated inhibition constants (K_i) are listed in **Table 2.16**. The cluster image of the compounds superimposed within the tunnel allosteric site of SHP2 is shown in **Figure 2.20**, where the compounds have been grouped into two clusters A and B (**Figure 2.20A** and **2.20B**) according to their orientation within the binding site. It can be observed herein that all compounds in cluster A and B oriented themselves

such that the (substituted phenyl)-1,3,4-thiadiazole moiety occupied the opening of the cavity opposite to the allosteric site. Our lead molecule according to *in vitro* IC_{50} data i.e., compound **STT13** ranks 6^{th} in its affinity towards SHP2 with a ΔG of -11.04 kcal/mol (**Table 2.16**).

Briefly, from the ranking order of **Table 2.17**, it can be inferred that the chloro and dichloro substitutions are conducive to better binding and interactions with SHP2 allosteric site as the top 5 molecules (**STT20**: ΔG = -11.94 kcal/mol, **STT21**: ΔG = -11.63 kcal/mol, **STT18**: ΔG = -11.29 kcal/mol, **STT17**: ΔG = -11.17 kcal/mol and **STT19**: ΔG = -11.10 kcal/mol) contain 4-chloro or 2,4-dichloro substitution at centre A. Among these, however, compounds **STT20** and **STT21** showed good correlation between *in vitro* IC_{50} value and *in silico* binding energy data. Further, loss of *in silico* binding affinity correlated well with *in vitro* activity in case of compounds **STT02** (IC_{50} = 3.144 ± 0.001 μM, ΔG = -9.72 kcal/mol) and **STT07** (IC_{50} = 2.945 ± 1.668 μM, ΔG = -9.57 kcal/mol). In all the cases, the triazole end i.e., centre A enters the allosteric cavity lined by Arg111, Phe113 and Glu250 where the ligands superimpose nicely with the piperidine ring of compound **SHP099**. Also, all 5 ligands are seen to interact strongly with the catalytic triad via H-bonding, pi-H bonding and van der Waals forces (**Figure 2.20**).

Table 2.16. Molecular docking data of compounds **STT01-STT21**

Compd Code	ΔG (Kcal/mol)	Calc. K_i[a] (nM)	Compd Code	ΔG (kcal/mol)	Calc. K_i[a] (nM)
STT01	-10.06	42.49	**STT12**	-10.74	13.32
STT02	-9.72	74.58	**STT13**	-11.04	8.06
STT03	-10.19	34.09	**STT14**	-10.13	37.37
STT04	-10.43	22.77	**STT15**	-10.19	33.80
STT05	-10.82	11.65	**STT16**	-11.17	6.51
STT06	-9.89	56.26	**STT17**	-10.96	9.24
STT07	-9.57	96.23	**STT18**	-11.29	5.31
STT08	-10.19	33.94	**STT19**	-11.10	7.36
STT09	-10.40	23.94	**STT20**	-11.61	1.77
STT10	-9.73	74.16	**STT21**	-11.63	3.00
STT11	-9.55	100.76	**SHP099**	-10.27	29.34

[a] K_i calculated from the binding energy of poses generated by AutoDockTools 4.2.

Table 2.17. Comparison of experimental and computational SHP2 inhibitory data

In vitro SHP2 Inhibition	**STT13 > STT05 > STT21 > STT06 > STT11 > STT20 > STT14 > STT17 > STT03 > STT10 > STT04 > STT12 > STT08 > STT15 > STT01 > STT09 > STT18 > STT19 > STT07 > STT02 > STT16**
In silico SHP2 (5EHR) binding	**STT20 > STT21 > STT18 > STT16 > STT19 > STT13 > STT17 > STT05 > STT12 > STT04 > STT09 > STT03 > STT08 > STT15 > STT14 > STT01 > STT06 > STT10 > STT02 > STT07 > STT11**

A. Binding data of compound STT20 within the crystal structure of 5EHR

Structural analysis of the 3D and 2D interaction of **STT20** with the tunnel allosteric site of SHP2 (**Figure 2.21A** and **2.22A**) explains its high affinity (ΔG = -11.94 kcal/mol) for the tunnel allosteric site of the enzyme and its relatively strong activity against allosterically activated SHP2 (IC_{50} = 0.913 ± 0.157 μM). The molecule occupies the intended site and half of it consisting of the 2,4-dichlorophenyl-triazole ring overlaps completely with **SHP099**, the native ligand. Due to its longer length, however, its distal end i.e., the *p*-methoxyphenyl-thiadiazole ring extends out of the cavity which results in better occupancy and binding of the molecule with SHP2 residues.

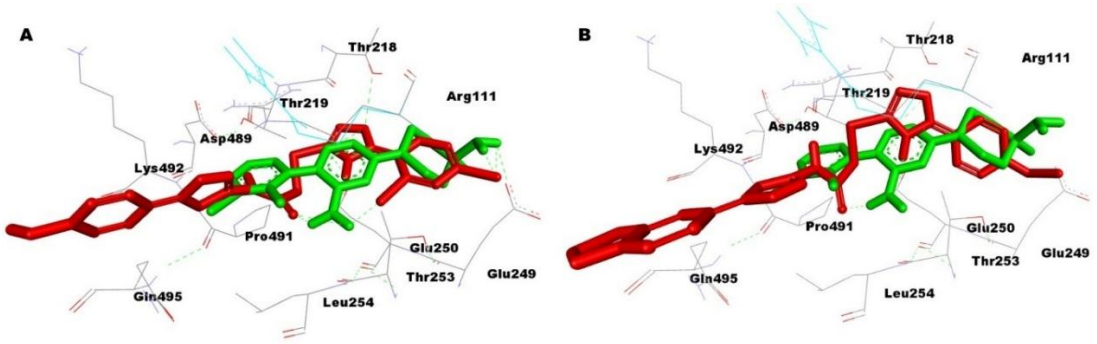

Figure 2.21. A) 3D orientation image of compound **STT20** (red) with **SHP099** (green) in the tunnel allosteric site of 5EHR, B) 3D orientation image of compound **STT13** (red) with **SHP099** (green) in the tunnel allosteric site of 5EHR.

The molecule shows multiple interactions with Arg111, whereby it is stabilized in its most active conformation by a sort of four-pronged tether formed by the following bonds with Arg111: conventional H-bonding with the thioether sulphur atom and the ring nitrogen of thiadiazole moiety, a pi-cation interaction with the triazole ring and a pi-donor hydrogen bond with the dichlorophenyl ring. The triazole ring nitrogen interacts via H-bonding with Leu216 which is a residue of the interdomain linker between C-SH2 and the PTP domain. This shows that **STT20** makes connections extending beyond the tunnel allosteric site. The *p*-methoxy substitution at centre B shows H-bonding with Ser499 of the PTP catalytic domain. As can be seen from **Figure 2.21A**, both ends of the molecule are exposed to the receptor surface with a solvent accessible surface area of 3341.21 $Å^2$. This results in better stabilization of the molecule inside the allosteric cavity of SHP2.

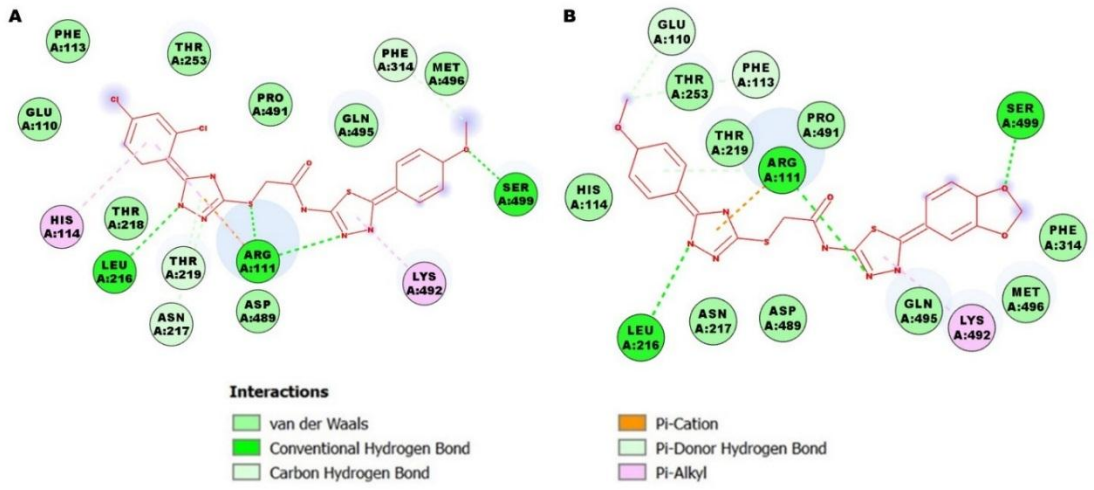

Figure 2.22. A) 2D interaction map of compound **STT20** (red) with the amino acid residues of the tunnel allosteric site of 5EHR, B) 2D interaction map of compound **STT13** (red) with the amino acid residues of the tunnel allosteric site of 5EHR**.**

B. Binding data of compound STT13 within the crystal structure of 5EHR

Figure 2.21B and **2.22B** show the binding pose and interaction map of compound **STT13** (IC_{50} = 0.318 ± 0.001 μM, ΔG = -11.04 kcal/mol) at the tunnel allosteric site of SHP2, a visual inspection of which reveals binding patterns similar as in the case of both the virtual leads (**STT20** and **STT21**). The ligand occupies the tunnel allosteric groove in an overlapping manner with **SHP099** with its benzodioxo end protruding out distally through the opposite end. The compound makes a number of crucial interactive bonds with the residues of the binding site, most prominent among which is its interactions with Arg111. Both the heterocycles interact with Arg111; the triazole ring via pi-cation forces and the thiadiazole ring via conventional H-bonding. The thiadiazole ring makes an additional bond with Lys492 using a Pi-sigma interaction whereas two additional H-bonds are formed with the ring nitrogen atom of the triazole ring (Leu216) and the benzodioxole oxygen atom (Ser499). The polar heteroatoms, including the extra heterocycle i.e., benzodioxole ring are thus important in extending

binding modalities and securing the molecule in its most stable conformation within the site. The *p*-methoxy carbon of the triazole-phenyl ring shows carbon-H bonds with Glu110 and Phe113. The entire complex is further stabilized through a number of van der Waals forces between the molecule and the following residues: His114, Asn217, Thr219, Glu250, Thr253, Leu254, Phe314, Asp489, Pro491, Gln495 and Met496.

2.3.4.2. Molecular dynamics simulation studies for compound STT13

In order to assess the extent and effect of the interactions of our lead compound **STT13** with SHP2 allosteric site, molecular dynamics simulation studies were carried out by Desmond module [109] (Schrodinger Release 2021.1: Desmond Molecular Dynamics System, D. E. Shaw Research, New York, NY, 2021). The simulation was done for 100 ns on Maestro graphical user interface (Maestro, Schrodinger, LLC, New York, NY, 2021) which was also used for the preparation of input files and visualization of results. The simulation interactions diagram for compound **STT13** with SHP2 (PDB ID: 5EHR) is shown in **Figure 2.23** which was analysed to determine the stability of the protein-ligand complex throughout the simulation period of 100 ns as well as to get an idea regarding the various contacts between the ligand and the protein. The root mean square deviation (RMSD) of the protein-ligand complex was analysed to determine the stability of the docked system. The protein and the ligand displayed different interactions throughout the course of the simulation (100 ns) viz. hydrogen bonds, hydrophobic interactions, ionic bonds and water bridges. From **Figure 2.23B**, we could conclude that compound **STT13** mainly stabilized SHP2 by forming hydrophobic interactions (violet histogram bars) with tunnel allosteric residue of SHP2 viz. Arg111 and also with His114, Leu233, Ala237, Leu254, Pro491 and Lys492. It made two ionic connections (red histograms), one with Thr108 and the other with Glu249. Importantly,

compound **STT13** interacted strongly with the tunnel allosteric triad member, i.e., Glu250 via hydrogen bonding (green bar) as well as by forming water bridge (blue bar). Glu250 and Phe113 showed a good degree of contacts with compound **STT13** throughout the simulation timeline (**Figure 2.23C**). In fact, Glu250 interacted with NH group of the ligand's triazole ring for 92% of the total simulation period (**Figure 2.23A**).

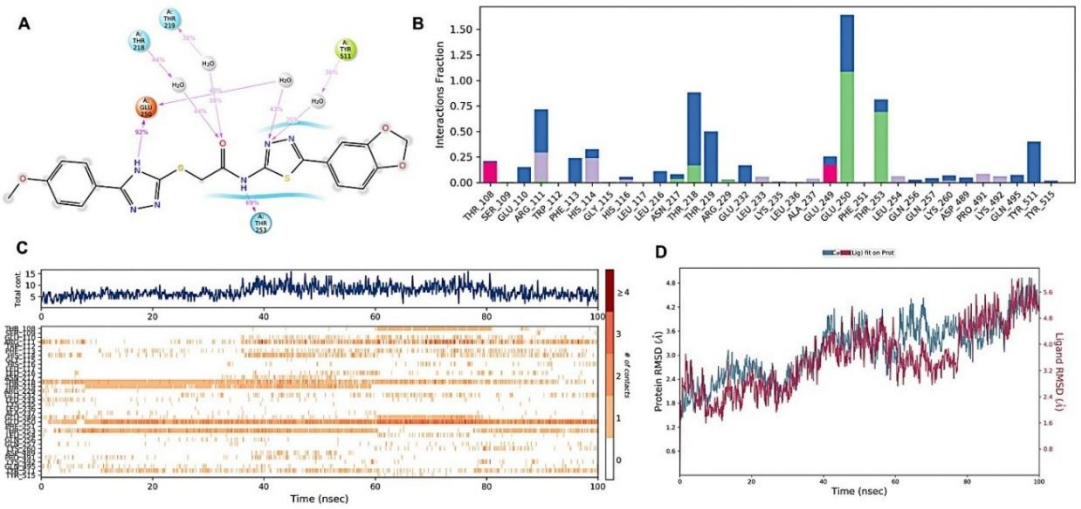

Figure 2.23. Protein-ligand contact diagrams ('simulation interactions diagrams') generated through Molecular Dynamics simulation of compound **STT13** with SHP2 (PDB ID: 5EHR). A) Percent interaction of ligand with protein (represented by purple arrow). Green spheres represent hydrophobic residues, red spheres represent electronegative species, blue spheres represent polar residues and solvent exposed areas are shown in grey. B) Stacked bar chart representing different types of protein-ligand contacts. Green histogram bars indicate hydrogen bond interactions; violet bars represent hydrophobic interactions whereas blue bars represent the water bridges between protein and ligand. Red bars represent ionic interactions. C) Protein-ligand contacts in timeline representation for 100 ns simulation; the top upper panel (blue) shows the number of contacts between protein and ligand throughout the simulation period and the bottom panel (orange) indicates the amino acid residues that interact with ligand at different time frame. D) Protein-ligand RMSD graph. Blue line represents apoprotein and red line represents ligand bound protein.

Analysis of the RMSD graph shown in **Figure 2.23D** tells us that association of SHP2 with compound **STT13** does not cause any significant conformational changes to the protein. Also, the RMSD value changes fall within the acceptable range of 1-3 Å (on an average, the change is of the order of 2.6 Å). Thus, it can be inferred from the MD simulation studies that compound **STT13** showed conserved interactions like H-bonding and hydrophobic interactions with crucial amino acid residues of tunnel allosteric site of SHP2 and conferred better stability to the complex on binding with the enzyme.

2.3.4.3. Predicted ADMETox parameters

The ADMETox properties of the final compounds **STT01**-**STT21** were predicted by Pre-ADMET online server (https://preadmet.webservice.bmdrc.org/, accessed on 23rd November 2022). The predicted ADME and toxicological properties of all compounds are given in **Tables 2.18 and 2.19** respectively. All compounds displayed similar skin permeability with a value around -4. The blood-brain barrier (BBB) permeability ranges from 0.0482 for compound **STT15** to 0.0175 for compound **STT13**. The lead compound **STT13** showed the least BBB permeability as well as very low Caco2 and MDCK permeability. It bound to plasma proteins by up to 92.32% and was predicted to be an inhibitor of CYP2C9 whereas a non-substrate of CYP3A4. From the ADME data it can be assumed that all the molecules of this series are rather lipophobic in nature and thus have better affinity for the polar amino acid residues lining most crucial parts of the enzyme. The toxicological data prediction also gave us an idea regarding the safety profile of the compounds. Expectedly enough, all compounds of this series were predicted to be mutagenic in Ames test (with the exception of **STT21**) as these comprise of five-membered nitrogen-containing heterocycles which are known to be of

mutagenic and genotoxic nature. Interestingly, all compounds showed negative carcinogenicity in mouse model and positive carcinogenicity in rat model and about 50% of the molecules posed high risk of hERG inhibition. In sharp contrast, **SHP099** though being a mutagen in Ames test, showed positive carcinogenicity in mouse model and negative in rats. It can thus be inferred from the toxicological data that all compounds fall within a normal range of safety as sought for newly developed drugs.

Table 2.18. Predicted ADME properties of compounds **STT01-STT21**

Compd	HIA (%)	Caco2	MDCK (nm/s)	SP (logKp, cm/h)	BBB	PPB (%)	CYP2C9	CYP2C19	CYP3A4
STT01	92.05	2.731	3.6829	-4.19	0.0276	91.78	Inhibitor	Non	Non
STT02	92.06	2.992	1.8354	-4.45	0.0344	90.56	Inhibitor	Non	Non
STT03	92.11	4.897	1.5011	-4.37	0.0284	89.58	Inhibitor	Non	Non
STT04	91.81	7.508	0.7128	-4.47	0.0274	90.36	Inhibitor	Non	Non
STT05	91.35	1.562	1.8171	-4.82	0.0235	93.71	Inhibitor	Non	Non
STT06	92.11	4.840	1.8870	-4.35	0.0189	88.64	Inhibitor	Non	Non
STT07	92.13	5.217	0.9563	-4.58	0.0221	87.76	Inhibitor	Non	Non
STT08	91.81	7.550	0.8527	-4.48	0.0203	87.53	Inhibitor	Non	Non
STT09	90.36	2.676	1.2208	-4.86	0.0198	90.82	Inhibitor	Non	Non
STT10	92.11	5.216	1.5011	-4.37	0.0179	89.89	Inhibitor	Non	Non
STT11	92.13	5.584	0.7766	-4.60	0.0208	89.04	Inhibitor	Non	Non
STT12	91.81	8.060	0.6810	-4.50	0.0184	88.63	Inhibitor	Non	Non
STT13	90.36	2.997	0.9438	-4.87	0.0175	92.32	Inhibitor	Non	Non
STT14	92.67	16.37	0.3405	-4.22	0.0383	91.39	Inhibitor	Non	Non
STT15	92.68	16.52	0.1981	-4.47	0.0482	90.63	Inhibitor	Non	Non
STT16	92.87	20.50	0.1731	-4.40	0.0282	88.82	Inhibitor	Non	Non
STT17	93.12	24.68	0.0975	-4.48	0.0215	90.10	Inhibitor	Non	Non
STT18	93.02	15.89	0.1961	-4.83	0.0187	93.01	Inhibitor	Non	Non
STT19	93.42	13.69	0.0634	-4.39	0.0957	91.31	Inhibitor	Non	Non
STT20	93.28	17.24	0.0599	-4.30	0.0476	88.81	Inhibitor	Non	Non
STT21	93.35	13.48	0.0481	-4.77	0.0255	92.12	Inhibitor	Non	Non
SHP099	95.49	20.89	0.1703	-3.03	0.0390	63.34	Inhibitor	Non	Non

HIA: Human Intestinal Absorption [0–20 (poor), 20–70 (moderate), 70–100 (well)], **Caco2**: In-vitro Caco2 cell permeability [<4 (low), 4–70 (moderate), >70 (high)], **MDCK**: Maden Darby Canine Kidney cell permeability [<25 (low), 25–500 (moderate), >500 (high)], **SP**: Skin permeability, **BBB**: Blood brain barrier permeability (C_{brain}/C_{blood}), **PPB**: In-vitro plasma protein binding.

Table 2.19. Predicted toxicological properties of compounds **STT01-STT21**

Compd	Ames test	Carcinogenicity (Mouse)	Carcinogenicity (Rat)	hERG inhibition
STT01	Mutagen	Negative	Positive	High risk
STT02	Mutagen	Negative	Positive	High risk
STT03	Mutagen	Negative	Positive	High risk
STT04	Mutagen	Negative	Positive	High risk
STT05	Mutagen	Negative	Positive	High risk
STT06	Mutagen	Negative	Positive	High risk
STT07	Mutagen	Negative	Positive	Medium risk
STT08	Mutagen	Negative	Positive	High risk
STT09	Mutagen	Negative	Positive	High risk
STT10	Mutagen	Negative	Positive	High risk
STT11	Mutagen	Negative	Positive	Medium risk
STT12	Mutagen	Negative	Positive	Medium risk
STT13	Mutagen	Negative	Positive	Medium risk
STT14	Mutagen	Negative	Positive	High risk
STT15	Mutagen	Negative	Positive	Medium risk
STT16	Mutagen	Negative	Positive	Medium risk
STT17	Mutagen	Negative	Positive	Medium risk
STT18	Mutagen	Negative	Positive	Medium risk
STT19	Mutagen	Negative	Positive	Medium risk
STT20	Mutagen	Negative	Positive	Medium risk
STT21	Non-mutagen	Negative	Positive	High risk
SHP099	Mutagen	Positive	Negative	Medium risk

Ames test-Ames test for mutagenicity in *Salmonella typhimurium*, **Carcinogenicity (Mouse)**-2 years carcinogenicity bioassay in mouse, **Carcinogenicity (Rat)**-2 years carcinogenicity bioassay in rat, **hERG Inhibition**-*In vitro* Human Ether-a-go-go Related Gene Channel Inhibition

2.4. Summary

In summary, pharmacophore-based virtual screening was performed on Enamine Advanced Database, an online bioactive library of more than 55,0000 potential anticancer molecules against an anti-SHP2 pharmacophore model built by creating hypothetical space regions on **SHP099** by MOE software. The screening exercise identified 37 hit molecules of diverse chemical classes which were subsequently filtered using rules-based filtering techniques like PreADMET, PAINS-Remover to get 35 virtual hits. Based upon the binding affinity of the molecules towards SHP2 (by molecular docking and MD simulation results), the topmost molecule **111675** [(2-((5-

(5-chloro-2-methoxyphenyl)-4*H*-1,2,4-triazol-3-yl)thio)acetyl)-D-tryptophanate] (SHP2 K_i = 0.118 μM) was synthesized, characterized and evaluated for SHP2 inhibition which unveiled its moderately potent SHP2 inhibitory activity (IC_{50} = 0.878 ± 0.008 μM). Unfortunately, **111675** did not possess strong antiproliferation activity against MCF-7 cells (GI_{50} > 1000 μM). Thus, to improve the pharmacological outcome, rational and systematic optimization was done on the molecule **111675** to design, synthesize and evaluate a series of novel heterocyclic hybrids of 1,3,4-thiadiazole and 1,2,4-triazole rings tethered by a thioacetamide linker.

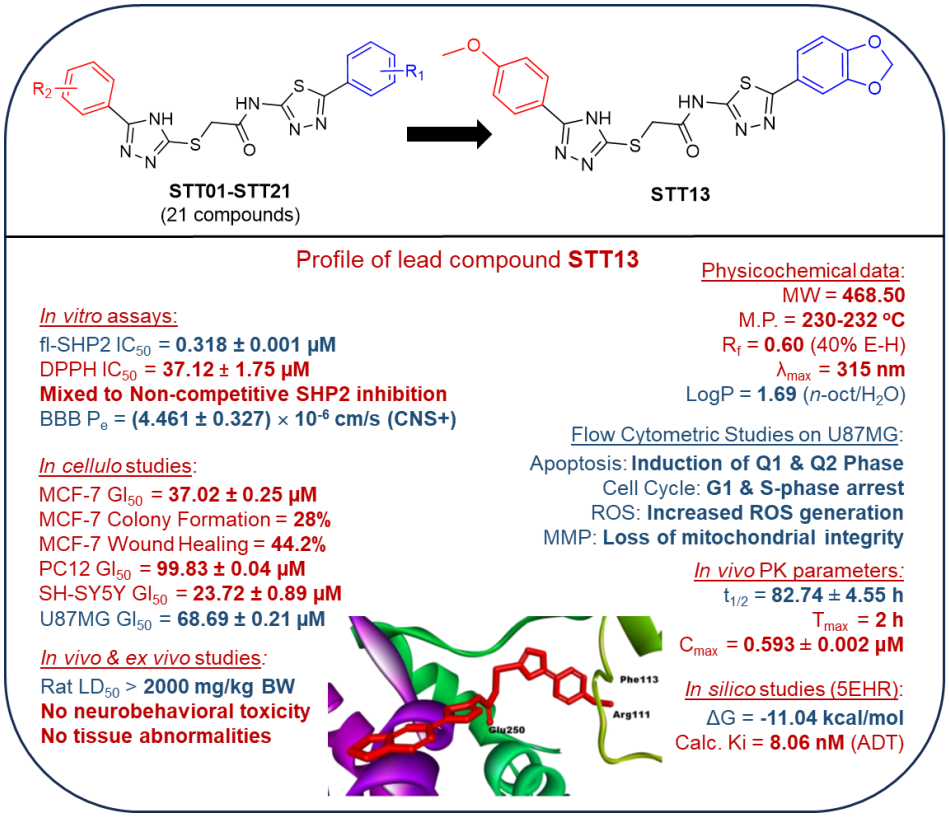

Figure 2.24. Summary of key outcomes of the current series of compounds **STT01-STT21**

The current series i.e., **STT series** is essentially a hybrid of 1,3,4-thiadiazole and 1,2,4-triazole rings tethered by a thioacetamide linker. A set of 21 homologues was designed, synthesized, characterized by NMR, FTIR & HRMS and evaluated for *in vitro* SHP2

inhibitory activity where compound **STT13** (*N*-(5-(benzo[*d*][1,3]dioxol-5-yl)-1,3,4-thiadiazol-2-yl)-2-((5-(4-methoxyphenyl)-4*H*-1,2,4-triazol-3-yl)thio)acetamide) emerged as the most potent SHP2 inhibitor (IC_{50} = 0.318 ± 0.001 μM) inhibiting the enzyme in a mixed to non-competitive manner indicating a possible allosteric mode of inhibition (**Figure 2.24**). An SAR study was done from the IC_{50} data and the corresponding structure of the **STT** homologues. *In silico* studies revealed that the lead inhibitor strongly binds to the tunnel allosteric site of SHP2.

Compound **STT13** possessed moderate antioxidant activity as determined by a DPPH assay (DPPH IC_{50} = 37.12 μM) and an effective *in vitro* BBB permeability value of (4.461 ± 0.327) × 10^{-6} cm/s indicating potential to cross the BBB. Further, cytotoxicity studies revealed that compound **STT13** caused death of SHP2-driven MCF-7 (GI_{50} = 37.02 ± 0.25 μM), U87MG (GI_{50} = 68.69 ± 0.21 μM), PC12 (GI_{50} = 99.83 ± 0.04 μM) & SH-SY5Y cells (GI_{50} = 23.72 ± 0.89 μM) in a dose-dependent manner and inhibited MCF-7 cell colony formation and migration. Moreover, flow cytometric analysis showed that it exerted its antiproliferative effect on U87MG cells by inducing early apoptosis (Q1 & Q2 phase) and inhibiting cell cycle progression at the G1 & S phase. Compound **STT13** was shown to increase oxidative stress in the U87MG cells by promoting ROS generation and loss of mitochondrial integrity. Interestingly, compound **STT13** displayed no systemic, haematological, histopathological or neurobehavioral toxicity in adult female Wistar rats on oral administration with an LD_{50} > 2000 mg/kg BW (acc. to OECD 423). RP-HPLC based *in vivo* pharmacokinetic study in rats revealed favourable oral pharmacokinetics of the molecule with a large half-life of elimination ($t_{1/2}$ = 88.72 h) and a C_{max} of 0.59 μM achieved at T_{max} of 2 h indicating rapid and significant oral adsorption of compound **STT13**.